Radioactive Fallout from Nuclear Weapons Tests

Proceedings of the Second Conference
Germantown, Maryland
November 3–6, 1964

Sponsored by the Fallout Studies Branch
Division of Biology and Medicine
U. S. Atomic Energy Commission

Alfred W. Klement, Jr.
Editor

November 1965

U.S. ATOMIC ENERGY COMMISSION / Division of Technical Information

Table 1 — COMPARISON OF RADIONUCLIDE PARTITIONS PREDICTED BY THE SEMIEMPIRICAL METHOD WITH OTHERS INFERRED FROM ANALYSIS OF NUCLEAR DEBRIS

Radionuclide	Predicted fractions			Fractions in 24-hr cloud of a high-yield, coral-surface burst	Fractions in a low-yield, silicate-surface burst		
	Local	Intermediate*	Worldwide		Local	Intermediate†	Worldwide
^{137}Cs	0.1	0.1	0.8	0.36 ± 0.36	0.00	0.22	0.78
^{89}Sr	0.1	0.1	0.8		0.02	0.24	0.74
^{90}Sr	0.15	0.1	0.75	0.11 ± 0.11	0.07	0.24	0.69
$^{140}Ba - ^{140}La$	0.25	0.1	0.65		0.20	0.26	0.54
^{132}Te	0.25	0.1	0.65		0.18	0.26	0.56
$^{95}Zr - ^{95}Nb$	0.65	0.1	0.25		0.72	0.19	0.09
^{99}Mo (coral)	0.65	0.1	0.25	0.02 ± 0.02	0.72	0.19	0.09

*Intermediate fraction taken as 25 to 50 μ in diameter.
†Intermediate fraction taken as 18 to about 90 μ in diameter.

particle-size distribution in the latter case differed considerably from that used in the model.

In summary, the present state of the art puts us in the position of the meteorologist who has to predict the weather even though he can't. We make the most reasonable attempt our knowledge permits and cross our fingers.

Second Phase of Predicting Fractionation Effects

We will now discuss the second, long-term phase of predicting fractionation effects, the phase concerned with piecewise refinement of weak links in the calculational chain. Figure 5 shows the fallout-formation processes that have to be taken into account in a fundamental approach. Our thinking on this is still the same as when we presented this diagram at the last conference.[5] Perhaps the weakest links are the definition of particle size and the absence of accounting for agglomeration effects, and next in importance is the transition from an equilibrium (thermodynamic) to a nonequilibrium (kinetic) approach. However, the definitive work being done by Russell on the first problem[10] and the need to properly plan our high-temperature experimental work has led us to attack the last problem first. Our efforts in this direction form the subject of this section of the report. One should not jump to the conclusion that the thermodynamic equilibrium treatment is inapplicable or that, even if it were, thermodynamic data are no longer required. As will be seen, each approach has its place in the overall development.

The plan of developing a kinetic model has been, first, to decide on a mechanism; second, to assemble useful, available theoretical and experimental results; and, third, to integrate these and fill in the missing steps to obtain the complete treatment. We are now in stage two. We are obviously not concerned so much at this point with developing a new theory of fallout formation as with the application of established theory.

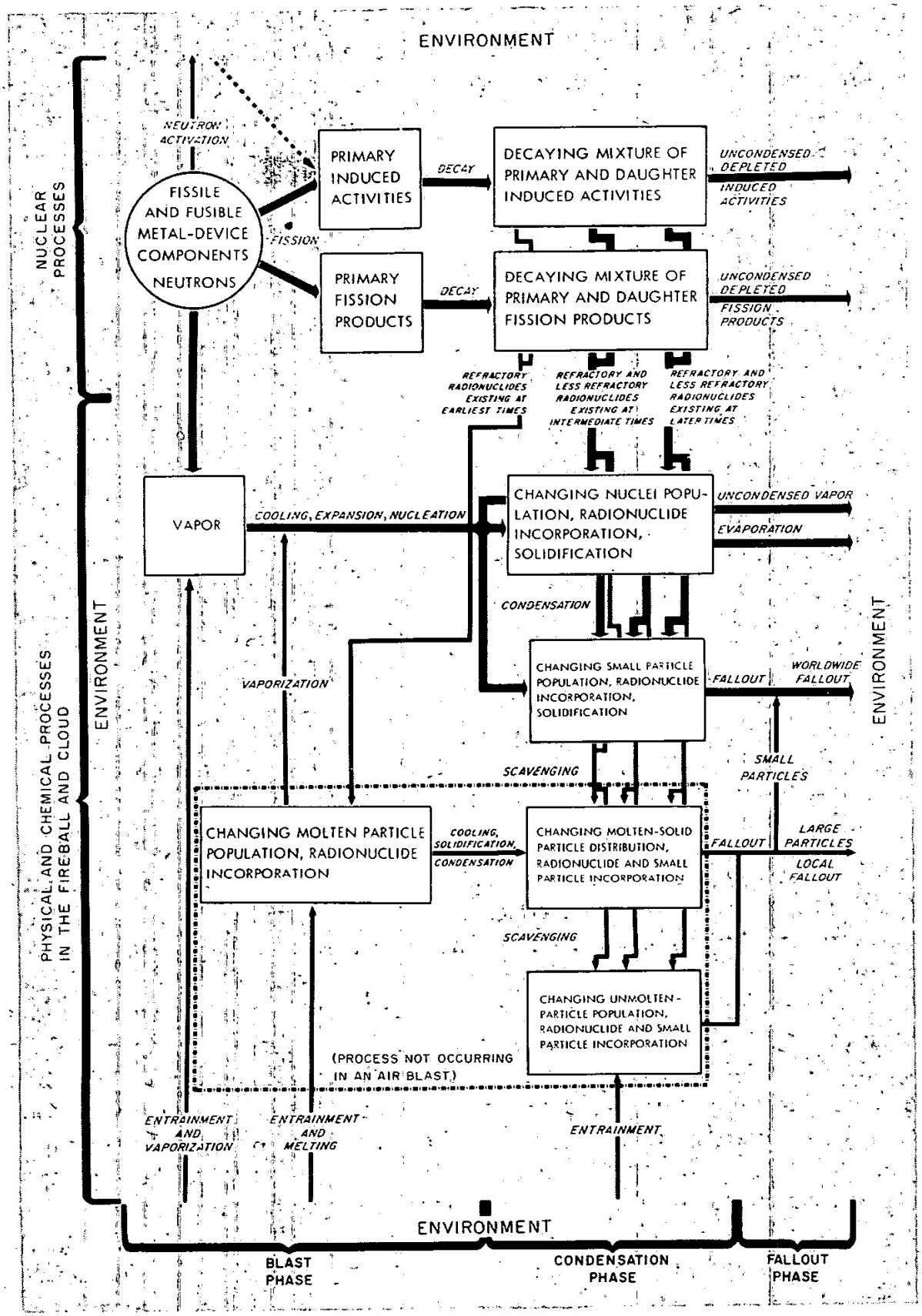

Fig. 5—Fallout-formation processes in air and surface bursts.

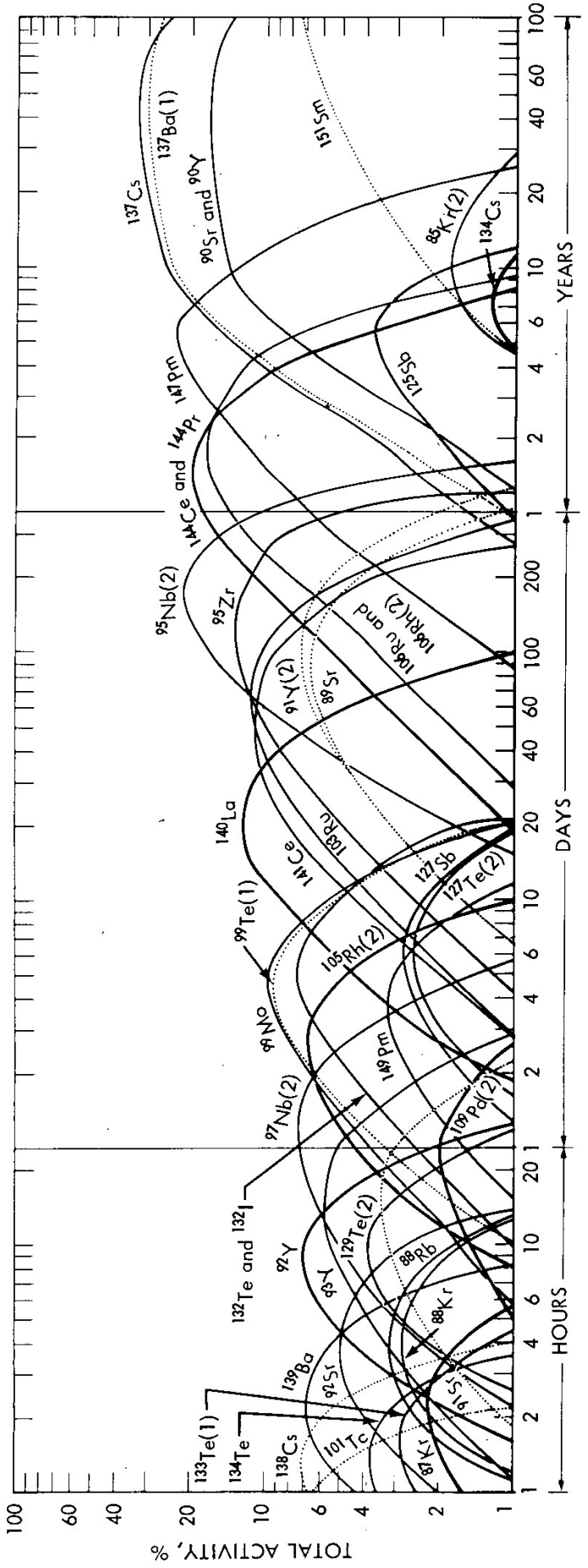

Fig. 11—Relative disintegration rates as a function of time for individual fission products in the case of ^{238}U fission produced by a thermonuclear neutron spectrum.

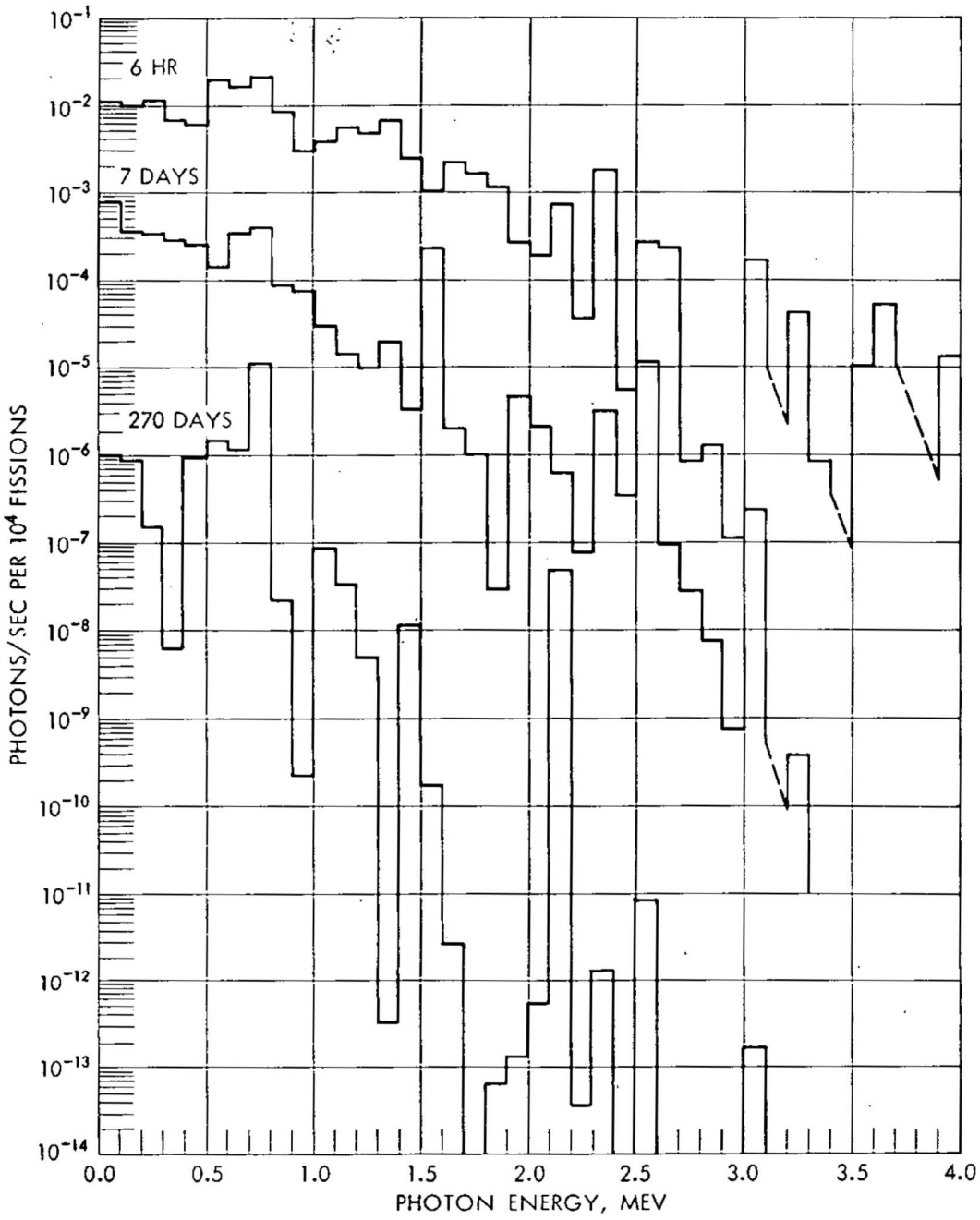

Fig. 12—Gamma-photon spectra from fission products at various times after ^{238}U fission produced by a thermonuclear neutron spectrum.

The relative contributions of the important gamma-emitting nuclides to the total dose-rate have been plotted vs. time in Fig. 14. It is interesting to note that from a few days onward much of the dose rate at any given time can be accounted for in terms of two or three nuclides and that volatilely behaving mass chains contribute prominently to the dose rate. The dose-rate contributions given here pertain, of course, to unfractionated debris. Since many of the hard emitters (e.g., cesium and iodine isotopes) are subject to fractionation, the relative dose-rate contributions will be greatly modified in the case of fractionated debris.

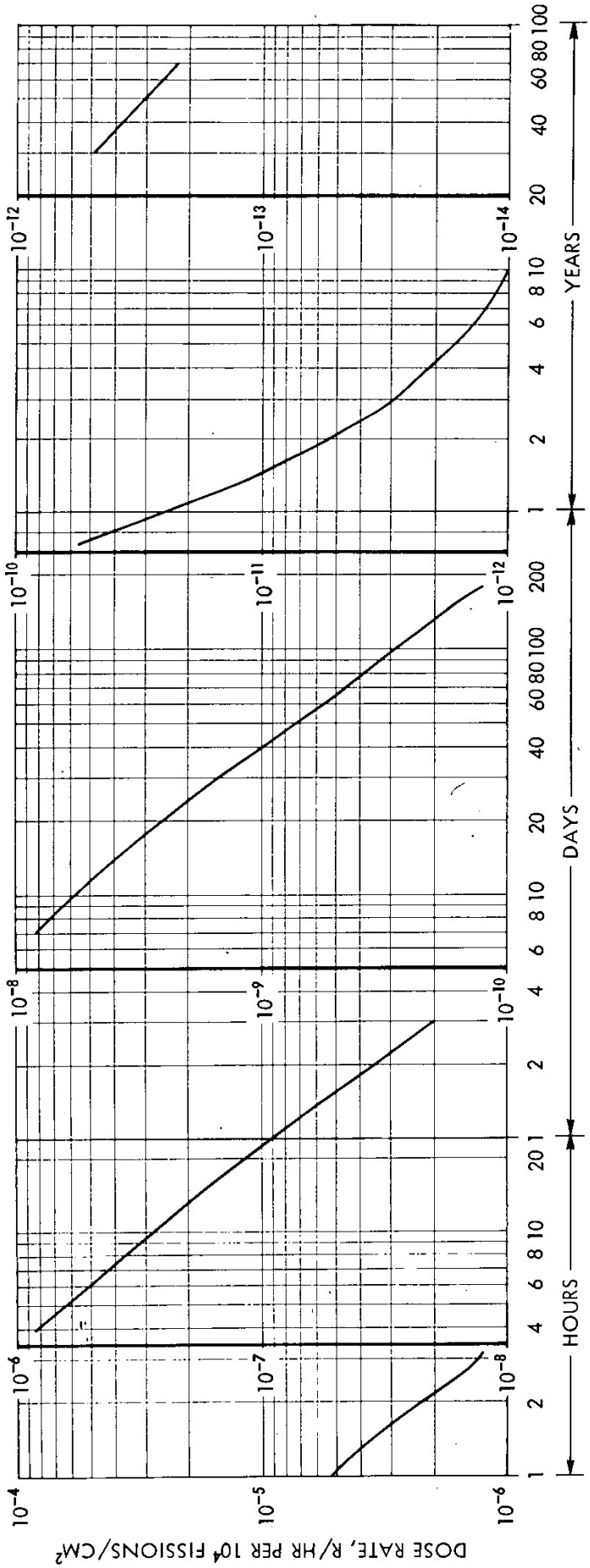

Fig. 13—Gross exposure-dose-rate decay for products of ^{238}U fission produced by a thermonuclear neutron spectrum.

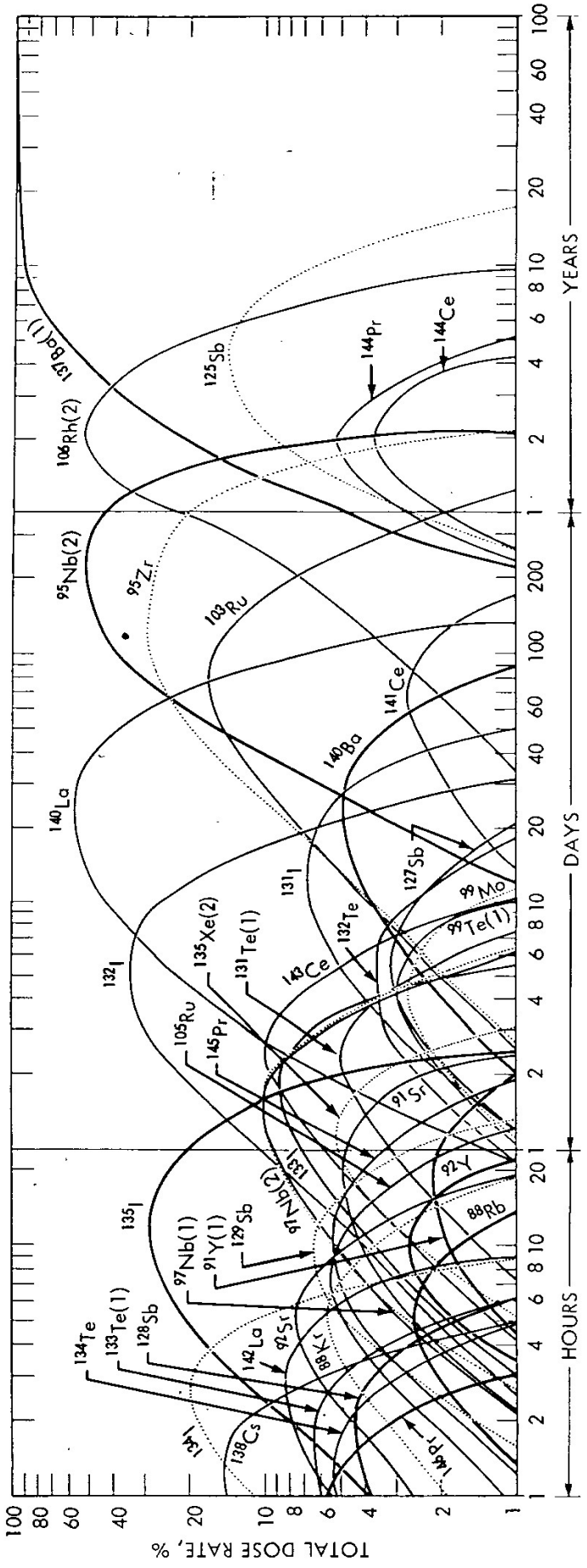

Fig. 14—Relative contributions to the exposure-dose rate as a function of time for individual fission products in the case of ^{238}U fission produced by a thermonuclear neutron spectrum.

The computed values of K_0 are plotted as a function of d_{50} in Fig. 4. It may be noted that the curves of i(100), i'(100), and K_0 given as a function of d_{50} in Figs. 2, 3, and 4 are very similar to the curve for i(100) plotted as a function of $\bar{d}$ in Fig. 1.

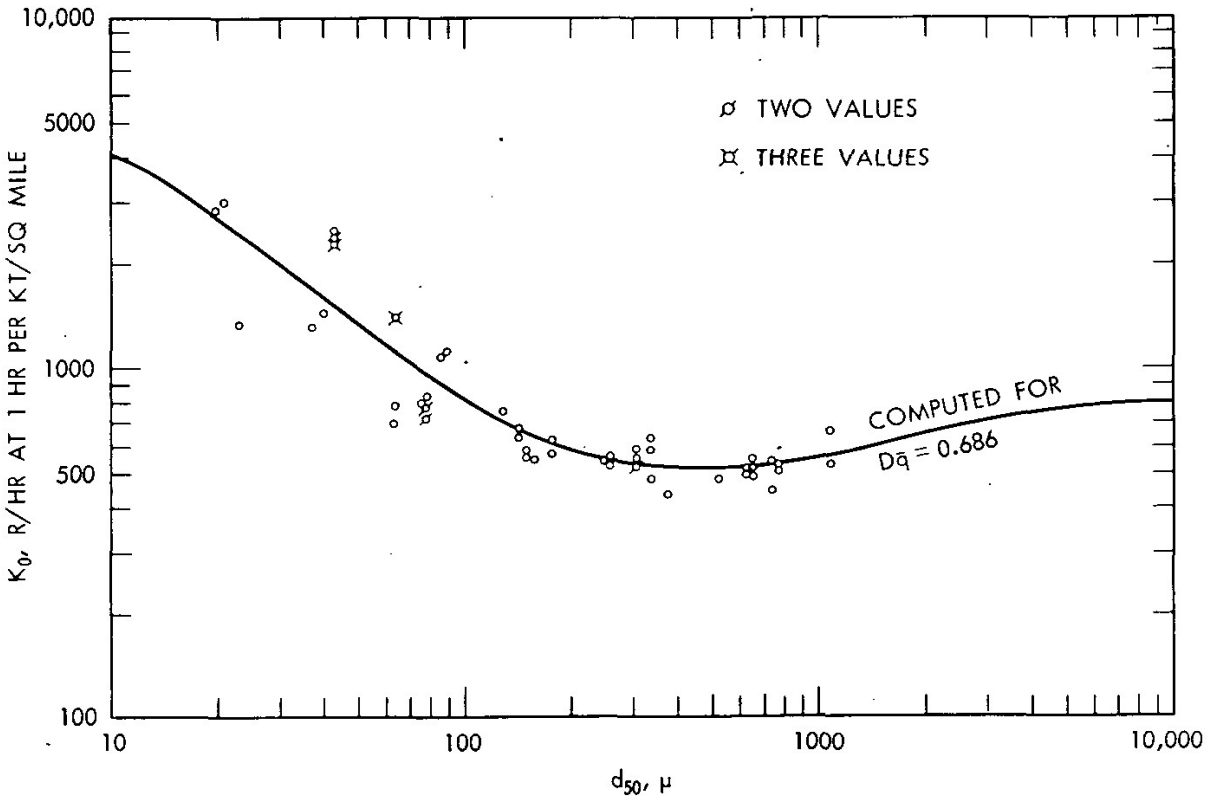

Fig. 4—Variation of K_0 with d_{50} for fallout-collecting stations.

The high values of K_0 for the stations in the 35- and 56-numbered series (Table 7) suggest that the I_s values are overestimated by correction of the monitoring data[1] to 1 hr with the $t^{-1.2}$ function. The adjustment of the two apparently different sets of reported A_f values[2] to a midvalue rather than correction of one of the two sets of data to be consistent with the other may have resulted in K_0 values that are either low or high by 25%. Further investigation of the reported data[3] together with theoretical analyses may suggest what corrections are appropriate.

The Dq terms of Eq. 12 can be evaluated using an appropriate value of k_{fp}. The selection of a value here is limited to the k_{fp} value for the fission products from the thermal-neutron fission of ^{235}U because the i(100) and r_{fp} values, as deduced from the ion-chamber measurements, are based on the response of the ion-chamber to the ^{235}U products. The calculated value[8] of k_{fp} is 3950 r/hr at 1 hr per kiloton per square mile. The Dq of Eq. 12 is given by

$$Dq = \frac{K_0}{3950\ r_{fp}} \qquad (21)$$

The values of $r_{fp}(100)$, $r'_{fp}(100)$, r_{fp}, r'_{fp}, K_0, and Dq for each station are summarized in Table 8. The value of K_0 in Table 8 for stations having more than one estimated value of K_0 in Table 7 is a median value. The terrain about the stations generally increased in roughness[1] proceeding from station 100 to station 707; however, this general increase in roughness is not reflected in a corresponding general decrease in Dq values for these stations. At the stations of the 800 series, the terrain was fairly smooth and flat at stations 813 and 814 and somewhat rougher at stations 815 and 816. The terrain features at the remainder of the stations were varied. At the stations in series 100 through 800, the GITR's were calibrated to have a response factor, D, near unity; thus for these stations the computed value of Dq is practically equal to q. For the other stations the response factor for the instruments and monitor has not been reported, but it is assumed to be about 0.7. Therefore, where the computed value of Dq is in excess of 0.7, either the I_s value is too large or the A_f value is too small (i.e., the r_{fp} value is too small).

Table 8—SUMMARY OF CALCULATED r_{fp}, r'_{fp}, K_0, AND Dq VALUES* FOR THE SMALL BOY SHOT FALLOUT-COLLECTING STATIONS

Station and sample No.	$r_{fp}(100)$	$r'_{fp}(100)$	r_{fp}	r'_{fp}	K_0, r/hr at 1 hr / kt/sq mile	Dq
100	0.338	0.369	0.194	0.304	511	0.667
101	0.355	0.425	0.204	0.346	589	0.731
103	(0.403)	(0.443)	(0.232)	(0.361)	595	0.650
200	0.456	0.469	0.262	0.382	758	0.724
201	0.340	0.398	0.195	0.324	494	0.642
202	(0.340)	(0.400)	(0.196)	(0.326)	530	0.685
203	0.341	0.400	0.196	0.326	515	0.666
204	(0.343)	(0.405)	(0.197)	(0.330)	515	0.663
207	(0.363)	(0.433)	(0.209)	(0.353)	540	0.678
209	(0.383)	(0.438)	(0.220)	(0.357)	578	0.665
300	(0.343)	(0.352)	(0.197)	(0.287)	519	0.691
303	0.335	0.361	0.192	0.294	485	0.640
305	0.338	0.381	0.195	0.310	518	0.673
309	(0.343)	(0.405)	(0.197)	(0.330)	531	0.684
311	(0.363)	(0.433)	(0.209)	(0.353)	549	0.665
400	(0.339)	(0.352)	(0.195)	(0.287)	551	0.717
401	0.344	0.354	0.198	0.289	441	0.564
403	0.346	0.357	0.199	0.291	561	0.715
405	0.350	0.362	0.202	0.295	590	0.741
407	0.350	0.362	0.202	0.295	545	0.684
409	(0.383)	(0.400)	(0.220)	(0.326)	589	0.678
501	0.362	0.378	0.208	0.308	549	0.669
502	(0.355)	(0.372)	(0.204)	(0.303)	540	0.671
503	0.350	0.362	0.202	0.295	530	0.665

(Table 8 continues on page 63)

Table 8—(Continued)

Station and sample No.	$r_{fp}(100)$	$r'_{fp}(100)$	r_{fp}	r'_{fp}	K_0, r/hr at 1 hr / kt/sq mile	Dq
505	0.359	0.372	0.206	0.303	549	0.674
507	0.399	0.415	0.230	0.338	598	0.659
509	(0.403)	(0.419)	(0.232)	(0.342)	610	0.666
513	(0.444)	(0.452)	(0.255)	(0.369)	657	0.654
601	(0.444)	(0.452)	(0.255)	(0.369)	693	0.688
603	0.428	0.443	0.246	0.361	572	0.590
605	0.415	0.431	0.239	0.351	542	0.575
607	(0.403)	(0.419)	(0.232)	(0.342)	553	0.605
700	(0.565)	(0.571)	(0.325)	(0.466)	670	0.523
701	(0.524)	(0.524)	(0.302)	(0.427)	530	0.445
703	(0.484)	(0.476)	(0.278)	(0.388)	571	0.522
704	(0.444)	(0.462)	(0.255)	(0.369)	655	0.644
707	0.431	0.449	0.248	0.366	658	0.673
813	0.573	0.557	0.330	0.454	1,133	0.870
814	0.576	0.562	0.332	0.458	1,094	0.836
815	1.100	0.924	0.633	0.753	1,330	0.533
816	1.037	0.880	0.596	0.718	1,450	0.617
18–9	0.638	0.605	0.367	0.482	805	0.556
18–10	0.625	0.595	0.360	0.485	830	0.585
18–11	0.625	0.595	0.360	0.484	775	0.546
18–12	0.625	0.595	0.360	0.485	725	0.511
27–1	0.735	0.662	0.422	0.540	697	0.418
27–2	0.735	0.662	0.422	0.540	1,395	0.838
27–3	0.726	0.657	0.418	0.535	793	0.482
27–4	0.735	0.662	0.422	0.540	1,390	0.835
35–17	0.980	0.843	0.564	0.687	2,510	1.128
35–18	0.980	0.843	0.564	0.687	2,320	1.043
35–19	1.000	0.852	0.575	0.695	2,390	1.053
35–20	1.090	0.905	0.626	0.737	2,320	0.939
56–11	1.573	1.272	0.905	1.037	1,335	0.374
56–12	1.695	1.367	0.975	1.113	3,020	0.785
56–14	1.760	1.414	1.012	1.152	2,860	0.717

*Values in parentheses are derived from estimated d_{50} values for the station.

The mean value of Dq for all the stations in the 100 to 700 series, for which d_{50} is given, is 0.686 ± 0.025. With this value of Dq, Eq. 12 becomes

$$K_0 = 2710\ r_{fp} \tag{22}$$

Thus K_0^0 for all the indicated stations is 2710 (i.e., K_0 with $r_{fp} = 1$).

The f_j values for the Small Boy shot fallout pattern were computed by constructing fallout patterns for a given range in particle size and evaluating the intensity–area integral for each pattern. The fraction of

I_s at each station contributed by each particle-size group was calculated from activity measurements on sieved fractions of the fallout samples. The constructed fallout patterns for several of the particle-size ranges and for the total fallout pattern are shown in Figs. 5 to 8. The activity–size distribution derived from this analysis is shown in Fig. 9. The median particle diameter for the distribution is 210 μ. The derived distribution is not lognormal.

The f_j values from which the distribution was determined are summarized in Table 9; also given in the table are the $f_j r_j$ and $f_j K_{0j}$ values leading to the estimates of $\bar{r}_{fp}$ and $\bar{K}_0$ for the whole fallout pattern. The sum of the intensity–area integrals, J_R, of the fallout patterns for the different particle groups is 580 r/hr at 1 hr per square mile; the value of J_R for the pattern of the gross I_s contours is 640 r/hr at 1 hr per square mile, about 11% larger. The yield of the Small Boy shot has not been reported, except that the yield was small.[9] With the use of the intensity–area integral for the I_s contours and the yield, the value of J_R/BW for the pattern thus could be estimated. With a $\bar{K}_0$ value of 1070 r/hr at 1 hr per kiloton per square mile, the value of C could be estimated; and the fraction of device, F_D, accounted for within the constructed fallout pattern of Fig. 8 could similarly be estimated.

The fallout patterns constructed for the various particle-size fractions do not include contributions from the regions of high I_s values near ground zero nor from the large area of low-level fallout that was deposited in northern Utah. These contributions are not included in the analysis because fallout samples for determining the distribution of radioactivity among the fallout particles deposited in these regions were not available for analysis. For the total fallout pattern, including the contributions to I_s from these areas, a J_R value of 1460 r/hr per square mile is obtained; this value is a factor of about 2.3 larger than that calculated for the fallout pattern constructed from the I_s values at the stations for which particle-size data are available.

The fraction of the device, F_D, accounted for within the larger fallout pattern, would therefore be 2.3 times that for the smaller pattern mentioned earlier. The ratio of the contributions to the intensity–area integral for the high-intensity region to the low-intensity region, as determined from integrals, is about 3 to 1. If an average r_j value of 0.29 is assumed for the fallout in the high-intensity region and an average r_j value of 1.5 for the low-intensity region, a value of $\bar{K}_0$ can be estimated for the larger pattern from the data of Table 9. Allocation of appropriate fractions of the intensity–area integral to the three areas gives a weighted average value for $\bar{K}_0$ of 1400 r/hr at 1 hr per kiloton per square mile; the corresponding

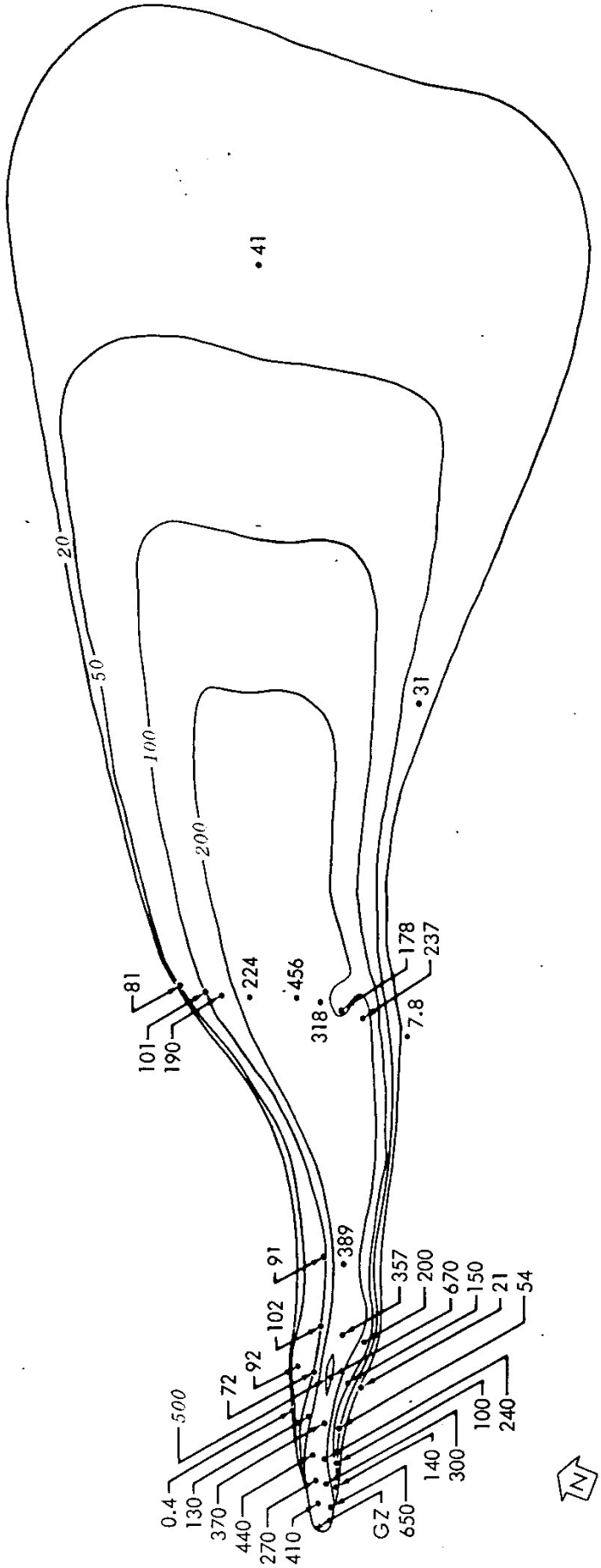

Fig. 5—Isointensity contours for 20- to 50-μ particle diameters in milliroentgens per hour at 1 hr.

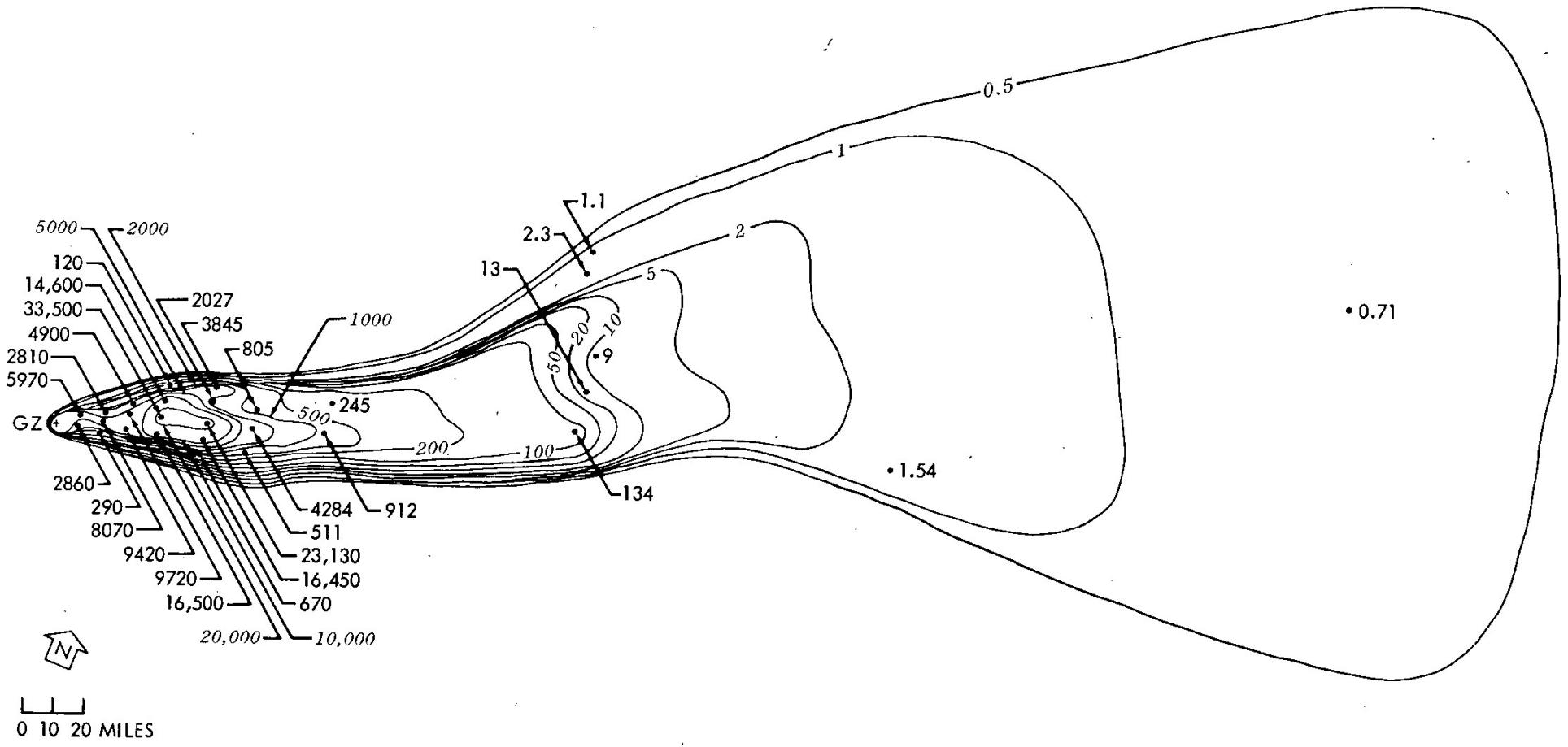

Fig. 6—Isointensity contours for 200- to 350-μ particle diameters in milliroentgens per hour at 1 hr.

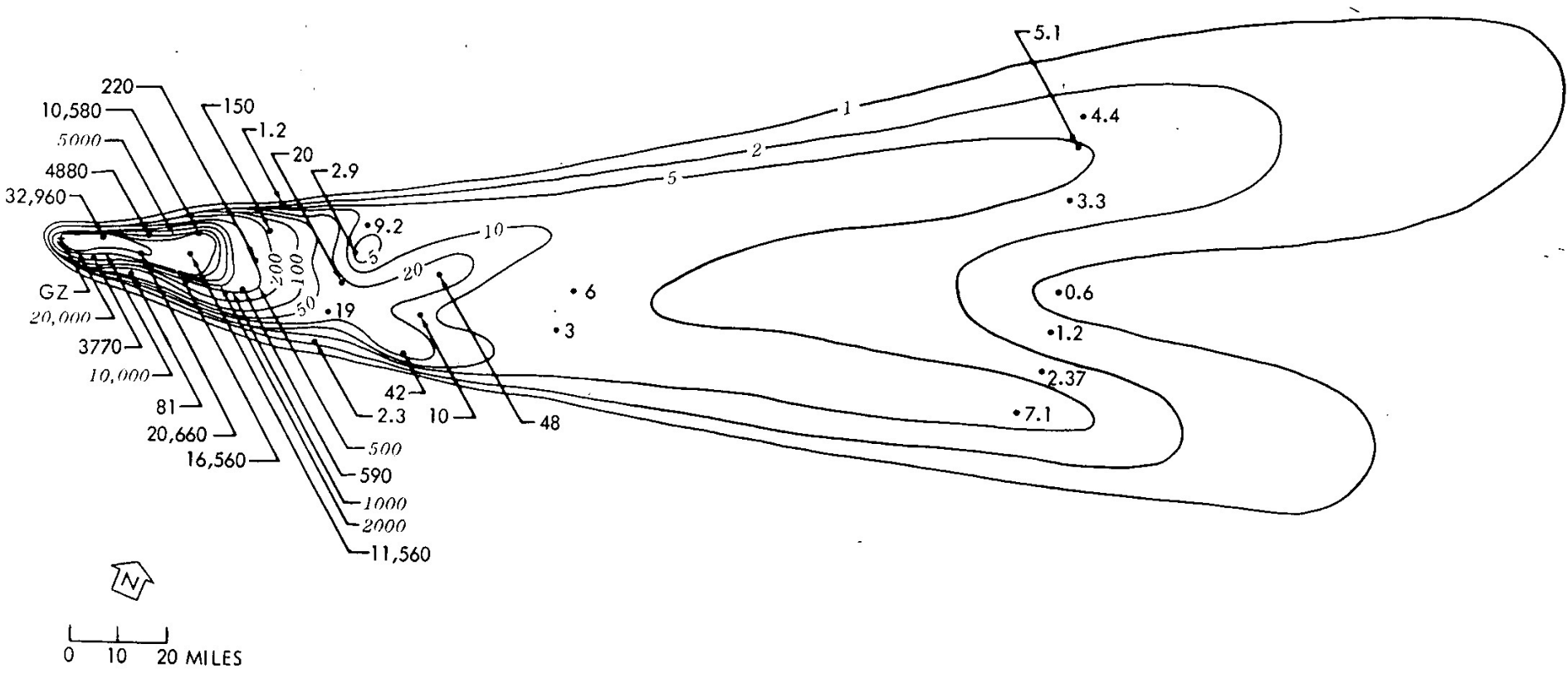

Fig. 7—Isointensity contours for 750- to 1000-μ particle diameters in milliroentgens per hour at 1 hr.

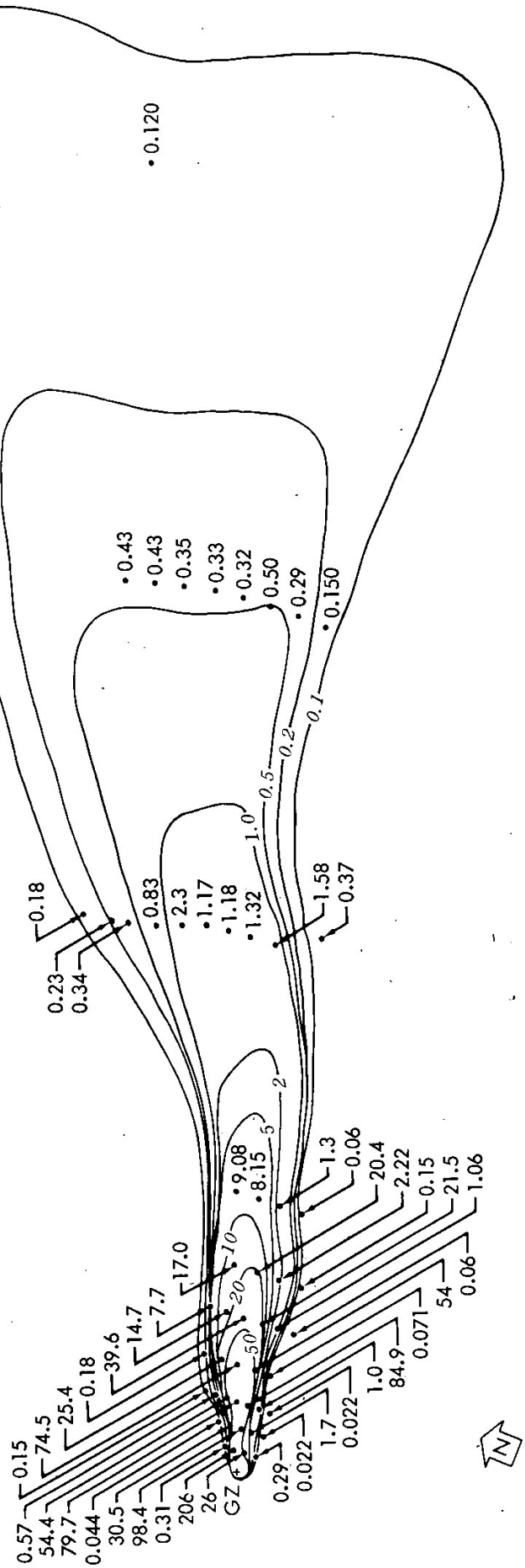

Fig. 8—Total fallout isointensity contours in roentgens per hour at 1 hr.

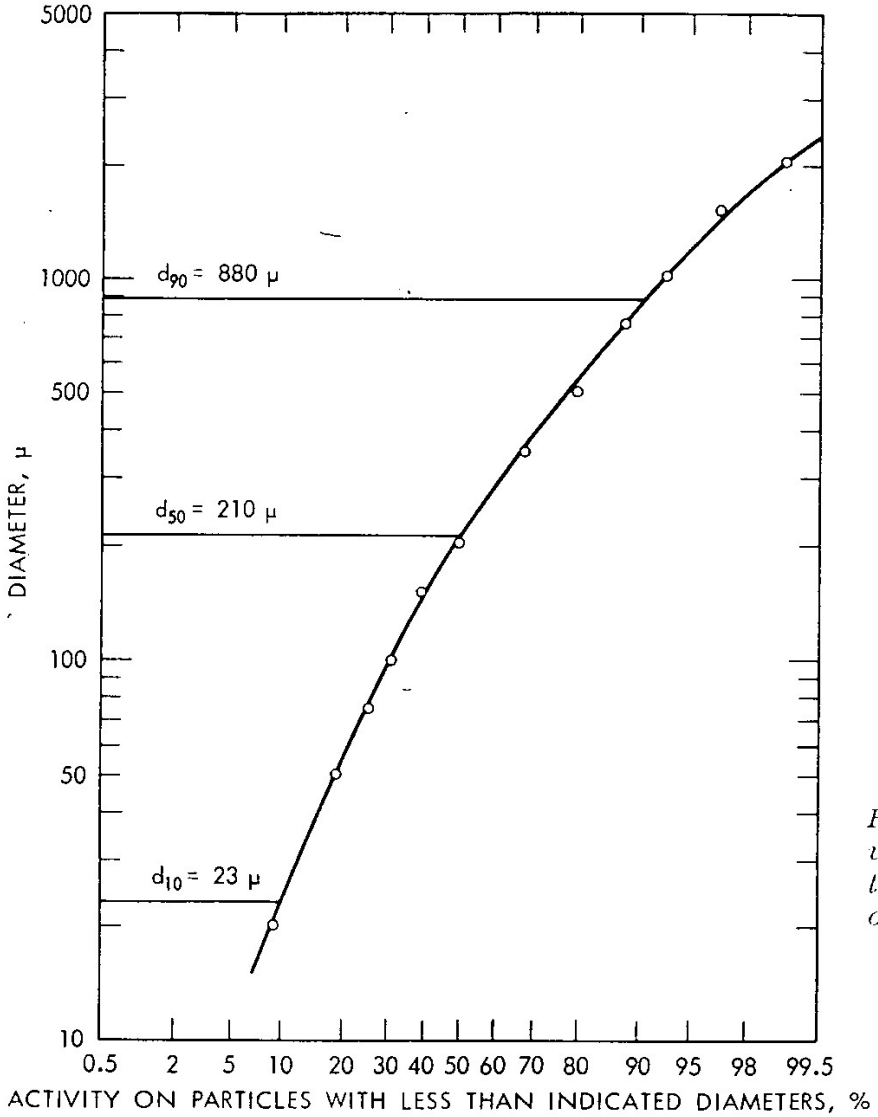

Fig. 9—Gross size vs. activity—area integrals for particles of different sizes.

Table 9—SUMMARY OF THE f_j VALUES FOR THE SMALL BOY SHOT FALLOUT AND THE CALCULATIONS FOR $\bar{r}_{fp}$ AND $\bar{K}_0$

Δd, μ	$\bar{d}$, μ	r_j	K_{0j}, r/hr at 1 hr / kt/sq mile	f_j	$f_j r_j$	$f_j K_{0j}$, r/hr at 1 hr / kt/sq mile
0 to 20	10	1.51	4090	0.091	0.137	372
20 to 50	35	0.665	1800	0.093	0.062	167
50 to 75	62.5	0.429	1160	0.075	0.032	87
75 to 100	87.5	0.334	905	0.049	0.016	44
100 to 150	125	0.269	729	0.076	0.020	55
150 to 200	175	0.232	629	0.108	0.025	68
200 to 350	275	0.204	553	0.182	0.037	101
350 to 500	425	0.195	529	0.122	0.024	64
500 to 750	625	0.194	526	0.082	0.016	43
750 to 1000	875	0.198	537	0.053	0.011	28
1000 to 1500	1250	0.210	570	0.040	0.008	23
1500 to 2000	1750	0.230	623	0.021	0.005	13
> 2000		0.292	791	0.0095	0.003	7
				Sum	0.396	1072

Notes: (1) $r_{fp} = \Sigma f_j r_j = 0.396$. (2) $\bar{K}_0 = \Sigma f_j K_{0j} = 1072$ r/hr at 1 hr per kiloton per square mile.

value of C for the larger fallout pattern could then be calculated if the yield were known.

A commonly used value of K_0^0 in Eq. 7 for estimating the fraction of a device in the fallout pattern, especially when experimental values of $D\bar{q}$ are not directly available, is 2000 r/hr at 1 hr per kiloton per square mile. If this value is used with the J_R value, 1460 r/hr at 1 hr per square mile, for the Small Boy fallout pattern, the estimated value of F_D could be compared to that obtained through use of the radiochemical analysis of the fallout material and the methods outlined in this report.

COMMENTS AND CONCLUSIONS

The computed r_{fp} values appear to be somewhat low, especially for the median particle diameters between about 200 and 800 μ. Further examination of the radiochemical data with respect to the fractionation of individual nuclides and to the fission yield of ^{95}Zr, as a measure of the number of fissions, could provide further information on the r_{fp} values. The major factors in determining the r_{fp} values, if the data from ion-chamber measurements are accepted as being by far the most accurate, are the fission content of the samples and the decay factors from 100 to 1 hr after detonation for the ion-chamber data. The absolute value of i_0 for the unfractionated mixture of radionuclides from thermal-neutron fission of ^{235}U rather than for fission by fission neutrons would result in a relatively small error in the r_{fp} estimates. It should be expected that the decay factors for the samples would approach those for i_0 as the $r_{fp}(100)$ values approach unity, indicating a relatively unfractionated mixture of radionuclides.

The Dq values derived from the data are consistent with other previously derived values of q for the Nevada Test Site terrain.[8] These values generally would not be influenced by possible future changes in the r_{fp} values since any change in r_{fp} would result in an equivalent change in the values of the K_0.

The example analysis of some of the Small Boy shot data applicable to evaluation of the intensity–activity ratio shows that the ratio is not a constant for a given fallout pattern but varies over the pattern depending on the particle sizes in the deposited fallout. However, when gross activity–size distribution data are evaluated, an average value of the ratio can be derived for the fallout pattern. On the other hand, the average value of the intensity–activity ratio is not required for estimating the fraction of the device within a fallout pattern. A value for this ratio for the fallout deposited uniformly over an ideal plane, an average terrain attenuation factor, and an instrument response factor, however, are needed for estimating the fraction of device in the pattern.

Further detailed analyses of the available data are needed to verify or adjust the values of several of the parameters, as described in this preliminary analysis of the reported data, for more accurate evaluations of the intensity–activity ratios and the fraction of device accounted for within the fallout pattern.

REFERENCES

1. P. D. LaRiviere, Hong Lee, and K. H. Larson, Ionization Rate Measurements, Project 2.11, Operation Sun Beam Report POR-2217, April 1964. (Classified)
2. P. D. LaRiviere, J. D. Sartor, W. B. Lane, and K. H. Larson, Fallout Collection and Gross Sample Analysis, Project 2.9, Operation Sun Beam Report POR-2215, October 1964. (Classified)
3. E. C. Freiling, L. R. Bunney, and F. K. Kawahara, Physiochemical and Radiochemical Analysis, Project 2.10, Operation Sun Beam Report POR-2216, October 1964. (Classified)
4. C. F. Miller, Response Curves for USNRDL 4-pi Ionization Chamber, Report USNRDL-TR-155, U. S. Naval Radiological Defense Laboratory, May 1957.
5. C. F. Miller and P. Loeb, Ionization Rate and Photon Pulse Decay of Fission Products from the Slow-Neutron Fission of U-235, Report USNRDL-TR-247, U. S. Naval Radiological Defense Laboratory, August 1958.
6. P. D. LaRiviere, Response of a Low-Geometry Scintillation Counter to Fission and Other Products, Report USNRDL-TR-303, U. S. Naval Radiological Defense Laboratory, February 1959.
7. W. B. Lane, Stanford Research Institute, private communication, July 1964.
8. C. F. Miller, Fallout and Radiological Countermeasures, Vol. I, Stanford Research Institute, Project IMU-4021, January 1963.
9. Samuel Glasstone (Ed.), *The Effects of Nuclear Weapons*, Revised Edition, U. S. Government Printing Office, Washington, D. C., 1962.
10. L. Machta, Meteorological Processes in the Transport of Weapon Radioiodine, *Health Phys.*, *9*(12): 1123-1132 (1963).

RADIOCHEMICAL-DATA CORRELATIONS ON DEBRIS FROM SILICATE BURSTS

GLENN R. CROCKER, FRANCIS K. KAWAHARA, and EDWARD C. FREILING
U. S. Naval Radiological Defense Laboratory, San Francisco, California

ABSTRACT

Local-fallout samples collected in 1962 in the Johnie Boy, Small Boy, and Sedan shots were analyzed radiochemically for ^{89}Sr, ^{90}Sr, ^{91}Y, ^{95}Zr, ^{99}Mo, ^{103}Ru, ^{106}Ru, ^{131}I, ^{132}Te, ^{136}Cs, ^{137}Cs, ^{140}Ba, ^{141}Ce, ^{144}Ce, ^{239}Np, and ^{239}Pu. These results, as reported by the project officers, have been correlated by plotting the log of the ratio of equivalent fissions of each nuclide, i, to equivalent fissions of ^{95}Zr, $r_{i,95}$, against the log of the similar ratio for ^{89}Sr and ^{95}Zr, $r_{89,95}$. The data were fitted to straight lines by linear regression; and slopes, intercepts, coefficients of correlation, and confidence limits were determined. The slope of such a line for a nuclide i is an indication of the degree of fractionation of the nuclide relative to the fractionation of ^{89}Sr. For all cases observed in these Nevada shots, the same group of nuclides (^{89}Sr, ^{90}Sr, ^{91}Y, ^{103}Ru, ^{106}Ru, ^{131}I, ^{132}Te, ^{136}Cs, ^{140}Ba, ^{137}Cs, ^{141}Ce, and ^{239}Np) fractionated from ^{95}Zr. The nuclides ^{99}Mo, ^{144}Ce, and ^{239}Pu did not fractionate appreciably from ^{95}Zr. For the Sedan shot the slope of the ^{137}Cs plot is near 1.0, but, for the remaining fractionating nuclides, the slopes lie within a narrow intermediate range. For the Johnie Boy and Small Boy shots, for which the results are quite similar, these slopes show much wider variation. The results of the correlation have been compared with those from similar correlations for a coral-surface burst and some air bursts. Aside from the fact that ^{99}Mo fractionated from ^{95}Zr in the air bursts and that ^{239}Np did not fractionate from ^{95}Zr in the coral-surface burst, the results indicate that differences in the fractionation behavior of the nuclides are of degree rather than of kind. Correlation of radiochemical results with particle size indicates increasing degree of fractionation with increasing particle size.

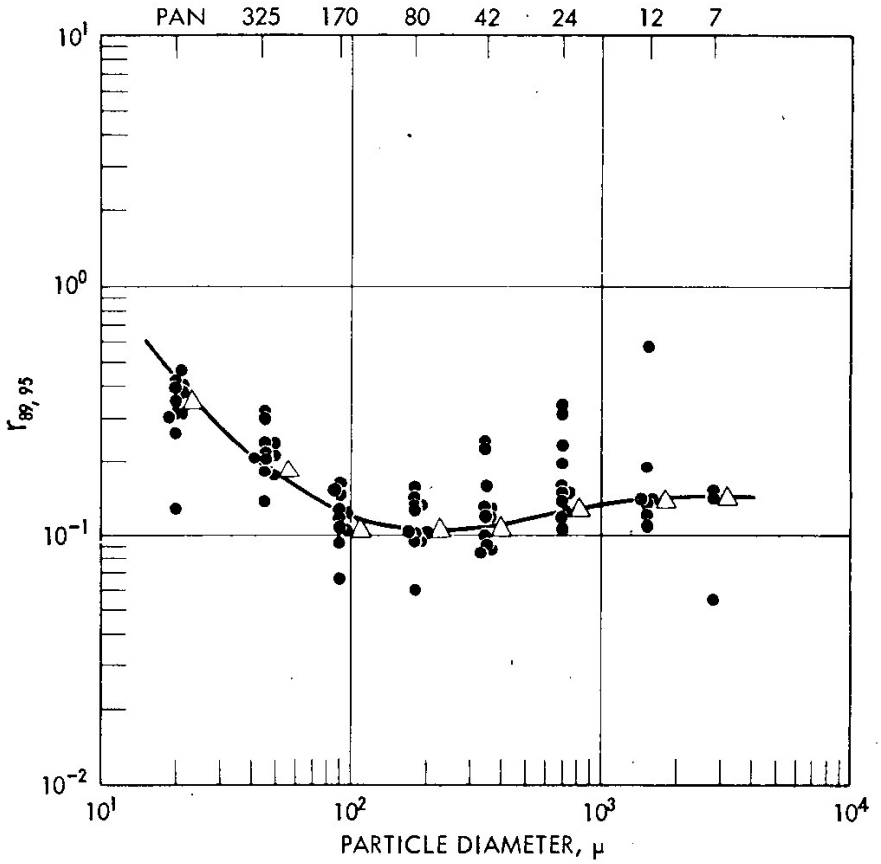

Fig. 5—Effect of particle size on fractionation ratio.

SUMMARY

Correlations indicate that the fractionation behavior of ^{89}Sr, ^{90}Sr, ^{91}Y, ^{137}Cs, ^{140}Ba, and ^{144}Ce relative to ^{95}Zr in silicate-surface bursts does not differ essentially from that observed in a coral-surface burst or in air bursts. Differences are noted for ^{99}Mo and ^{239}Np. For ^{103}Ru, ^{106}Ru, ^{131}I, ^{132}Te, ^{136}Cs, ^{141}Ce, and ^{239}Pu, some differences in degree of fractionation are indicated, and further study of these nuclides is recommended.

ACKNOWLEDGMENTS

In addition to the U. S. Atomic Energy Commission, the Defense Atomic Support Agency contributed generously to the support of this study. Some of the data were obtained from U. S. Air Force sources.

REFERENCES

1. D. E. Clark, F. K. Kawahara, and W. C. Cobbin, Fallout Sampling and Analysis: Radiation Dose Rate and Dose History at 16 Locations, Report POR-

2289, U. S. Naval Radiological Defense Laboratory, Oct. 24, 1963. (Classified)
2. E. C. Freiling, L. R. Bunney, and F. K. Kawahara, Physicochemical and Radiochemical Analysis, Report POR-2216, U. S. Naval Radiological Defense Laboratory, Oct. 28, 1964. (Classified)
3. W. B. Lane, Some Radiochemical and Physical Measurements of Debris from an Underground Explosion, USAEC Report PNE-229F, Jan. 7, 1964.
4. E. C. Freiling, Radionuclide Fractionation in Bomb Debris, *Science, 133* (3469): 1991–1998 (1961).

PHYSICAL CHARACTERISTICS OF SINGLE PARTICLES FROM HIGH-YIELD AIR BURSTS

P. BENSON, C. E. GLEIT, and L. LEVENTHAL
Tracerlab, A Division of Laboratory for Electronics, Inc.,
Richmond, California

ABSTRACT

Particles, isolated from high-altitude nuclear explosions, were separated and their physical parameters determined. The particles varied in color from colorless to black. They were generally spherical, and some had satellites that were a result of collisions of small particles with larger particles before complete solidification had occurred. Particles with diameters greater than 2 μ were isolated.

The beta radioactivity of the particles was measured at 25 days and was found to be related to the diameter expressed in the following way: $A = aD^b$, where b showed values of 3.06 ± 0.08, 3.22 ± 0.16, and 3.01 ± 0.30 for the three shots studied. Since the standard deviations were due to variations in activities of the particles and not in experimental errors, it was concluded that the activity was directly proportional to the particle volume. The standard deviations were found to be unrelated to particle size and color, but the value of a was found to be a function of the weapon yield. The value of b, however, was not related to weapon yield.

Individual particles were allowed to decay to determine the decay rate of the fission-product mixtures. On the average, the particles followed the relation $A = kt^{-1.10}$. Values of the decay slopes varied from 0.7 to 1.4. The distributions of the decay slopes of the individual particles from the average was found to be Gaussian. The deviations were not a function of particle size or color; they are explained as being a result of the widely different radionuclide content of the particles.

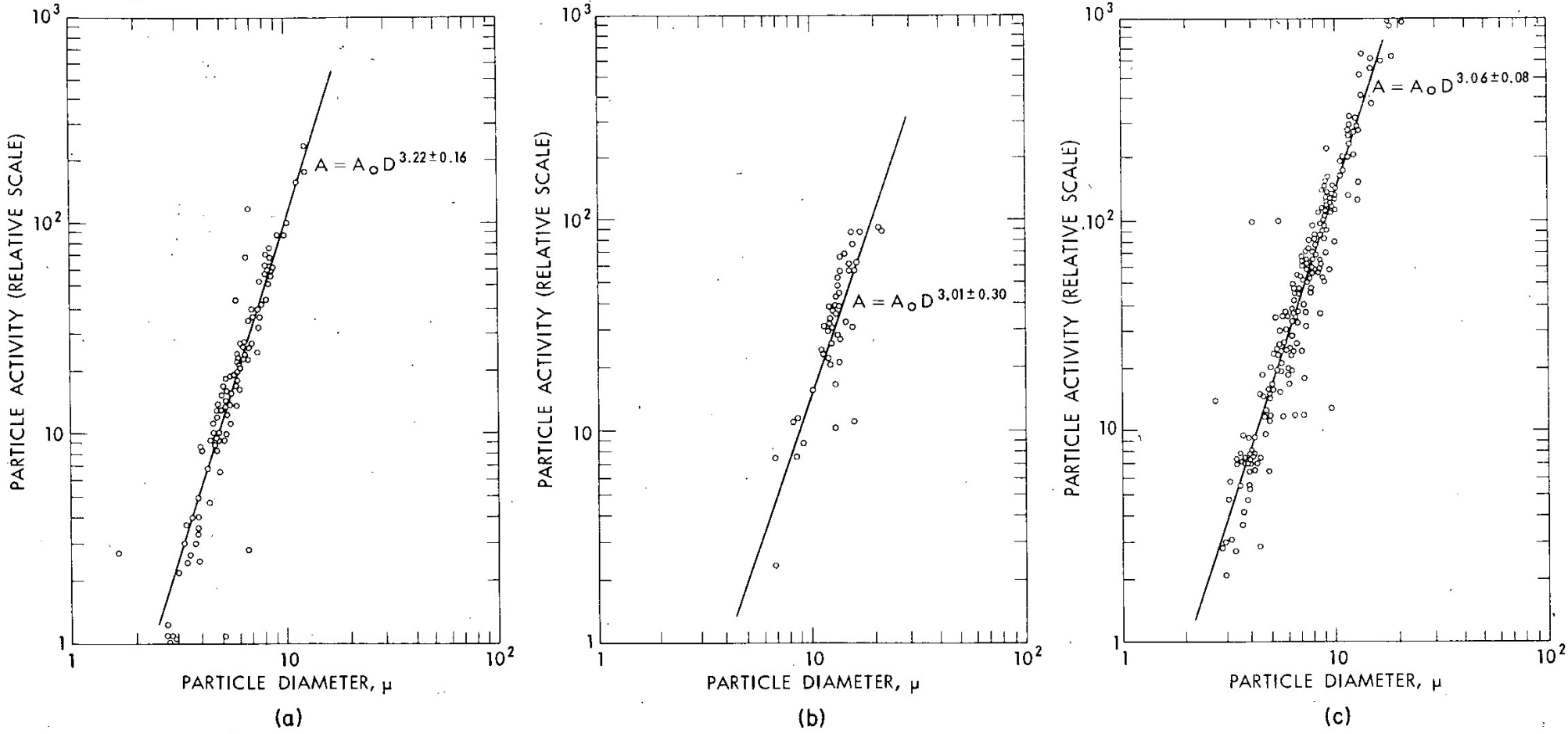

Fig. 2—Total beta activity as a function of particle diameter.

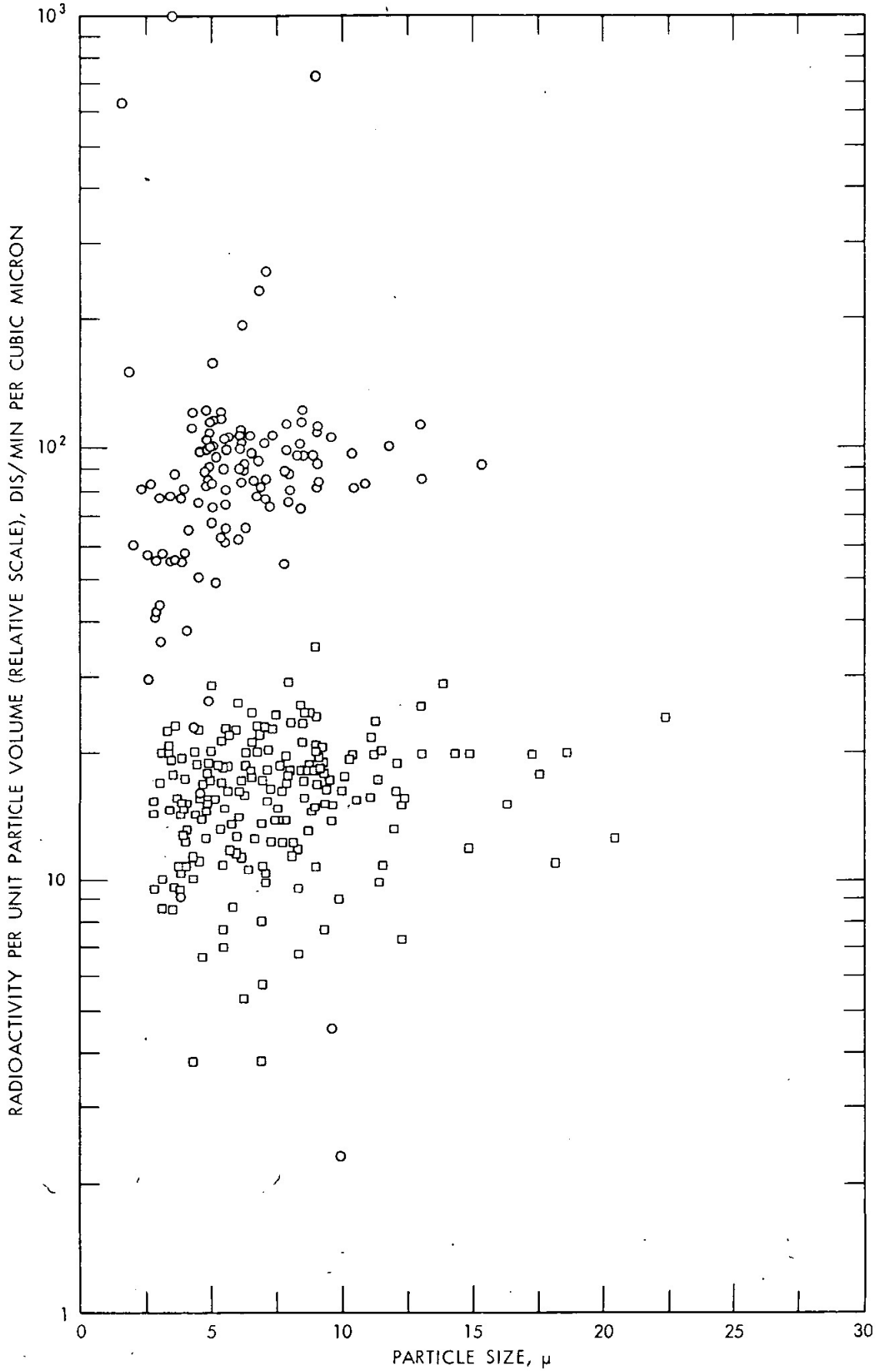

Fig. 3—Radioactivity per unit particle volume for two shots as a function of particle size.

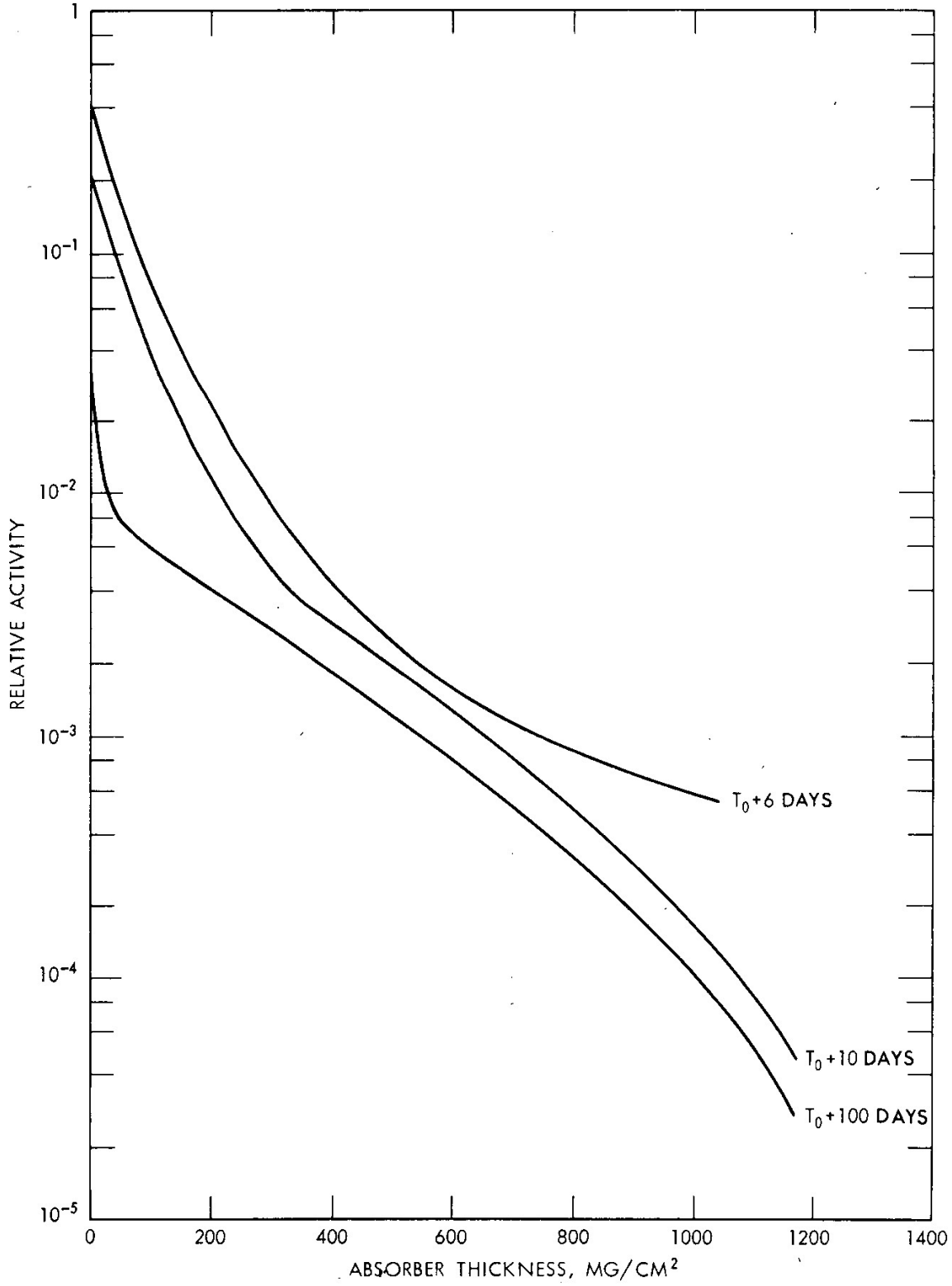

Fig. 4—Aluminum absorption measurements as a function of time.

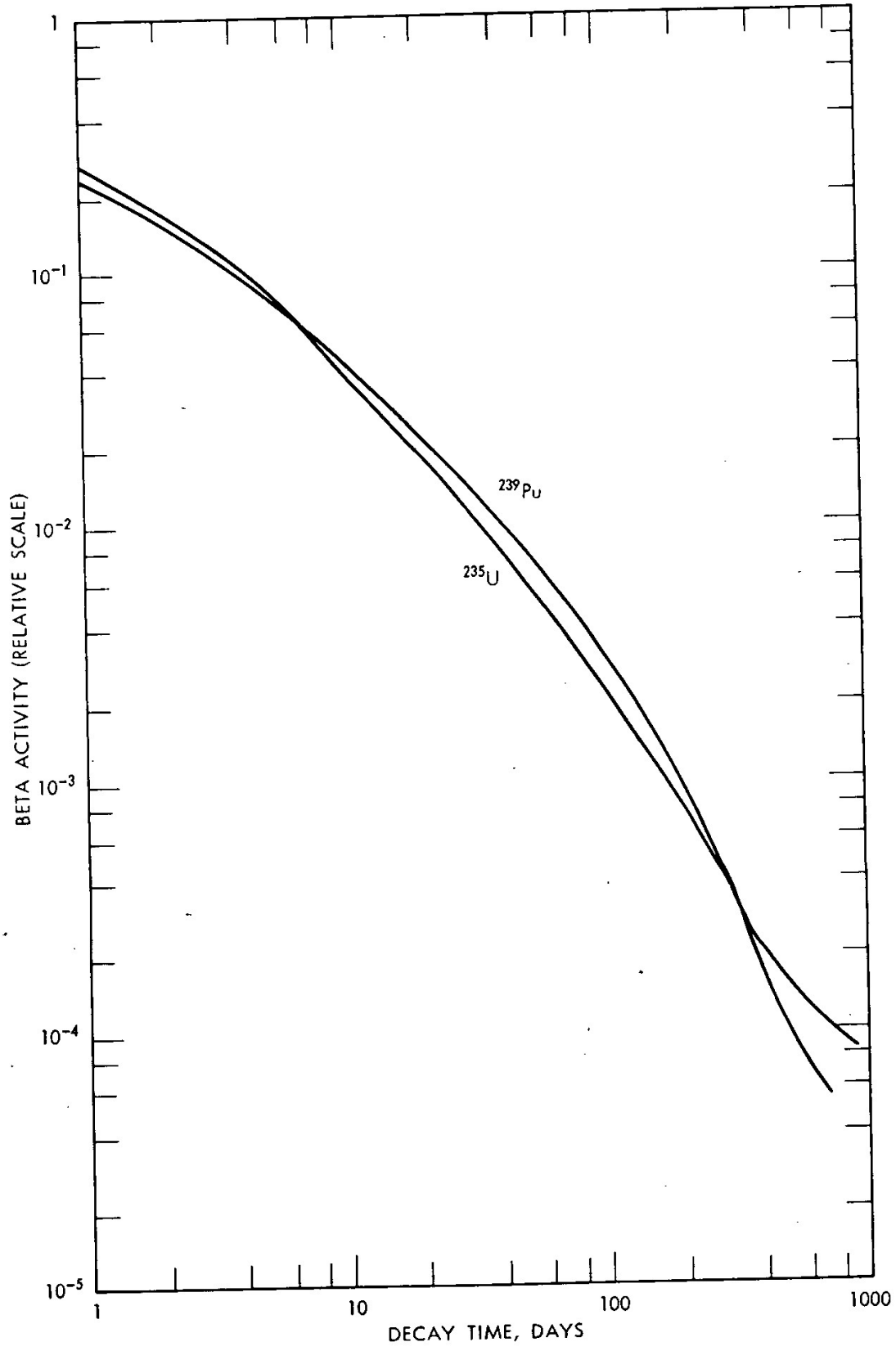

Fig. 5—Beta-activity decay of unfractionated ^{235}U and ^{239}Pu fission-product mixtures.

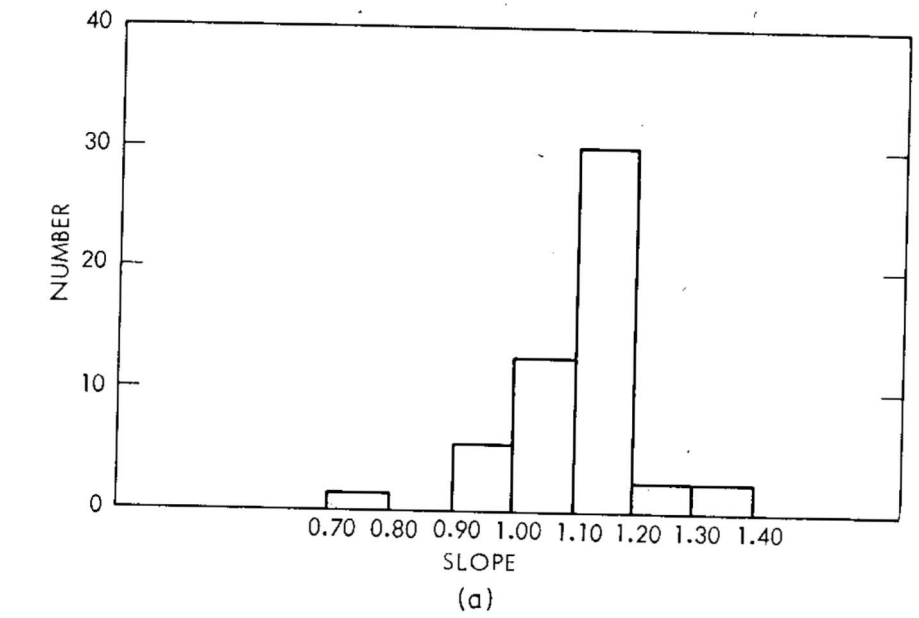

(a)

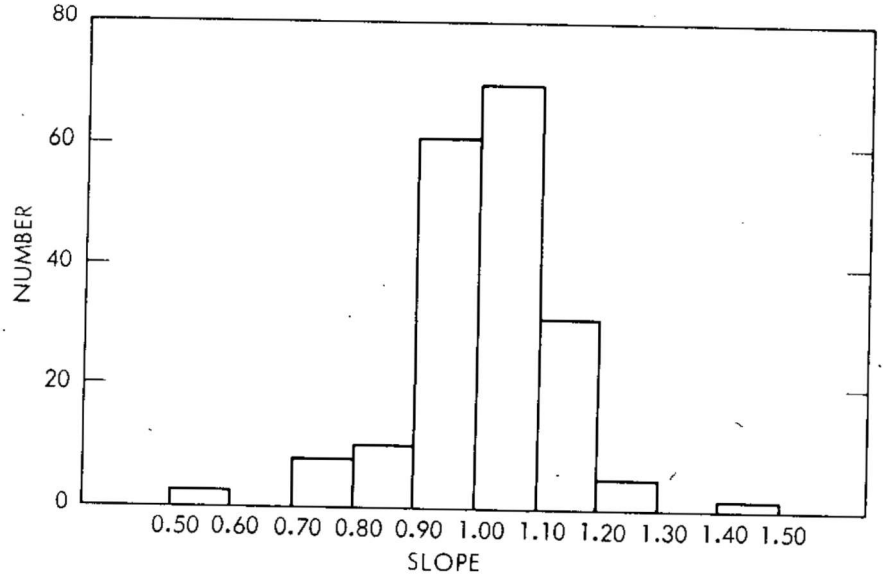

(b)

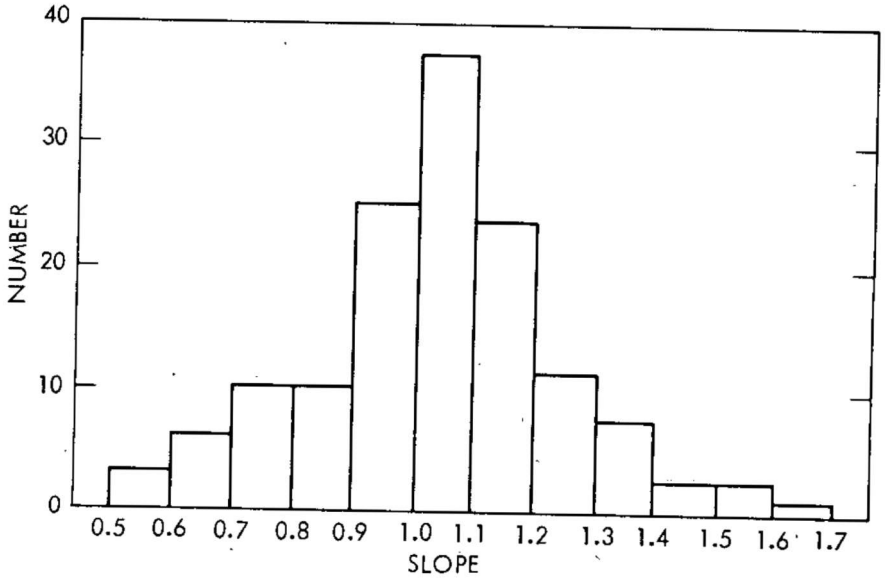

(c)

Fig. 6—The number of particles observed with various decay slopes.

RADIOCHEMICAL FRACTIONATION CHARACTERISTICS OF SINGLE PARTICLES FROM HIGH-YIELD AIR BURSTS

P. BENSON, C. E. GLEIT, and L. LEVENTHAL
Tracerlab, A Division of Laboratory for Electronics, Inc.,
Richmond, California

ABSTRACT

The radiochemical fractionation characteristics from two Operation Dominic high-yield air bursts were studied. Particles measuring from 2.5 to 20.0 μ were isolated from filter-paper matrices by autoradiographic registration and confirmed by optical microscopy. After physical measurements radiochemical and/or gamma-spectroscopy studies were performed on individual and aggregates of particles. Of particular interest was the distribution of volatile and refractory nuclides for each particle size. The nuclides radiochemically analyzed were ^{99}Mo, ^{89}Sr, ^{90}Sr, ^{95}Zr, ^{129m}Te, ^{132}Te, ^{137}Cs, ^{140}Ba, ^{141}Ce, ^{144}Ce, ^{147}Nd, ^{237}U, and ^{239}Np. Gamma-spectra analysis was used to determine the ^{95}Zr and ^{140}Ba concentrations in 334 particles. A computer technique for resolving these nuclides and ^{99}Mo, ^{103}Ru, ^{131}I, ^{132}Te, ^{137}Cs, ^{141}Ce, ^{144}Ce, ^{147}Nd, and ^{239}Np was developed.

The particles were found to be extremely fractionated. A logarithmic fractionation correlation plot for ^{140}Ba was determined which compared within the limits of error with data plotted by Freiling for high-yield water bursts. The logarithms of ^{95}Zr and ^{140}Ba activities were plotted as functions of the particle diameters for the two shots. The slopes for the regression plot for ^{95}Zr were 3.41 ± 0.18 and 3.09 ± 0.37. These values imply a cubic relation. The slopes for the regression plot for ^{140}Ba were 2.63 ± 0.24 and 2.32 ± 0.50, somewhat between a square and a cubic relation. These results point toward condensation of the refractory nuclides initially with subsequent precipitation of the volatiles on the particles at later times.

PREDICTION OF FALLOUT FROM SUBSURFACE NUCLEAR DETONATIONS

JOSEPH B. KNOX
University of California, Lawrence Radiation Laboratory,
Livermore, California

ABSTRACT

A numerical simulation model has been developed for the prediction of fallout from subsurface nuclear detonations that produce craters through spall and the action of the cavity gas. The physical processes modeled are atmospheric transport, lateral eddy diffusion, and gravitational sedimentation of radioactive particulates. This cratering fallout model is normalized to the observed external gamma-dose-rate fields of the Sedan (100 kt) and the Danny Boy (0.43 kt) cratering shots conducted at the Nevada Test Site. Calculations of the fallout patterns for additional shots, used for testing the prediction capability of the cratering fallout model, indicate that the model gives estimates of the external gamma dose rate at H + 1 hr with a maximum error of a factor of 2 to 3 in the gamma dose rate vs. distance along the hot line of the pattern.

INTRODUCTION

During the past few years, a small but continuing effort has been expended in developing a model for predicting fallout from subsurface nuclear detonations. In this report the experience in predicting fallout from surface bursts that is transferable to the construction of a fallout model for subsurface detonation is summarized, the development of the fallout model for subsurface nuclear detonations (the cratering fallout model) is described, the predictive capability of the model is illustrated by means of independent test cases, and some of the problems asso-

ciated with the prediction of fallout from row-charge subsurface nuclear detonations are discussed. This paper is limited to research or development in which the investigator has been personally involved within the Plowshare Program of the Lawrence Radiation Laboratory.

CRATERING FALLOUT MODEL

Basis of Model Construction

For prediction of the area affected by radioactive fallout from a subsurface detonation of a nuclear explosive and of the gross external gamma dose rate in the surface-fallout pattern, knowledge of the following factors are needed:

1. The heights of the base, the top, and the radius of each radioactive cloud (i.e., the main cloud and the base surge) formed by the detonation at the time the clouds cease to rise in the atmosphere. This time is defined as the time of cloud stabilization. The cloud heights are prescribed in terms of height above surface zero.

2. The total yield of the explosive, W_T; the fission yield of the explosive, W_f; the depth of burial of the explosive, z; the fraction of the fission-product gamma emitters expected to appear in the fallout pattern beyond the estimated radius of direct ejecta, F_c; and the equivalent fission-yield gamma needed to simulate the gamma dose from induced activities.

3. The activity–particle size distribution in both the main cloud and the base surge and the fraction of F_c in each.

4. The terminal fall velocity of the fallout particles (in still air) as a function of particle size and height in the atmosphere.

5. The time and space prediction of the horizontal wind at the level of each cloud top along with the specification of the wind-shear tangential and normal to the wind for the layer through which particles fall. This knowledge is required because in a fallout calculation involving two clouds (main cloud and base surge), the calculation of the fallout pattern for each cloud is done separately. The total surface-fallout pattern of the shot is found by summing the patterns from the base surge and the main cloud.

6. The effect of horizontal eddy diffusion on the growth of the horizontal radius of the disks of radioactive particles as the disks fall earthward. The initial debris cloud is subdivided into disks of debris in the model as a function of initial height in the cloud and of particle size.

The preceding information (items 1 through 6) provides the simplest, but still adequate, basis for constructing a cratering fallout model. In addition to this information, it is assumed that the fission-

product radioactivity is unfractionated and that 1 kt of unfractionated fission products spread uniformly over 1 sq mile corresponds to an (H + 1)-hr dose rate of 3380 r/hr at a height of 3 ft above an infinite plane.[1] This normalization constant of 3380 r/hr is corrected for terrain shielding by a factor of 0.8.

Certain atmospheric processes or effects have been neglected in developing the cratering fallout model, just as these same effects were neglected in developing the land surface-burst fallout model:[2]

1. The effect of synoptic-scale vertical motions on the vertical displacement of the falling disk of particles.
2. The effect of the mean divergence of the horizontal wind on the radius of the disk of falling particles during descent.
3. The effect of vertical eddy diffusion.
4. The time from detonation to cloud stabilization.
5. The development of subsynoptic-scale wind systems.
6. Changes in time and space of the shear tangential and normal to the horizontal wind at cloud-top level.
7. The effect of water products of condensation on the size and fall rate of radioactive particles.

Fraction of Gamma Activity in the Close-in Pattern

For calculation of the close-in fallout pattern from a subsurface detonation, the fraction of the gamma activity produced by the fission yield and appearing in the close-in fallout pattern, F_c, must be known. Thus far, experimental data from the Sedan, the Teapot ESS, the Jangle U, the Neptune, the Jangle S, and other surface-burst shots have provided a basis for estimating F_c. The measured fallout patterns from these shots have been integrated[3] from the radius of direct throwout to the limit of the measured pattern. The results are shown in Table 1.

These F_c calculations were performed by assuming a normalization constant of 3380 r/hr per kiloton of fission yield per square mile at H + 1 hr and a terrain shielding factor of 0.8. The graphical presentation of F_c as a function of z/W is shown in Fig. 1. In construction of the experimental F_c curve, the following asymptotes were used: (1) an

Table 1 — EXPERIMENTAL DATA

Shot	W, kt	z, ft	F_c	Medium
Sedan	100	635	~0.10	Alluvium
Teapot ESS	1.2	67	0.46	Alluvium
Jangle U	1.2	17	0.64	Alluvium
Neptune	0.115	100	0.005	Tuff
Jangle S	1.2	0	0.50	Alluvium
Danny Boy	0.43	109	0.04	Basalt
Blanca	19	835	0.0005	Tuff

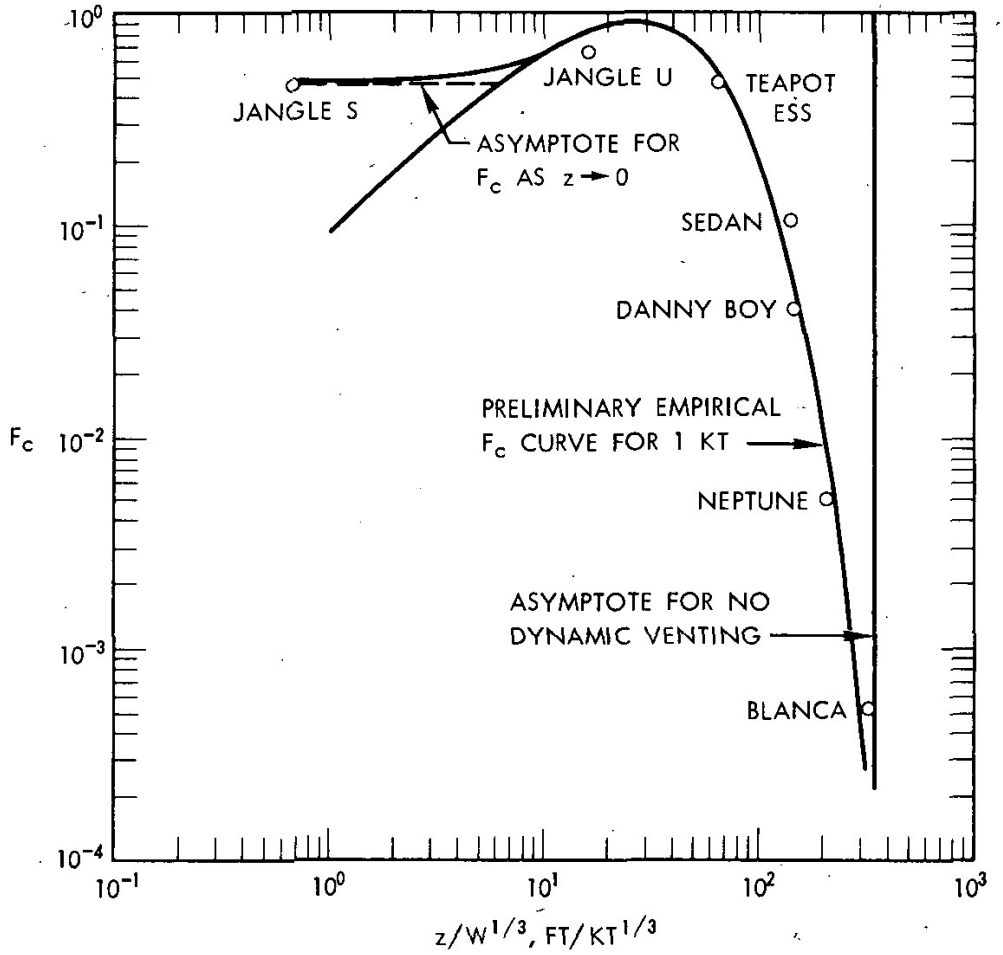

Fig. 1—Fraction of gamma activity appearing in the close-in fallout pattern.

asymptote of $F_c = 0.50$ for $z = 0$, suggested by the Jangle S data in Table 1 and supported by previous work,[4] and (2) an asymptote of no dynamic venting for $z/W^{1/3} = 330$ ft/kt$^{1/3}$, supported by experimental evidence[5] and by studies of containment physics.[6]

It should be noted that the value of F_c (estimated by pattern integration) for the Sedan shot departs considerably from the curve fitted to the whole sample of F_c data. This departure could arise because of an F_c yield dependency that is inadequately known at this time. In the absence of knowledge of such a dependency, F_c estimates made from the curve in Fig. 1 for high-yield cratering events (of the order of 100 kt and above) should be considered as uncertain by a factor of 2. It should be further stated that F_c estimates derived from Fig. 1 are made with the tacit assumption that the nuclear explosive is fully tamped and that no additives for fission-product gamma-radiation suppression have been placed around the explosive.

It should also be mentioned that the maximum value of F_c (0.75 at $z/W^{1/3} \approx 30$) occurs at very nearly the same value of $z/W^{1/3}$ as the maximum base-surge radius (crosswind) in a neutral atmosphere, reported

in Ref. 7. The author believes that this coincidence of maximums at $z/W^{1/3} \approx 30$ is physically consistent.

Cloud Geometries

The geometrical definition of the top, the base, and the radius of both the main cloud and the base surge at the time of cloud stabilization is shown in Fig. 2. In addition to the definitions given in Fig. 2, the

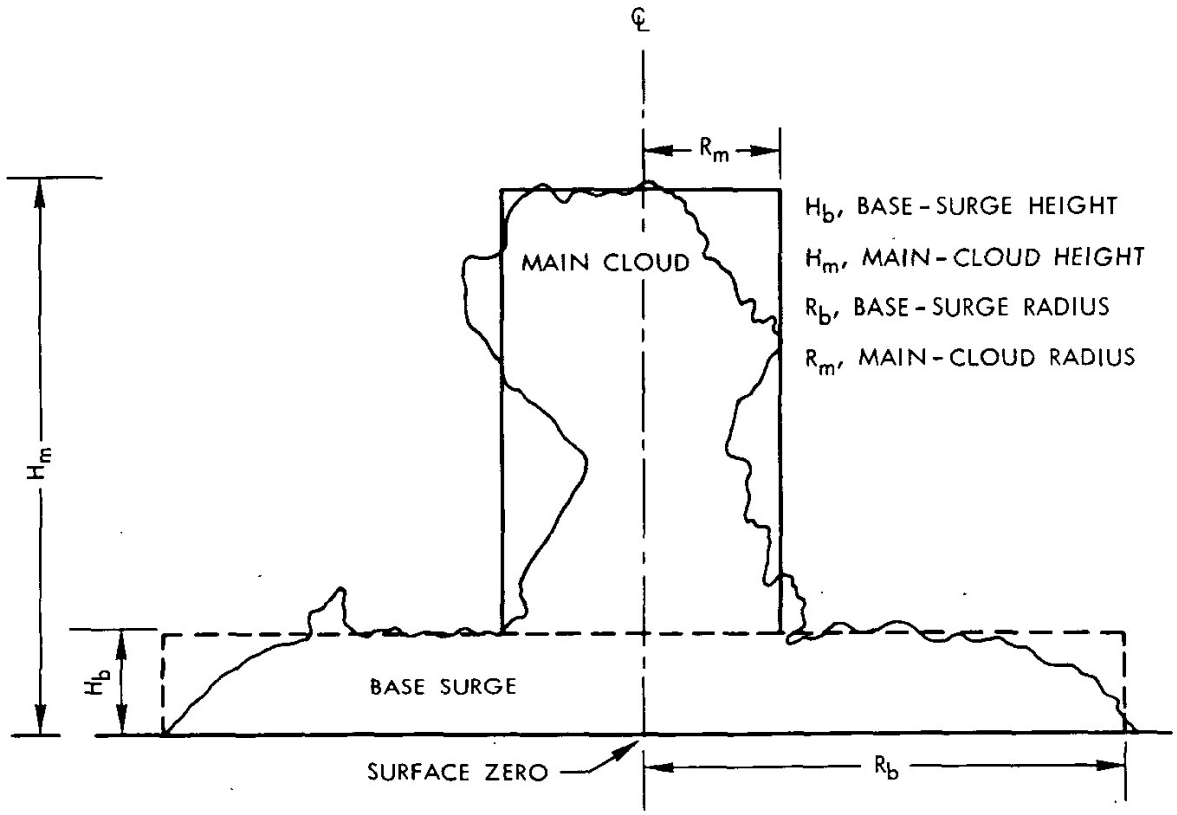

Fig. 2—Definition of cloud dimensions and symbols.

height of the base of the main cloud is defined as being equal to the height of the base-surge top, H_b, in the model.

Evidence suggests that the geometry of these two clouds at the time of stabilization is a function of the total explosive yield, the material in which the detonation occurs, the depth of burial of the explosive, and the meteorological conditions existing during the development of the clouds.[7] At present, the cloud-geometry parameters (R_b, H_b, R_m, and H_m) must be evaluated experimentally as functions of total yield and depth of burial. Reasonable samples of experimental data exist for alluvium and basalt materials. Examples from one of the most useful summaries of cloud-geometry data for alluvium[8] are shown in Figs. 3b to 3g. (Figure 3a is a computational aid to the acquisition of input to Figs. 3b to 3g. In these figures, z denotes depth of burial and D_a denotes the depth of apparent crater.) This summary utilizes all the known

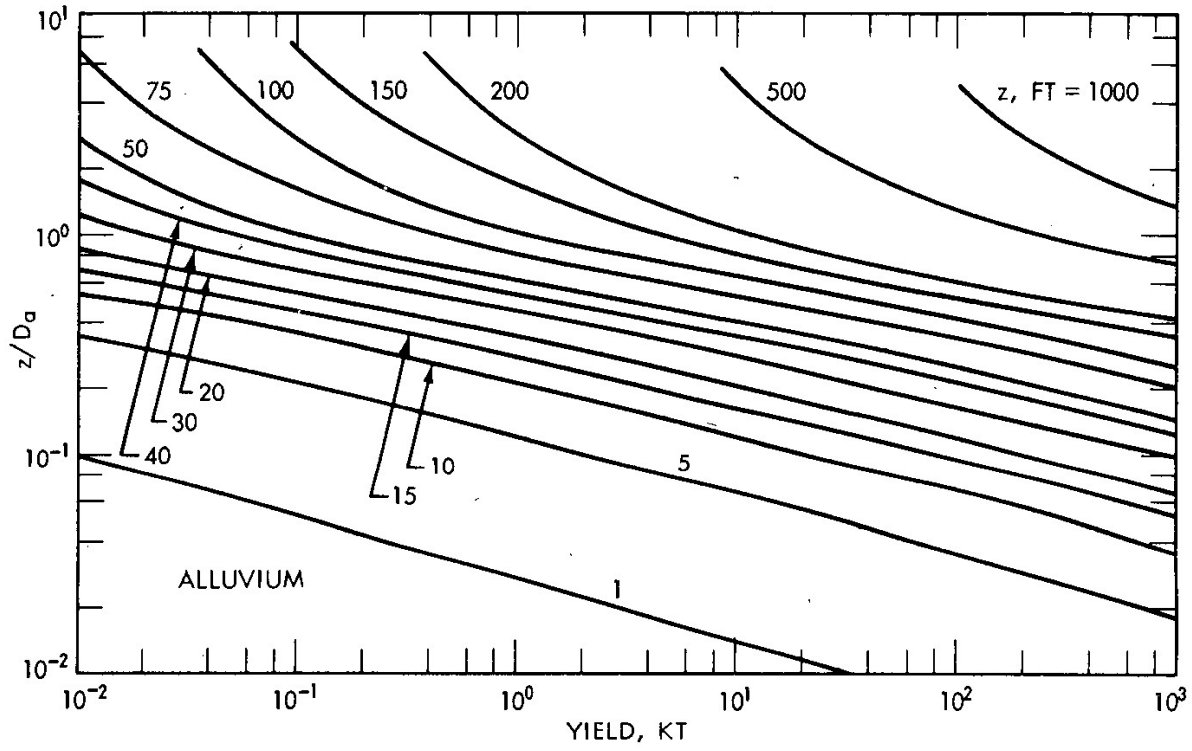

Fig. 3a—Computational aid to the acquisition of input data to the cloud-dimension graphs of Figs. 3b to 3g.

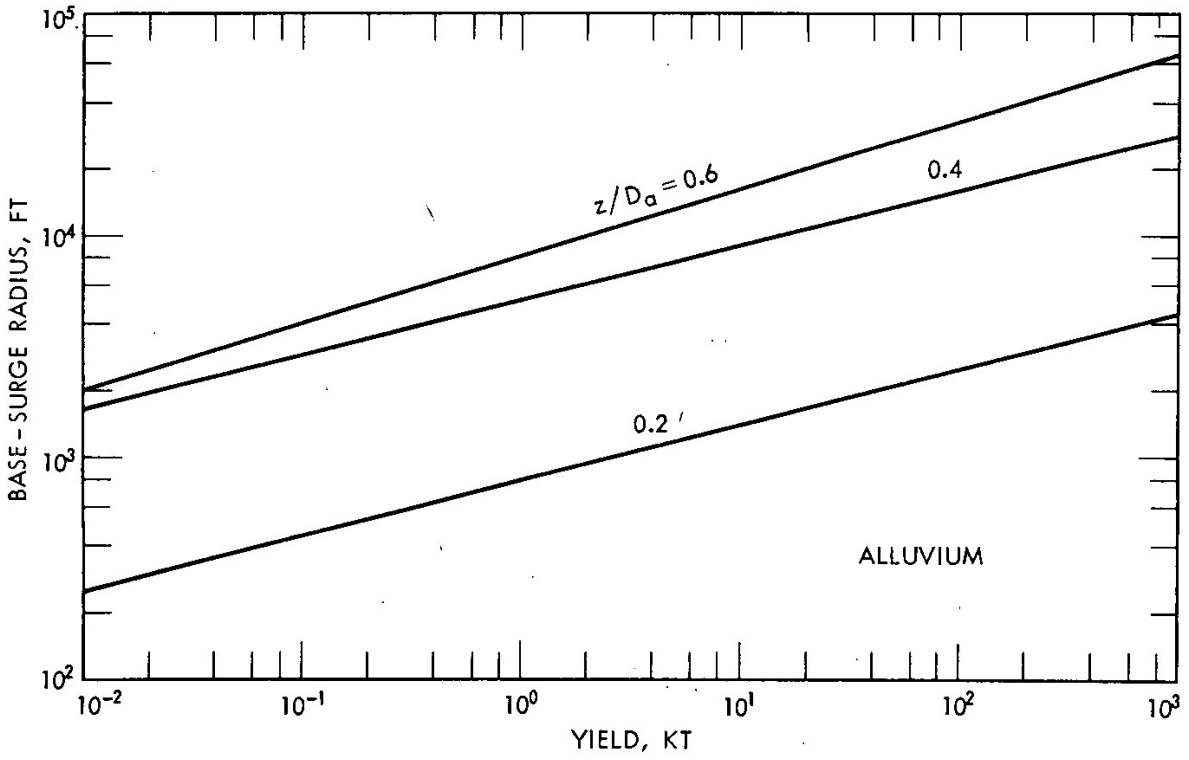

Fig. 3b—Base-surge radius as a function of the total yield and the parameter z/D_a.

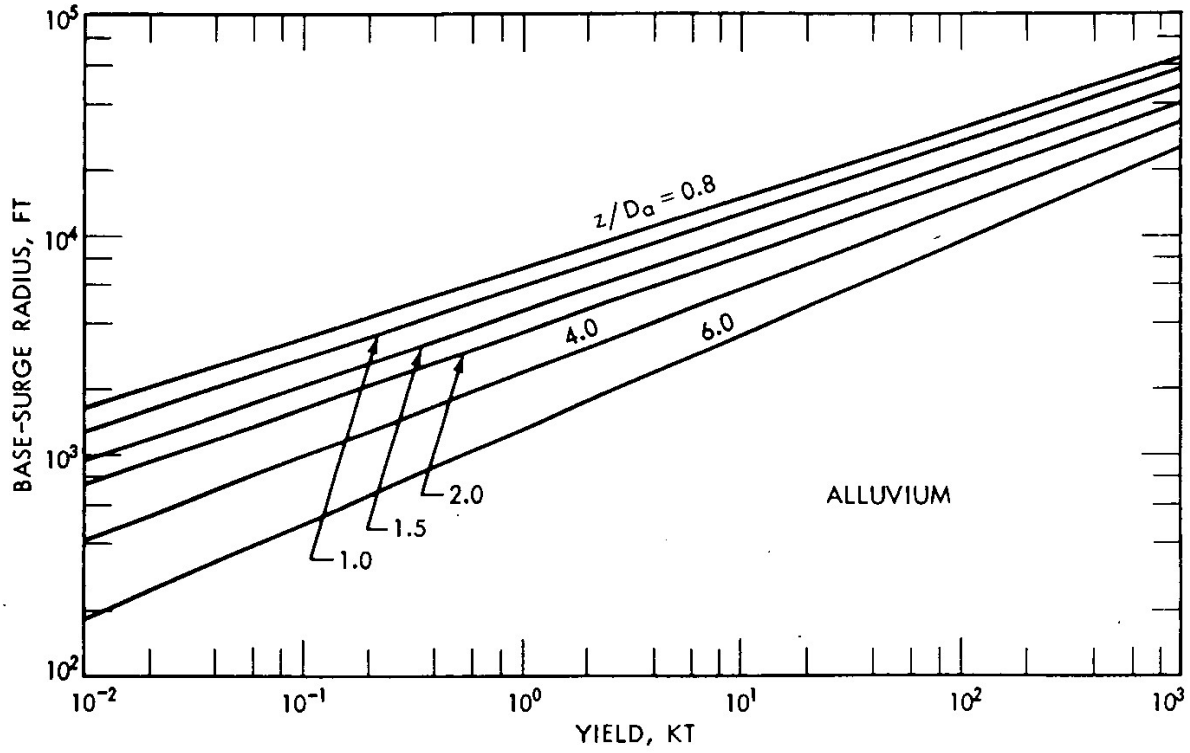

Fig. 3c —Base-surge radius as a function of the total yield and the parameter z/D_a.

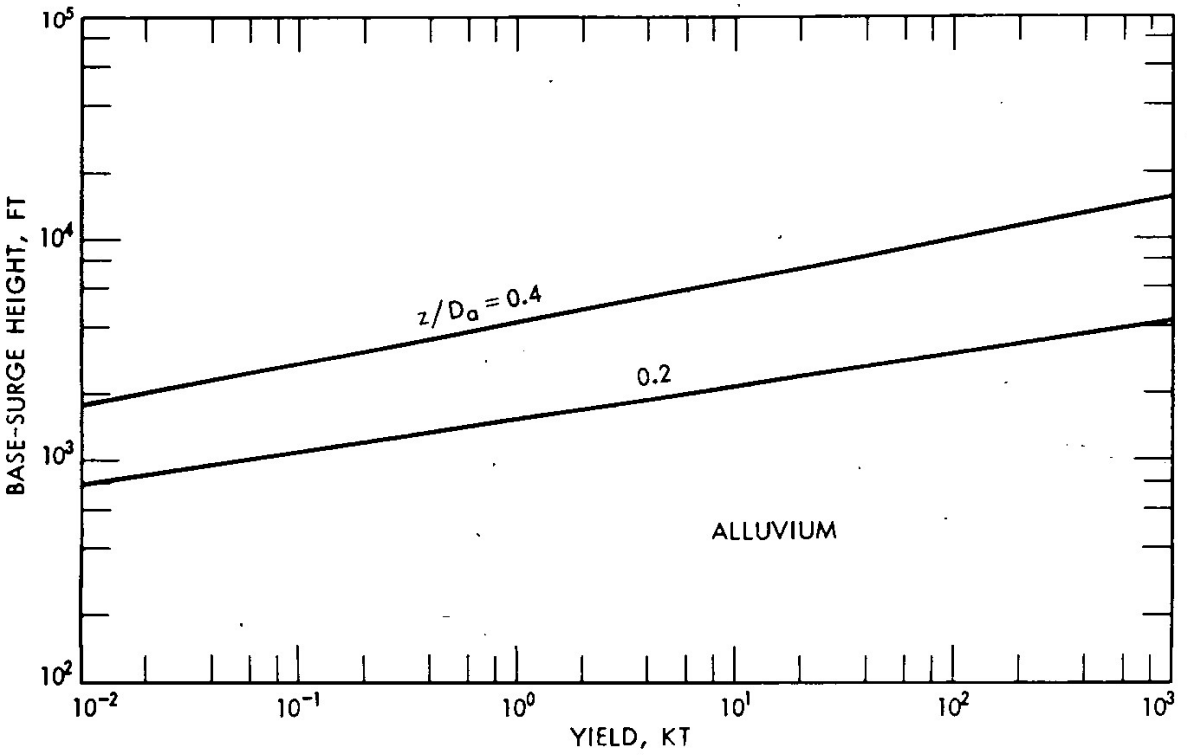

Fig. 3d —Base-surge height as a function of the total yield and the parameter z/D_a.

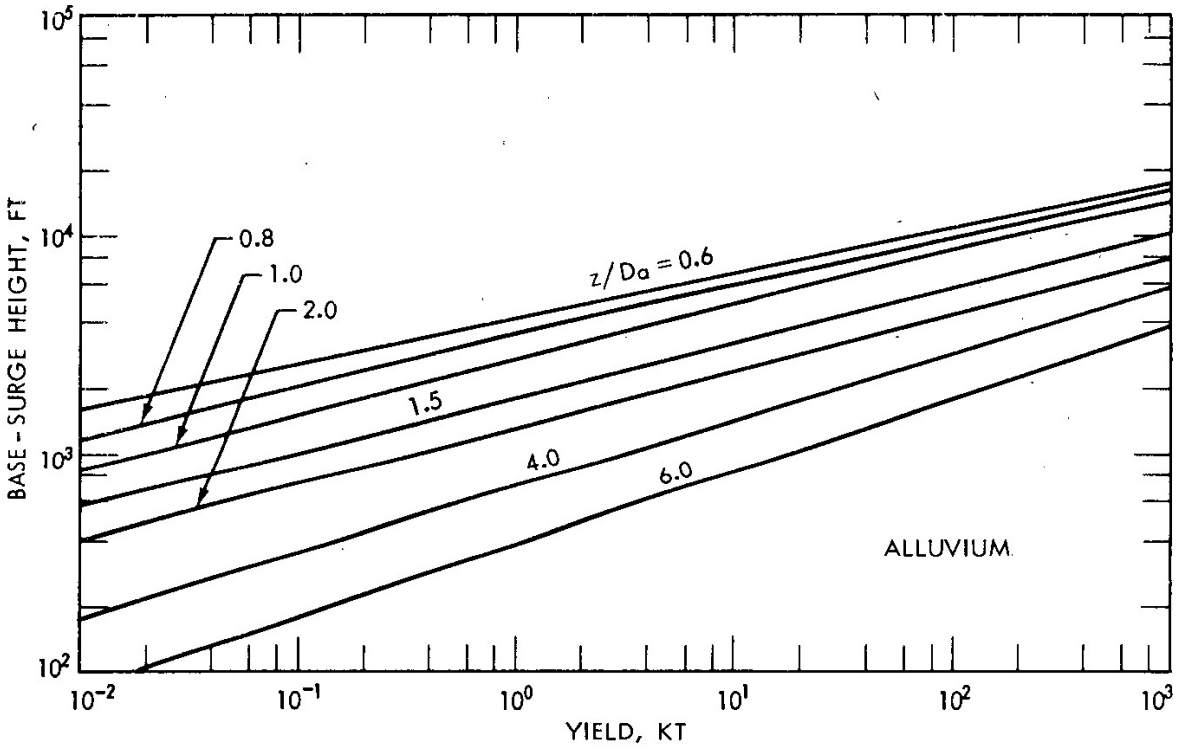

Fig. 3e—Base-surge height as a function of the total yield and the parameter z/D_a.

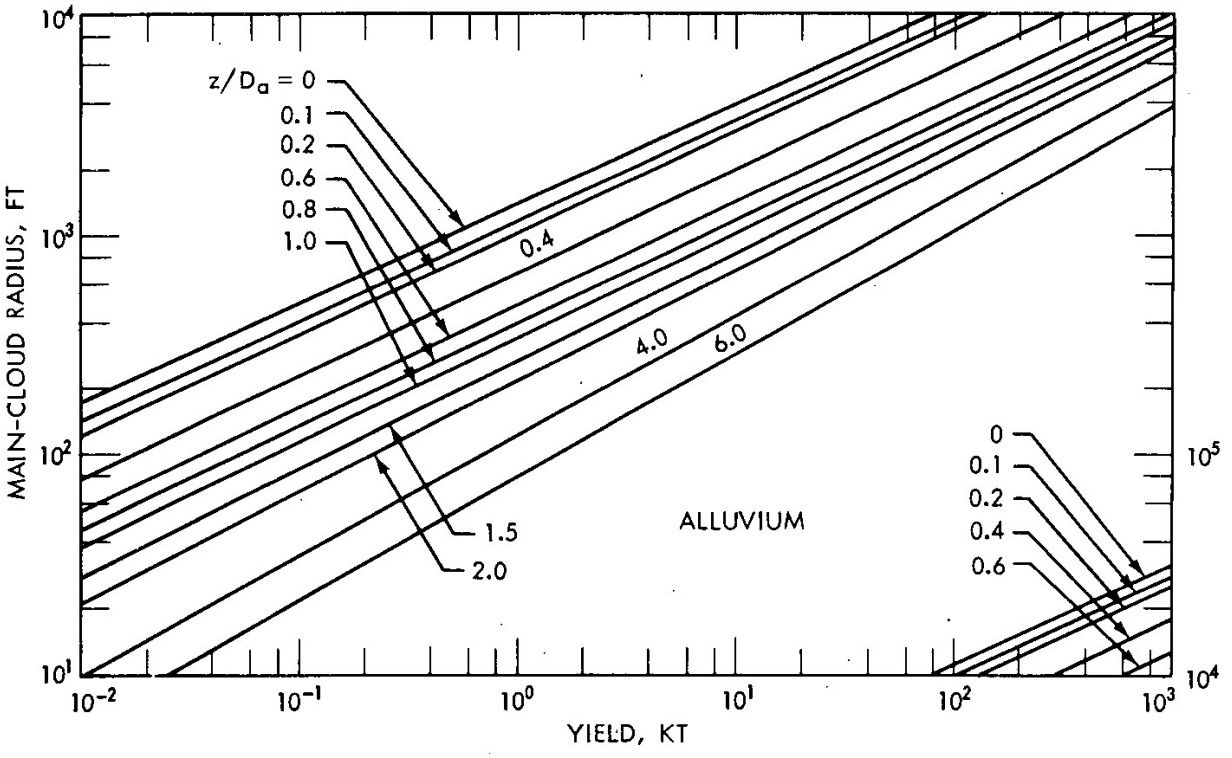

Fig. 3f—Main-cloud radius as a function of the total yield and the parameter z/D_a.

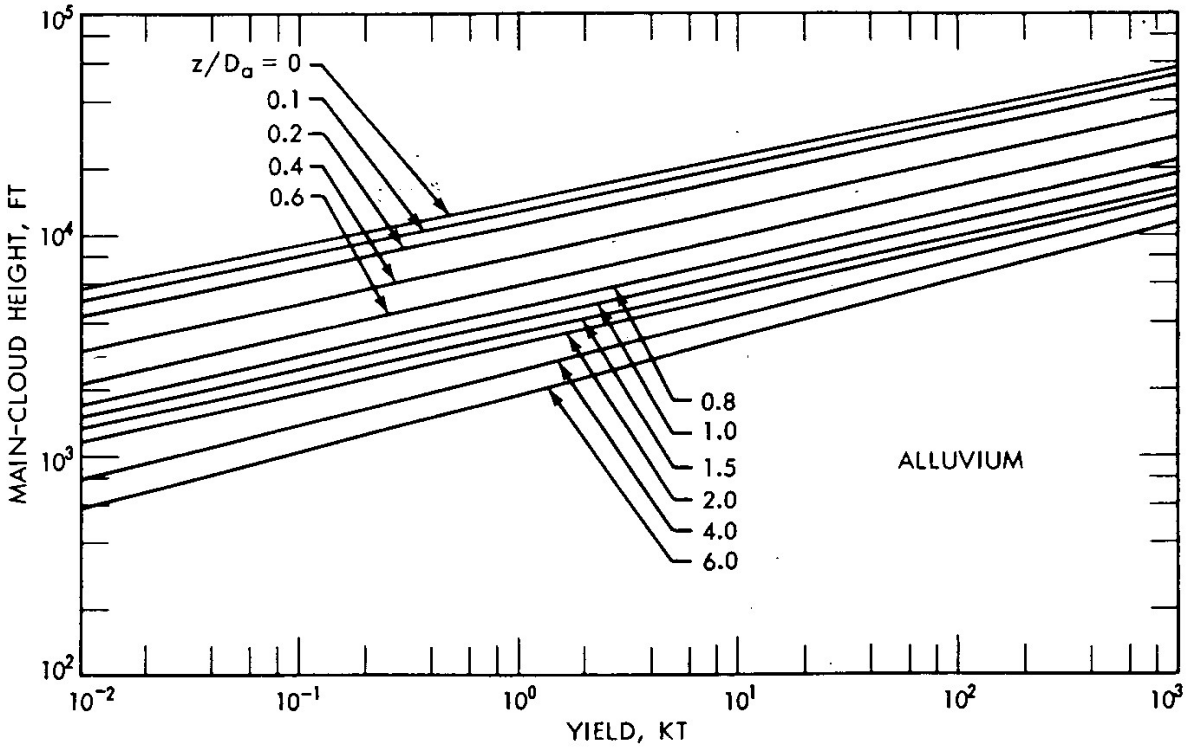

Fig. 3g—Main-cloud height as a function of the total yield and the parameter z/Da.

cloud-geometry data from high-explosive and nuclear-explosive detonations conducted by the U. S. Atomic Energy Commission in alluvium and basalt. Implicit in the summary is the assumption that a high explosive and a nuclear explosive detonated in the same material at identical depths of burial and under similar meteorological conditions produce the same cloud geometries.

Activity–Particle Size Distributions

In a typical subsurface nuclear detonation in alluvium, two clouds are formed. The main cloud is composed mostly of vented cavity gas and particulates (originating from either condensation or injection and entrainment of soil). The base surge is composed of ejecta and suspended fine particulates. For a nuclear cratering shot in alluvium, it is assumed that 80% of the F_c gamma activity is in the main cloud and 20% is in the base surge. The 0.8 F_c main-cloud activity is assumed to be subdivided between two lognormal activity–particle size distributions. The first activity–particle size distribution contains the activity $0.8\ w_m(1)F_c$ and is characterized by the mean $\ln \bar{r}_m(1)$ and the standard deviation $\sigma_m(1)$. The second activity–particle size distribution contains the activity $0.2\ w_m(2)F_c$ and is characterized by the mean $\ln \bar{r}_m(2)$ and the standard deviation $\sigma_m(2)$. The activity of the first distribution is assumed to be homogeneously mixed through the whole main cloud, whereas that of the second distribution is assumed to be homoge-

neously mixed only in the lower fifth of the cloud. A similar prescription of activity–particle size is used for the base surge. Figure 4 summarizes the parameters governing the activity–particle size distributions in the two clouds at the time of cloud stabilization. These parameters governing the activity–particle size distributions in the

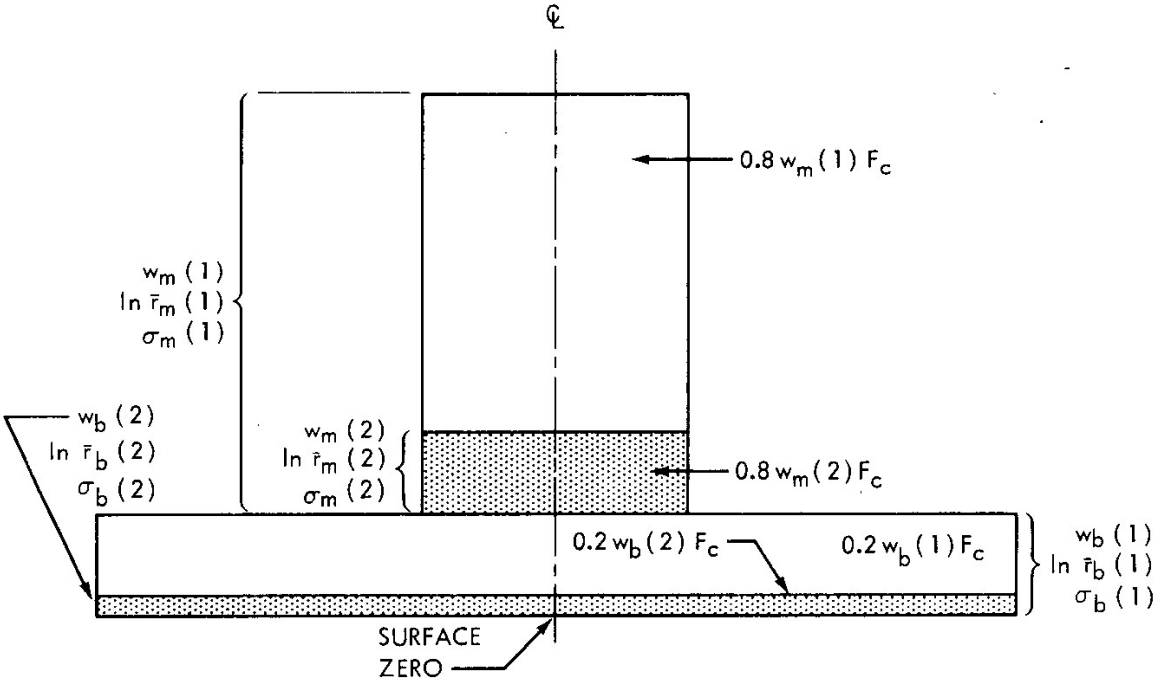

Fig. 4—Schematic drawing of an idealized cloud from a subsurface detonation showing spatial relations of the activity–particle size distribution assumed in the model.

cratering fallout model have been determined by mathematical experimentation with the model in the re-creation of the observed fallout patterns for the Sedan and the Danny Boy shots. Results of these calibration calculations will be discussed in a later section.

Terminal Fall Velocity of Fallout Particles

The vertical fall velocities of the fallout particles are modeled as the terminal fall velocities of smooth spheres of density 2.5 g/cm^3 in an International Civil Aeronautical Organization standard atmosphere as computed by McDonald[9] for both the Stokes'-law region and the aerodynamic region (wherein the Reynolds number exceeds 1). If some fallout particles are a cluster of small spheres attached to a large central particle, these complex particles are assumed to fall with the speed of the equivalent smooth spherical particle of the same mass. Experimental evidence has been obtained by Rapp and Sartor[10] to support this assumption.

Specification of the Horizontal Wind Field for the Model

The horizontal wind field that transports the debris-disk centroids during their fall to the earth's surface may be specified in two ways in the cratering fallout model:

1. Idealized Wind Hodograph. If H denotes height above surface zero, then the horizontal wind, $\underset{\sim}{v}_h$, at height H for a simple wind hodograph (see Fig. 5) is

$$\underset{\sim}{v}_h(H) = \underset{\sim}{v}_h(H_m)\frac{A(p)}{A(p_m)} - S(H_m - H)\underset{\sim}{n}$$

where $\underset{\sim}{v}_h(H_m)$ = steady-state wind at cloud-top level H_m (or it can be specified as a function of time and space in either wind component form or by means of a stream function)

$A(p)$ = wind-shear component tangential to the horizontal wind at cloud-top level and is evaluated from shot-time winds in a diagnostic fallout calculation or from preshot wind information for a predictive fallout calculation (it is held constant in time for the period of fallout deposition)

$A(p_m)$ = value of $A(p)$ at cloud-top level (normally it is set equal to 1)

S = wind-shear component normal to the horizontal wind at cloud-top level (it is evaluated from shot-time winds or preshot wind information, depending on the purpose of the fallout calculation, and is held constant in time)

$\underset{\sim}{n}$ = unit vector normal to $\underset{\sim}{v}_h(H_m)$ in a right-handed system

p = atmospheric pressure corresponding to H

2. Arbitrary Hodograph. The horizontal wind can be specified in wind-component form for as fine a vertical interval as desired or for which wind information exists.

Debris-disk Radius as a Function of Time

For estimation of the radius of a debris disk expanding by horizontal eddy diffusion during its fall to earth, it is proposed that the disk radius as a function of time $R_e(t)$ be represented by

$$R_e(t) = (R_{e,0} + 2Dt')^{1/2}$$

where t' is the distance traveled by the disk centroid divided by the mean horizontal wind speed in the layer through which the disk has settled, $R_{e,0}$ is the debris-disk radius at time of stabilization, and D is the horizontal eddy-diffusion coefficient.[2] The diffusion coefficient D is estimated as the Richardson's diffusion coefficient $0.2 \times l^{4/3}$, where

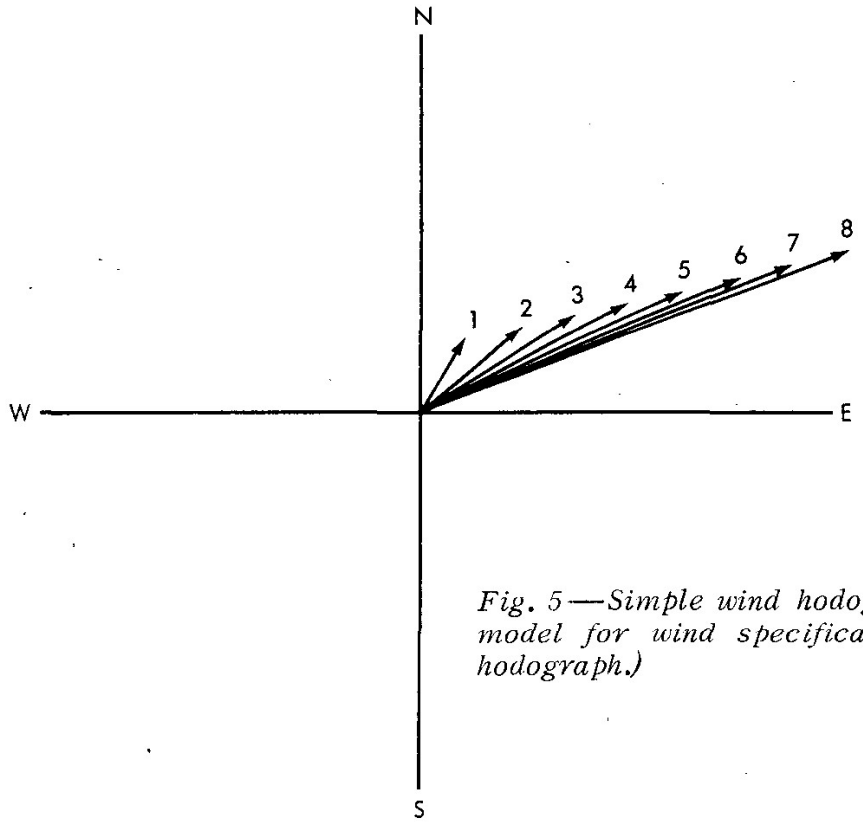

Fig. 5—Simple wind hodograph assumed in the model for wind specification. (Idealized wind hodograph.)

ℓ is the standard deviation of the position of the particles (in the disk) from the disk centroid. Since ℓ is poorly known in nuclear-debris clouds, it is usually set equal to $R_{e,0}$ or $2R_{e,0}$ if accelerated relative diffusion is to be approximated in the fallout model.

Physical Processes Simulated in the Model

The principal physical or meteorological processes simulated by the cratering fallout model are (1) the transport of the debris disks by the mean wind in the layer through which the disks are falling, (2) the relative advection of the debris disks by the horizontal wind field containing both a speed and a directional shear, and (3) the lateral eddy diffusion, which expands the disks falling earthward.

The first two processes are simulated by calculating the transport of the disk centroids by the ambient horizontal wind field during the disk's earthward fall until the disk centroid is on the ground surface by using either the idealized wind hodograph or the arbitrary hodograph for the horizontal wind specification. The result of this calculation is the position vector from surface zero to the predicted ground position of each disk centroid and the time of arrival at the ground surface of each disk. The lateral eddy-diffusion process is modeled by the expression for $R_e(t)$ which estimates the debris-disk radius at the time of arrival of the disk centroid on the ground surface.

The debris disks tracked earthward are defined as follows: In each cloud (main cloud and base surge), 11 disks of particle size r_I are defined at each isobaric surface p_p such that

$$\ln r_I = \ln r_L - \frac{I}{10}(\ln r_L - \ln r_s)$$

where I is equal to 0, 1, 2, ..., 10; r_L is the radius of the largest particle modeled in the cloud; and r_s is the radius of the smallest particle modeled in the cloud. The term p_p is equal to $p_B - [P/10(p_B - p_m)]$, where P is equal to 0, 1, 2, ..., 10; p_B is the pressure at the base of the cloud at the time of cloud stabilization; and p_m is the pressure at the top of the cloud at the time of cloud stabilization.

The (H + 1)-hr external gamma dose rate (for a height 3 ft above an infinite plane) is calculated by using the method of Batten, Iglehart, and Rapp[11] modified to account for the effect of normal shear and lateral eddy-diffusive disk growth.

The following quantities are calculated in the model and are output in the indicated modes:*

	Printout	Cathode-ray-tube display
Position of surface zero		x
(H + 1)-hr dose rate at the predicted ground position of each disk centroid for each cloud	x	
Predicted ground position of each disk centroid for each cloud	x	x
Envelope containing the area affected by the fallout from each cloud		x
Time of beginning and end of fallout deposition at each ground-position centroid for each cloud	x	
Isopleths of the (H + 1)-hr dose rate for any specified interval of dose rate (each contributing cloud and total pattern)		x
(H + 1)-hr dose rate as a function of distance along the hot line (each cloud and total pattern)		x

DIAGNOSTIC CALCULATION FOR SEDAN

For calibration of the cratering fallout model on the Sedan shot, the observed shot-time winds, the observed cloud geometry of the main cloud and the base surge, the estimated $F_c = 10\%$, and the appropriate fission yield were input to the model. A first guess of the 12 activity–particle size parameters, to be discussed later, was also input to the

*About 0.25 min of IBM 7094 computer time is required for the calculations for a two-cloud nuclear-cratering fallout problem, and 2.4 min of Livermore Advanced Research Computer time is required for the cathode-ray-tube displays indicated above.

model. The main cloud was assumed to contain 80% of F_c; the base surge, 20%. The parameters governing the activity–particle size distributions have been determined from the observed Sedan gross gamma fallout pattern by mathematical experimentation. The values of these parameters are as follows:

$$w_m(1) = w_b(1) = 0.9$$

$$w_m(2) = w_b(2) = 0.1$$

$$\ln \bar{r}_m(1) = \ln \bar{r}_b(1) = 2.9$$

$$\ln \bar{r}_m(2) = \ln \bar{r}_b(2) = 5.0$$

$$\sigma_m(1) = \sigma_b(1) = 0.69$$

$$\sigma_m(2) = \sigma_b(2) = 0.59$$

Figure 6 shows the calculated and the observed gamma dose rate* at H + 1 hr from fission products vs. distance along the hot line for the Sedan shot.

DIAGNOSTIC CALCULATION FOR DANNY BOY

The Danny Boy shot was a 0.42-kt nuclear cratering detonation emplaced at a depth of 109 ft in dry basalt. The observed gamma fallout pattern for Danny Boy has been published.[4] By mathematical experimentation with the cratering fallout model, the activity–particle size distribution parameters can be adjusted to duplicate the observed Danny Boy fallout pattern. In this shot no visible main cloud was observed.[4] Thus, in the diagnostic calculation with the cratering fallout model, it is assumed that 100% of the F_c gamma activity is in the base surge and that there is a preliminary value of 0.05 for F_c. The activity–particle size distribution parameters determined in this calculation are given below:

$$w_b(1) = 0.9$$

$$w_b(2) = 0.1$$

$$\ln \bar{r}_b(1) = 3.0$$

$$\ln \bar{r}_b(2) = 5.7$$

$$\sigma_b(1) = 0.69$$

$$\sigma_b(2) = 0.59$$

*The observed (H + 1)-hr gamma dose rate for fission products derived from the observed total gamma dose rate at H + 24 hr, assuming that 52% of the (H + 24)-hr gamma dose rate was from tungsten.[12]

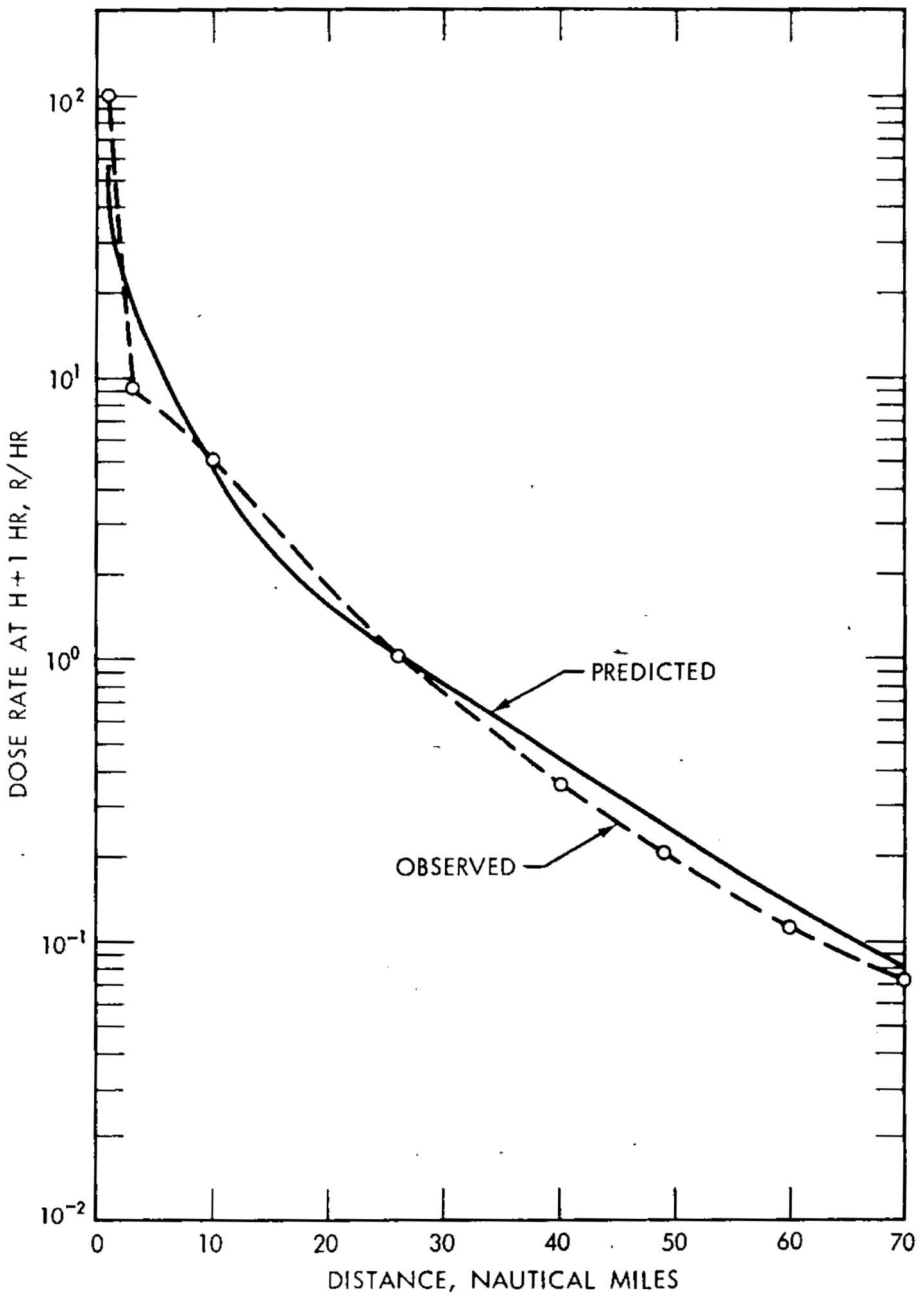

Fig. 6—The calculated and observed gamma dose rate at H + 1 hr as a function of distance along the hot line of the Sedan pattern (diagnostic calculation).

Figure 7 shows the calculated (H + 1)-hr dose rate vs. distance curve from the model, and the observed (H + 1)-hr dose rate vs. distance. As was previously mentioned, the value of F_c used in the cratering-fallout-model calculation was 0.05. If a value of 0.04 for F_c (as reported in Ref. 4) had been used, the agreement between the calculated (H + 1)-hr dose rate and the observed (H + 1)-hr dose rate vs. distance would have been better than shown in Fig. 7.

Recently effort has been expended to obtain machine capability of plotting the calculated (H + 1)-hr dose-rate patterns for an arbitrarily selected interval of dose rate. Figure 8 shows the machine-plotted dose-rate pattern for the Danny Boy diagnostic calculation. The computer-

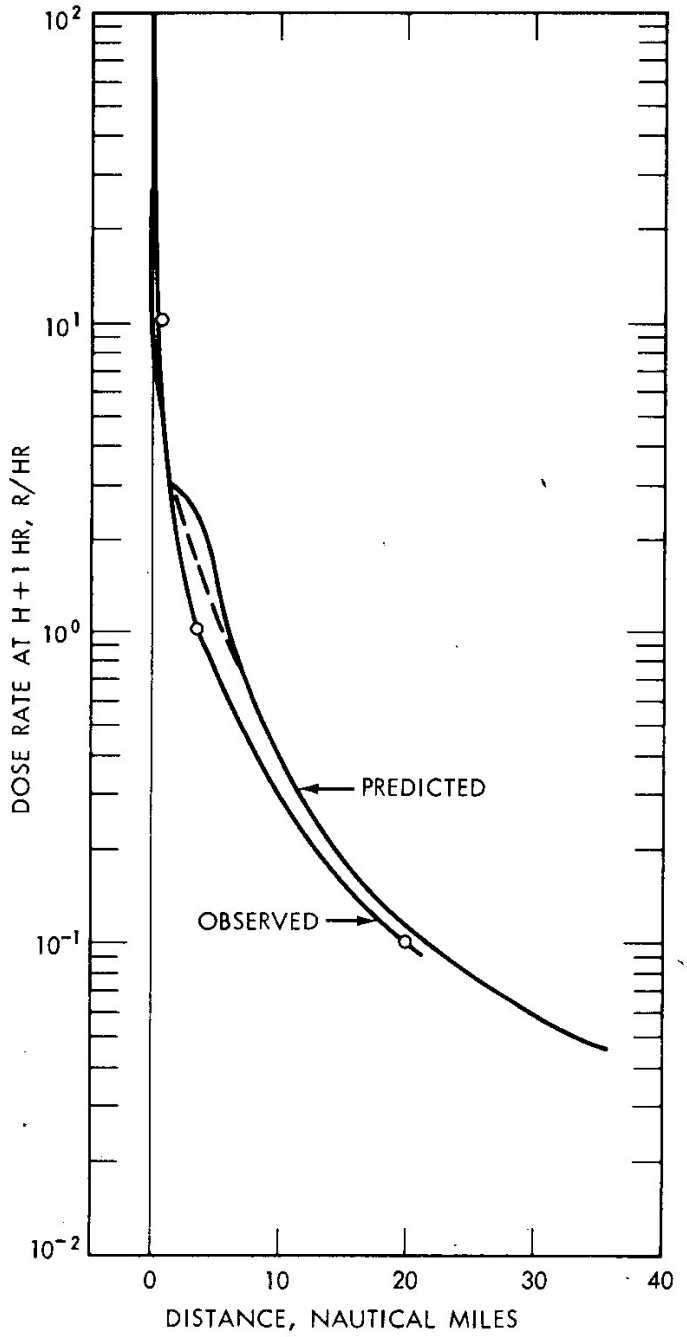

Fig. 7—The calculated and observed gamma dose rate at H + 1 hr as a function of distance along the hot line of the Danny Boy pattern (diagnostic calculation).

pattern breadth at 25 miles downwind is about 7 miles; the observed-pattern breadth at 25 miles downwind is 5.5 miles. It should be noted that the closure of the isodose-rate line of 10^{-4} r/hr at H + 1 hr in the plotted pattern is artificial and is the result of the logic used for the computer plotting rather than of the logic used for the cratering fallout model. All isodose-rate lines will apparently be closed at the downwind edge of the pattern if computed dose-rate information is insufficient for their appropriate extension downwind. The observed (H + 1)-hr gamma-dose-rate pattern for Danny Boy is shown in Fig. 9 for comparison with the computer-plotted pattern.

INDEPENDENT TESTS OF THE MODEL

An independent test calculation of the cratering fallout model (calibrated on Sedan) was performed by using data from the Teapot ESS

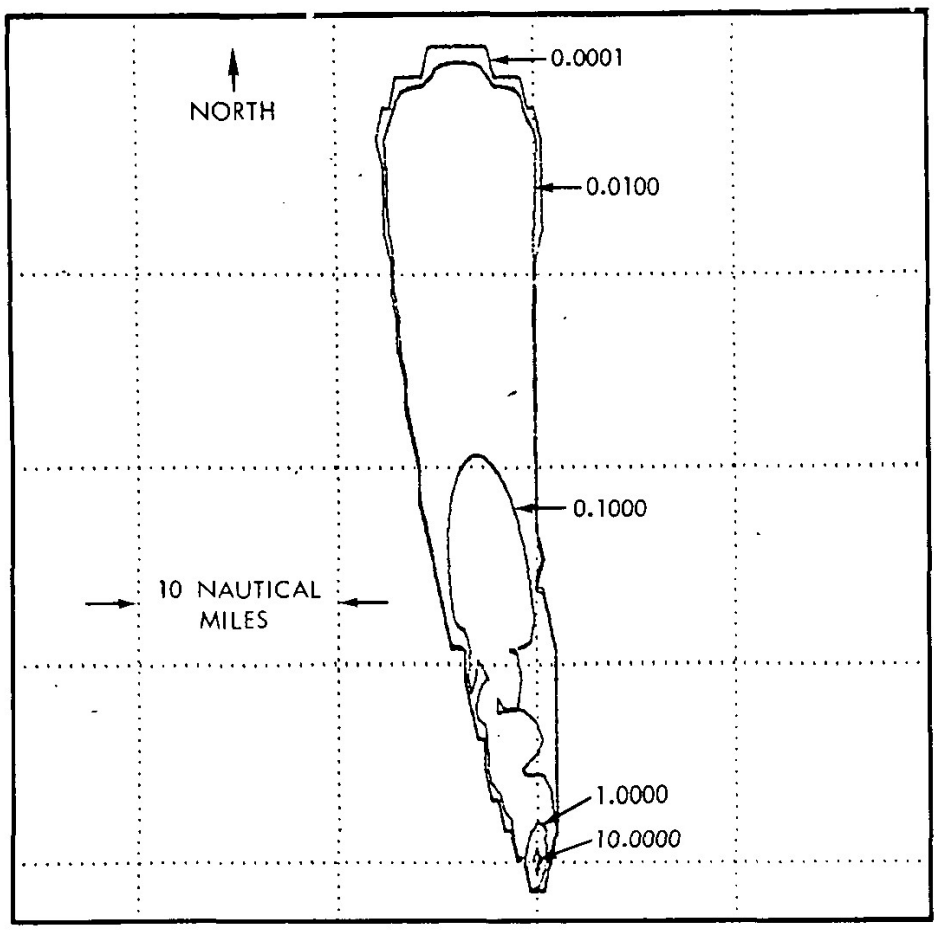

Fig. 8—The machine-plotted (H + 1)-hr gamma-dose-rate pattern for the Danny Boy shot (diagnostic calculation), roentgens per hour.

shot. The observed winds at shot time, the observed cloud geometry, the published fission yield of 1.2 kt, and a value of 0.85 (an early preliminary value) for F_c were input to the model. Figure 10 shows the calculated and the observed (H + 1)-hr gamma dose rate as a function of distance along the hot line of the pattern. A comparison of these two dose rate vs. distance curves shows that the largest error between calculation and observation is of the order of a factor of 2.5. An examination of the radiosonde observation near shot time at the Nevada Test Site indicates that the vertical temperature distribution of the layer through which the particles were falling was slightly superadiabatic. Under such conditions, it is possible that the vertical eddy diffusion on the day of the Teapot ESS shot was larger than average. If enhanced vertical eddy diffusion were operative, the dose rate would have been slightly less near ground zero and would have been enhanced downwind.

Other model confirmation tests have been performed. These include calculations with the surface-burst version of the model on the Apple II and the Zucchini shots[2] and on several other atmospheric shots for which the data are still classified. The results of these additional tests were satisfactory.

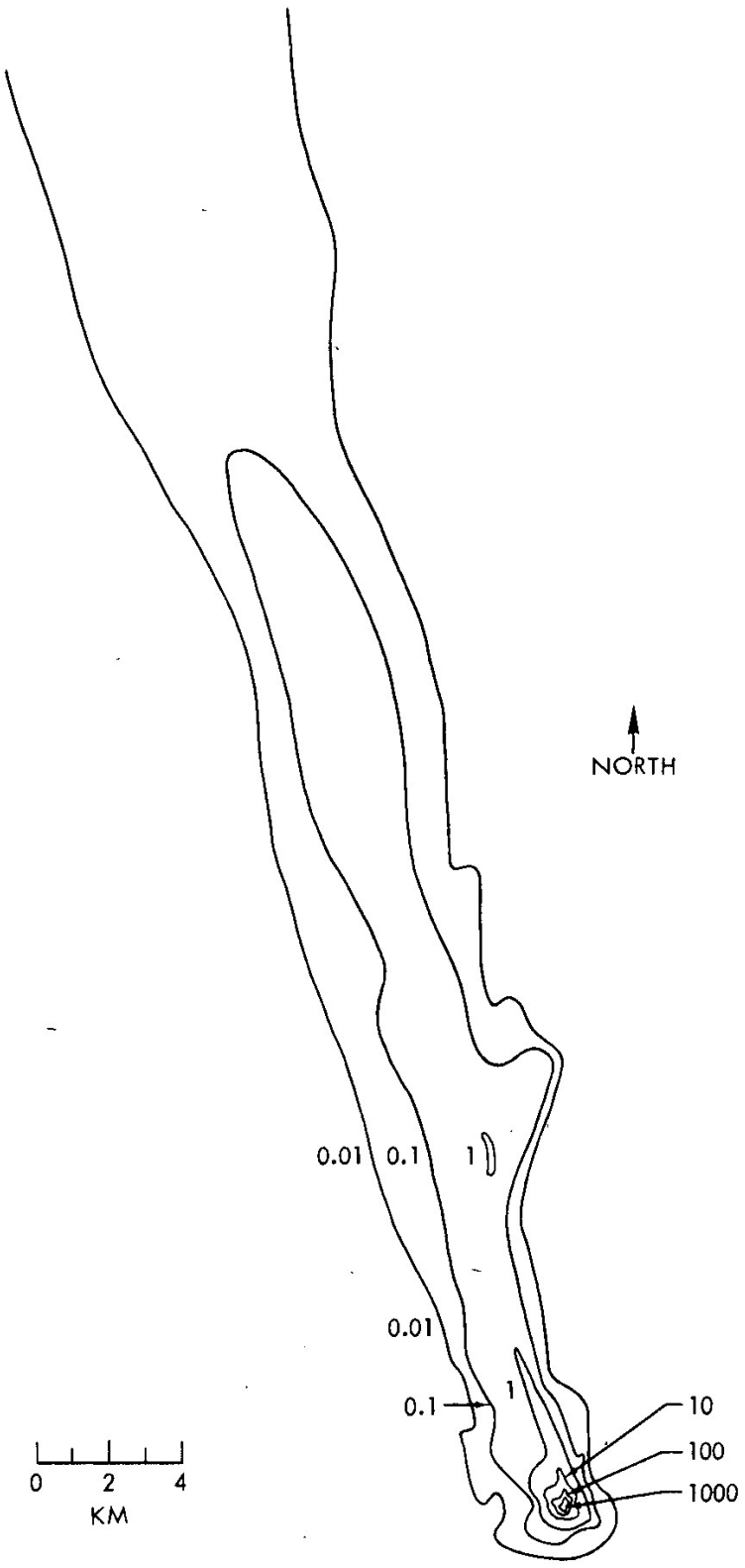

Fig. 9—Preliminary gamma-isodose-rate contours observed at H + 1 hr.[4] Readings in roentgens per hour minus H + 1 hr. Data taken from Nuclear Defense Laboratory ground surveys (close in); Edgerton, Germeshausen & Grier, Inc., aerial surveys (intermediate range); and U.S. Geological Survey aerial survey (long range).

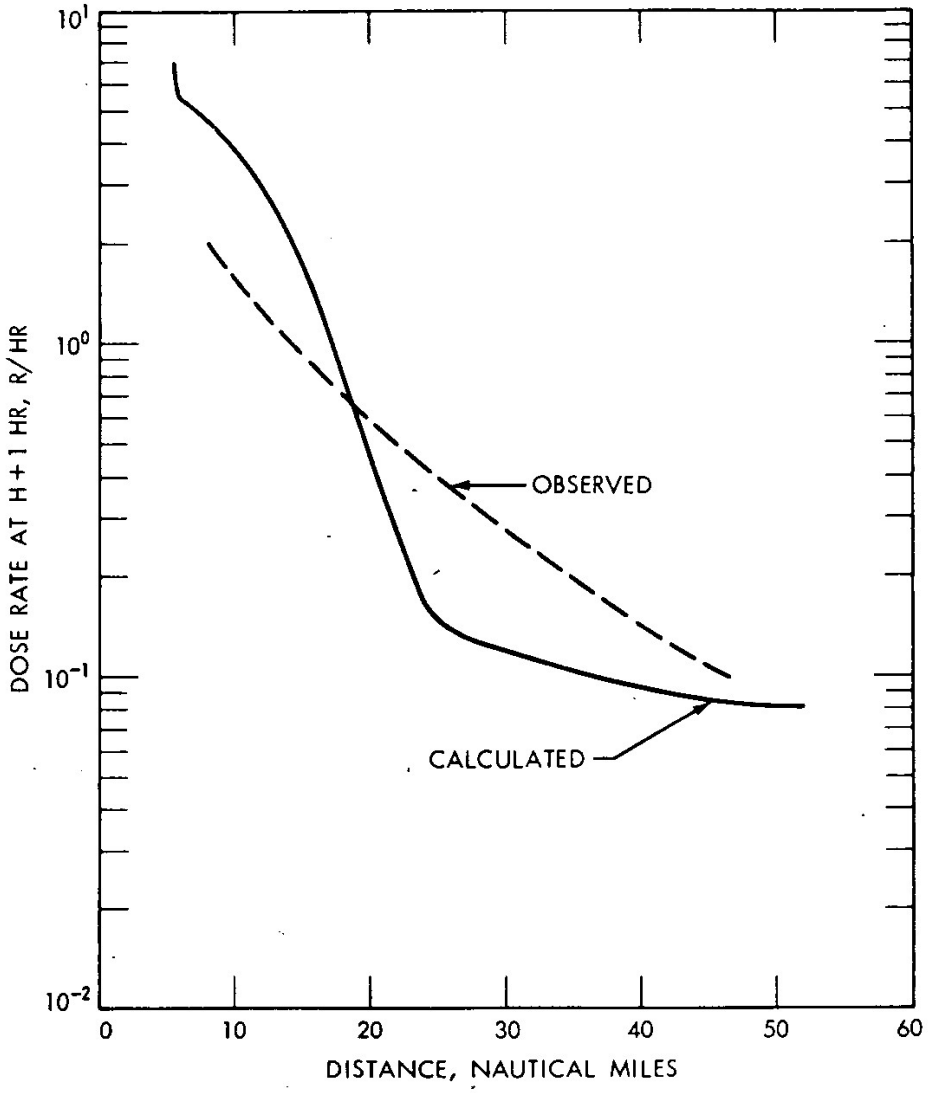

Fig. 10—The calculated and the observed gamma dose rates at H + 1 hr as a function of distance along the hot line of the pattern (predictive calculation) from the Teapot ESS shot.

PREDICTION OF FALLOUT FROM ROW-CHARGE SHOTS

In principle, the fallout pattern from a row of subsurface nuclear detonations may be estimated with the cratering fallout model, provided the model input parameters are adequately known for row-charge events. In the current state of knowledge, the cloud-geometry input parameters and the value of F_c appear to be the most difficult to specify. Study of time-lapse photography of the main-cloud and the base-surge evolution from past high-explosive row-charge tests give significant experimental information on the cloud-geometry parameters. For example, empirical methods of predicting crosswind radius and height of the base surges originating from high-explosive row-charge shots have been studied.[7] In this study it was shown that for five equal-weight charges, equally spaced and emplaced at the same depth of burial, the

resulting base surge has approximately the same radius as the base surge from a large single shot of the same total yield and emplaced at the same scaled depth. The base-surge height for a five-charge row shot is reasonably well approximated by scaling the height of the base surge for a single-charge event by the 0.2 power of the total yield of the row-charge shot.

A first approximation to the geometries of the individual main cloud may be obtained by treating each main cloud independently and estimating the top and the radius of each cloud from the work of Day.[8] Examination of the high-explosive row-charge documentary photographs of the Rowboat, the Dugout, and the Pre-Buggy shots indicates that such an approximation is reasonable. This approximation can, of course, be in error if main-cloud interactions occur. There is a need to evaluate the uncertainty in fallout prediction for multiple-charge shots in cases where cloud interactions lead to the injection of radioactivity at levels higher in the atmosphere than predicted.

Concerning the F_c for row-charge shots, preliminary experimental results for high-explosive single- and row-charge shots have been reported previously.[13] In this study, results of the measured vented fraction of ^{140}La tracer from single- and row-charge high-explosive shots were given. The experimental evidence suggests that the vented fraction from row-charge shots may be about twice that from single-charge shots. One of the most pressing needs for fallout prediction from row-charge shots is the establishment, through either experiment or theory, of the dependency of the F_c on yield, depth of burial, or charge spacing.

The development of computer aids for the row-charge fallout-prediction problem, however, can proceed independently of the solution of the two previously cited problems: (1) the specification of initial cloud geometry and (2) the specification of F_c. Therefore the capability of plotting fallout patterns for multicloud and/or multidetonation events has been developed. Figures 11 and 12 show, respectively, the (H + 1)-hr dose-rate patterns computed for 10 Danny Boy detonations on an east to west line with charge centers separated by 33.5 m and for 10 Danny Boy detonations on a north to south line with charge centers separated by 33.5 m. For the purpose of these calculations, each detonation is assumed to vent 5% (e.g., $F_c = 0.05$), each cloud is assumed to be the same as that for Danny Boy, and the input wind for each cloud fallout problem is assumed to be the same as the shot-time wind for Danny Boy. These two row-charge fallout patterns, although detectably different as determined from the printout, appear to be very similar. Calculational results suggest that the fallout pattern from a small-scale row-charge shot is not sensitive to the orientation of the wind to the alignment of the charges.

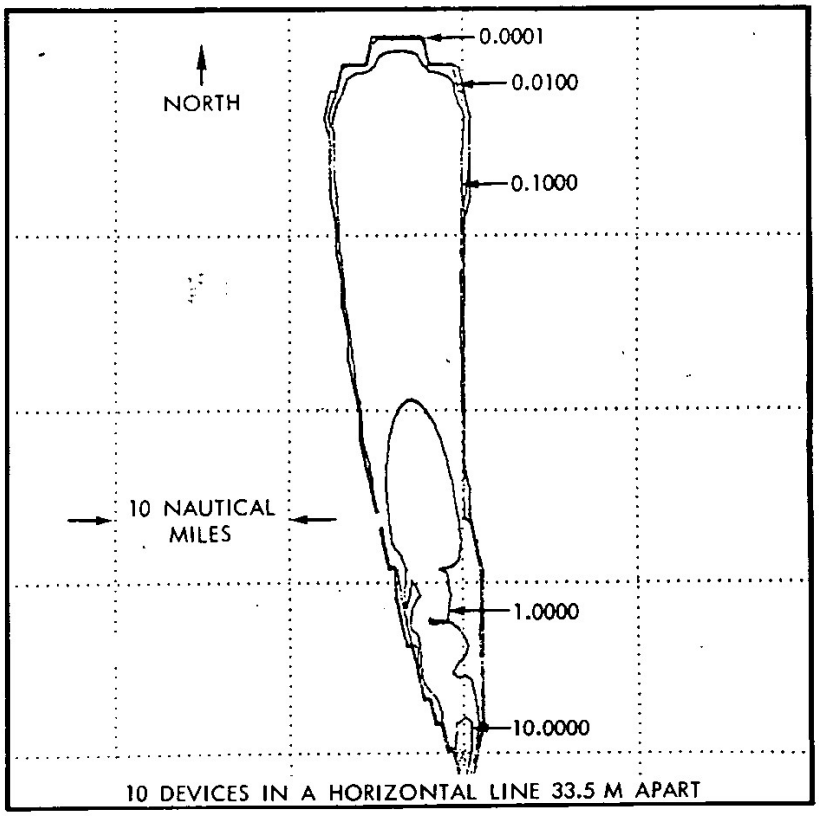

Fig. 11—The (H + 1)-hr gamma-dose-rate pattern computed for 10 Danny Boy detonations on an east to west line with charge centers separated by 33.5 m. Values are in roentgens per hour.

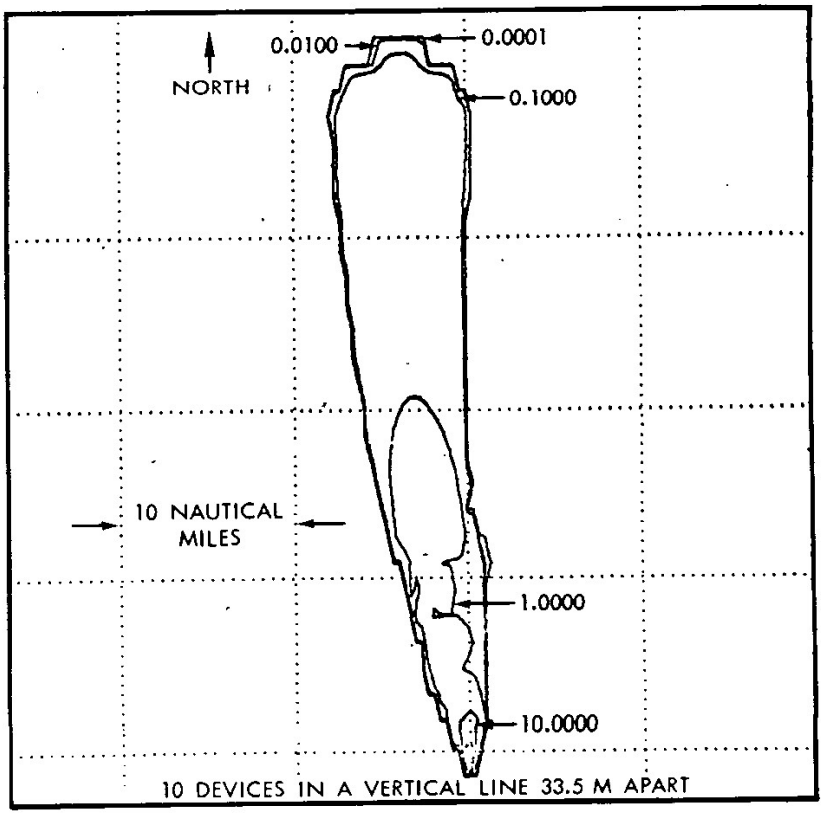

Fig. 12—The (H + 1)-hr gamma-dose-rate pattern computed for 10 Danny Boy detonations on a north to south line with charge centers separated by 33.5 m. Values are in roentgens per hour.

CONCLUSIONS

In conclusion, it may be stated that the cratering fallout model developed gives reasonable results for the prediction of the area of the pattern, the geometry of the dose-rate contours, and the (H + 1)-hr dose rate vs. distance along the hot line. The independent testing of the model should be extended to include more than the Teapot ESS case described and the several others cited.

Meteorological improvements in the cratering fallout model could well include the following items:

1. The prediction of synoptic-scale changes in the normal- and tangential-shear components.
2. A better understanding of the growth of the debris disks through horizontal eddy diffusion during their earthward fall.
3. The prediction of diurnal change of wind at low levels and close to ground zero.
4. The inclusion of the effects of topography on the evolution of the horizontal wind field.
5. The effect of terrain-induced circulations on fallout deposition.
6. A better solution to the cloud-rise problem for cratering detonations.

Before embarking on the development of these meteorological improvements in fallout predictions, however, one must consider potential improvements that may come from other areas. Areas of promise are cratering physics and filtration theory for the vented-fraction problem, special emplacement for control of vented fraction, and improvement of nuclear explosives.

ACKNOWLEDGMENTS

The author wishes to acknowledge the interest often expressed by Gary Higgins and the late A. Vay Shelton in the work herein reported, as well as programming support given by Mrs. Leota Barr and Roger Fulton.

REFERENCES

1. G. H. Higgins, Calculation of Radiation Fields from Fallout, USAEC Report UCID-4539, University of California Lawrence Radiation Laboratory, Jan. 25, 1963.
2. J. B. Knox, The Prediction of Wind and Fallout, USAEC Report UCID-4662, University of California Lawrence Radiation Laboratory, November 1962.
3. M. M. Williamson, private communication, 1964.
4. M. D. Nordyke and W. Wray, Cratering and Radioactivity Results from a Nuclear Cratering Detonation in Basalt, *J. Geophys. Res.*, *69*(4): 675-689 (1964).
5. G. H. Higgins, University of California Lawrence Radiation Laboratory, private communication, 1964.

6. J. B. Knox, University of California Lawrence Radiation Laboratory, unpublished data, 1963.
7. J. B. Knox and R. Rohrer, Project Pre-Buggy. Base Surge Analysis, USAEC Report PNE-304, University of California Lawrence Radiation Laboratory, Sept. 1, 1963.
8. W. Day, University of California Lawrence Radiation Laboratory, private communication, 1964.
9. J. D. McDonald, Rates of Descent of Fallout Particles from Thermonuclear Explosions, *J. Meteorol., 17:* 380-381 (1960).
10. R. R. Rapp and J. D. Sartor, Rate of Fall Through the Atmosphere of Irregularly Shaped Particles, Report RM-2006, RAND Corporation, Nov. 1, 1957.
11. E. S. Batten, D. L. Iglehart, and R. R. Rapp, Derivation of Two Simple Methods for the Computation of Radioactive Fallout, Report RM-2460, RAND Corporation, Feb. 18, 1960.
12. J. B. Knox, Status Report on Cratering Fallout Models, USAEC Report UCID-4663, University of California Lawrence Radiation Laboratory, Jan. 30, 1963.
13. E. Graves, W. R. Wray, and R. B. Pierce, Scope of Chemical Explosive Cratering Experiment, USAEC Report PNE-300, University of California Lawrence Radiation Laboratory, May 15, 1963.

REED: Dr. Knox, when you talked about F_c decreasing in row charges, was that for special tests? Would it go up a factor of maybe 5 for rows of 15 or 20 charges?

KNOX: In fallout from row-charge detonations, F_c, the fraction of the gamma activity appearing in the close-in fallout pattern, is not well known. The paper I presented utilizes F_c data from USAEC Report PNE-300. This report describes the F_c experiments and measurements for tracer-loaded high-explosive sources detonated as single charges and as rows in alluvium (Pre-Buggy I). These measurements of F_c for row-charge shots and the corresponding measurements of F_c for single-charge shots indicate that F_c for a row charge does not exceed that for a single charge by more than a factor of 2. It is not thought that F_c is a linear function of the number of charges. However, a definite need exists to obtain better information on the vented fraction for row charges since the number of experiments contained in the Pre-Buggy Program is small.

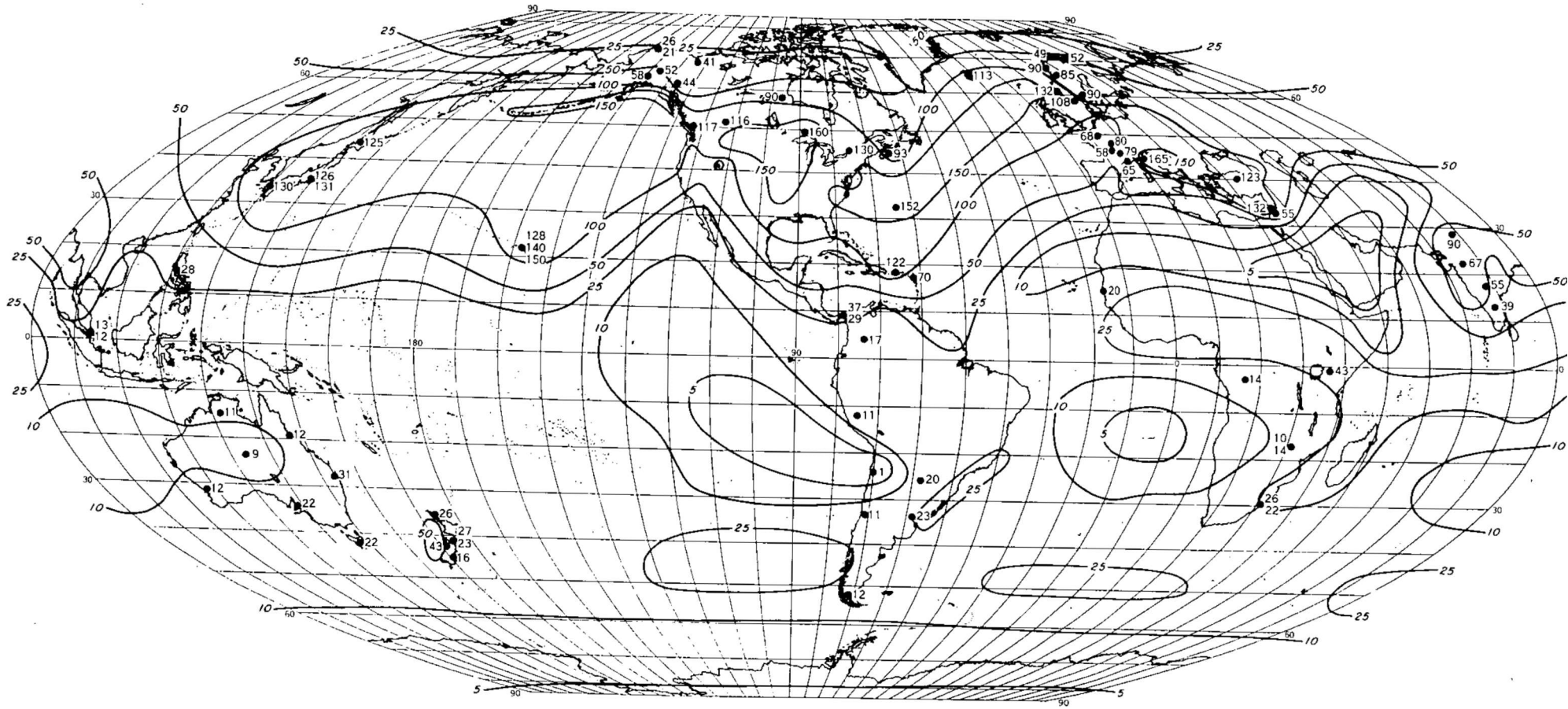

Fig. 5—Strontium-90 in soil determined from the 1963 and early 1964 survey, millicuries per square mile. Isolines are based on observed data and mean precipitation patterns.

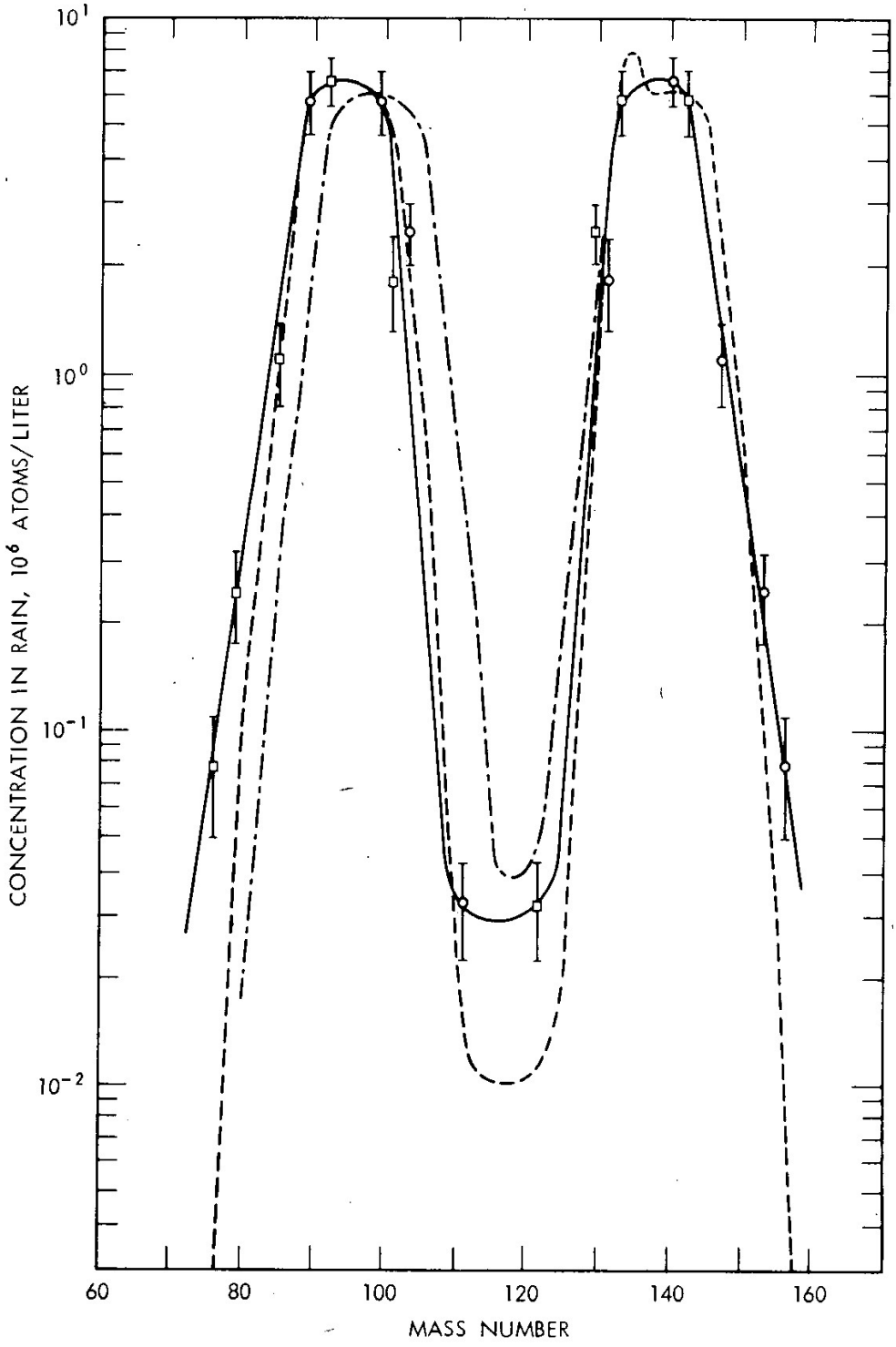

Fig. 7—Fission products in the Oct. 26, 1964, rain collected at Fayetteville, Ark. The concentrations in rain are expressed in terms of 10^6 atoms per liter of rain as of Oct. 16, 1964 (the date of the nuclear explosion). The vertical bars indicate the magnitude of decay of the longer lived nuclides since December 1962.

REFERENCES

1. P. K. Kuroda, Radiostrontium in Rain Water, in Radiological Physics Division Semiannual Report, July through December 1957, USAEC Report ANL-5829, p. 167, Argonne National Laboratory, February 1958.
2. H. L. Hodges, Radiochemical Determination of ^{90}Sr, ^{89}Sr, and ^{140}Ba in Nuclear Debris, Ph. D. Dissertation, University of Arkansas, January 1964.

DISTRIBUTION OF RADIOACTIVITY WITH HEIGHT IN NUCLEAR CLOUDS

GILBERT J. FERBER
U. S. Weather Bureau, Washington, D. C.

ABSTRACT

During Operation Dominic I at Christmas Island in 1962, aircraft sampling of nuclear clouds was done soon after cloud stabilization to investigate the amount of radioactive debris that stabilizes in the troposphere and its distribution with height. The detonations studied were all air bursts over water. Some data for surface bursts obtained during Operation Redwing in 1956 are used for comparison. Results indicate that for air bursts less than 1% of the total radioactivity is present in the stem of the nuclear cloud. It is estimated that about one-third of the total debris from the Christmas Island clouds initially stabilized in the troposphere.

Project Stemwinder has shown that in-cloud dose-rate monitoring by aircraft is a relatively simple and economical way to obtain information on the distribution of radioactive debris in a nuclear cloud. Used in conjunction with limited radiochemical analysis of samples, this type of monitoring could produce a reliable inventory of the debris in a nuclear cloud.

INTRODUCTION

The objective of Project Stemwinder was to probe and sample nuclear clouds as soon as possible after cloud stabilization to investigate the amount of radioactive debris that stabilizes in the troposphere and its distribution with height. Sampling was done with RB-57 aircraft of the 1211th Test Squadron under the scientific direction of the Atmospheric Radioactivity Research Branch, U. S. Weather Bureau.

The detonations investigated were all air bursts over water during Operation Dominic I at Christmas Island in 1962. Some data for surface detonations obtained by aircraft sampling during Operation Redwing in 1956 are used to compare with the Project Stemwinder data.

The project was conceived as an attempt to utilize available sampling aircraft to narrow the area of uncertainty involved in two related problems. The first problem was concerned with the operational need for prediction of the possible local hazards due to rainout of radioactive debris from a portion of a nuclear cloud that might pass over Christmas Island shortly after an air burst. Since the tops of rain clouds in the Christmas Island area were generally below 20,000 ft. and often below 10,000 ft, the amount and distribution of activity in the stem of the mushroom cloud was of primary concern. The second problem was concerned with the partitioning of nuclear debris between the stratosphere and the troposphere as a function of nuclear yield, tropopause height, burst height, and, possibly, other factors. Such partitioning has been an important consideration in estimating the long-range fallout from nuclear tests since nuclear debris has a mean residence time of several weeks in the troposphere (intermediate fallout) as opposed to many months or years in the stratosphere (worldwide fallout), depending on the latitude and altitude of injection. The fraction of the debris which remains in the troposphere may be particularly important in considering the possible hazards from relatively short-lived nuclides such as ^{131}I since the stratospheric portion usually decays to insignificant amounts before it can return to the surface of the earth.

It is emphasized that the preceding remarks apply only to the very small particles that contribute to the intermediate and the worldwide fallout. In the case of surface detonations, much of the radioactivity is associated with relatively large particles that comprise the local fallout. These large particles are not affected by the tropopause and appear in the local fallout regardless of whether they are initially injected into the troposphere or into the stratosphere.

CLOUD HEIGHTS OF AIR BURSTS IN A TROPICAL ATMOSPHERE

Operation Dominic I shot data (including those for yield, burst height, and cloud-top, base, and tropopause heights) are given in the Project Stemwinder final report.[1] Since there was no scientific program to document cloud heights, a "best guess" was made for each cloud by evaluating estimates made by observers on the ground and in the sampling aircraft and by using the dose rates reported at the various sampling altitudes to verify, where possible, the visual observations. Variations in the burst heights did not appear to have any

consistent effect on the cloud heights. Evidently, the effect of the burst height was masked by the influence of meteorological factors and/or the errors in the cloud-height estimates.

Selected data[2] were added from other Pacific test series to aid in drawing the mean curve and the curves for the estimated range of cloud heights (see Fig. 1). Almost all the detonations in previous U. S.

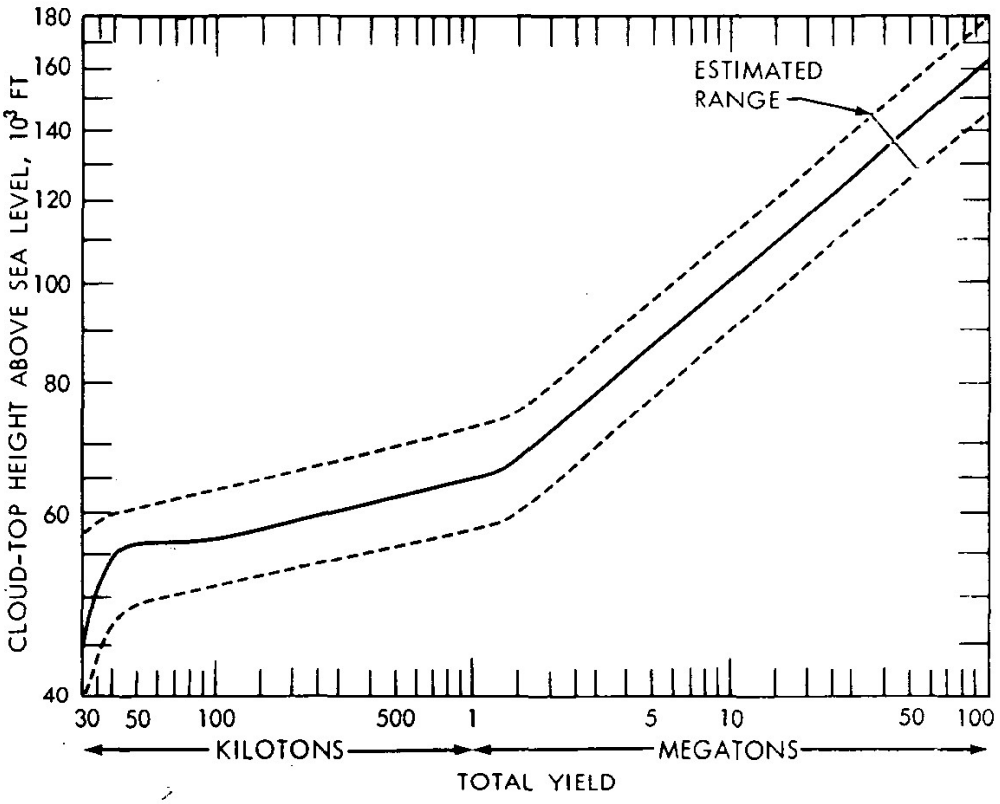

Fig. 1—Cloud-top heights and estimated range for air bursts ($180Y^{0.4}$ < burst height < 0.15 H_T) in a tropical atmosphere.

tests in the Pacific had been surface bursts, and the documentation of nuclear cloud dimensions had been generally poor. The curves shown in Fig. 1 are intended to be valid only for air bursts in a tropical atmosphere and for burst heights less than about 15% of the expected cloud-top heights. For this purpose, an air burst may be defined as a detonation at an altitude equal to or greater than $180Y^{0.4}$, where Y is the total yield in kilotons. It is emphasized that there are no reliable cloud-top data for yields greater than about 5 Mt, and the extrapolation of the curves beyond this point represents little more than an educated guess. Indeed, over the entire range of yields shown in Fig. 1, the dashed curves indicate only the expected range of cloud heights for the stated conditions and should not be interpreted as representing absolute limits.

STEM-CLOUD PENETRATIONS

An RB-57 aircraft was available for stem-penetration missions immediately following seven of the Dominic I detonations. The navigator was provided with a dose rate meter with a range from 0.01 to 2000 mr/hr and was instructed to record the dose rate as the aircraft penetrated the stem cloud at specified altitudes. The dose rates measured in the cockpit were then used to estimate the amount of activity in the cloud.

The relation between cloud concentration and dose rate in a uniform infinite cloud[3] is given by

$$C = \frac{D\rho}{\rho_0} \frac{84\rho_0}{(3.7 \times 10^4)(1.6 \times 10^{-6})E} \tag{1}$$

where C = cloud concentration, $\mu c/cm^3$
D = dose-rate, r/sec
ρ_0 = standard density of air at sea level = 1.293×10^{-3} g/cm^3
ρ = density of air at sampling altitude, g/cm^3
E = average gamma energy, Mev
84 = energy absorbed per roentgen, ergs per gram of air
1.6×10^{-6} = ergs/Mev
3.7×10^4 = dis/sec per microcurie

If the unit of dose rate is converted to roentgens per hour and the concentration to megacuries per cubic mile,

$$C = 2.1 \frac{\rho}{\rho_0} \frac{D}{E} \tag{2}$$

For stem penetrations within an hour after the burst, E was assumed to be 1 Mev. For the sampling missions between 2 and 5 hr after the burst, a value of 0.86 Mev was used.[4] Figure 2 gives the value of ρ/ρ_0 as a function of altitude for a typical tropical atmosphere.[5] With the use of appropriate values for E and ρ/ρ_0 in Eq. 2, the dose rates recorded during stem penetration were converted to cloud concentrations. An estimate of the stem diameter was then used to estimate the total volume of cloud in a 1000-ft-thick layer. The total amount of activity in the layer and the fraction of the bomb represented by that activity was then determined by multiplying the concentration by the volume. The results are shown in Fig. 3 as a plot of the fraction of the bomb present in a 1000-ft-thick layer of the stem cloud vs. height (indicated as percent of the total stem height). The three highest Dominic I data points are derived from the extended sampling missions described later in this paper. The Redwing data used for the figure

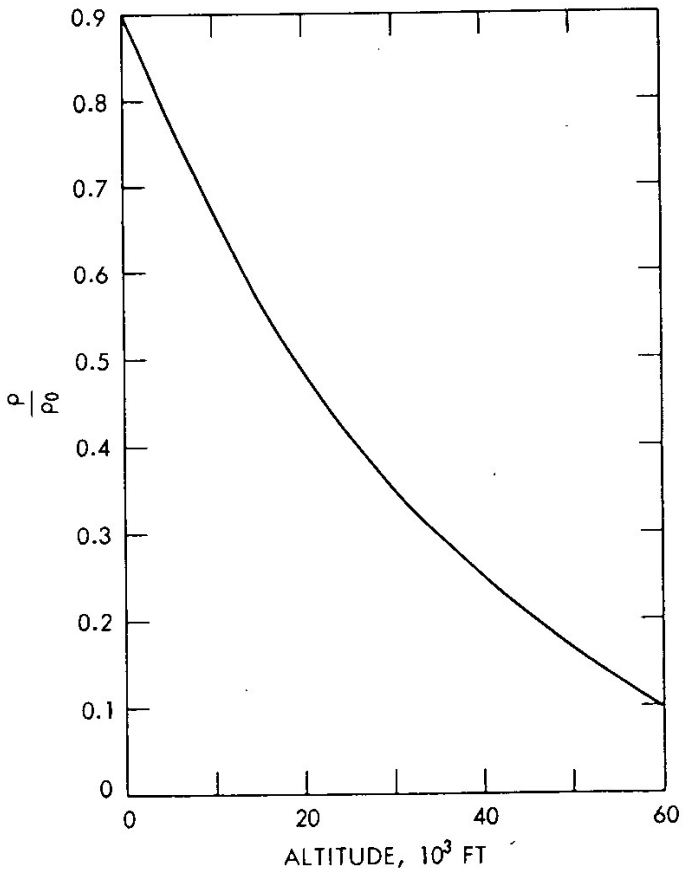

Fig. 2—Ratio of air density (ρ) to standard sea-level air density ($\rho_0' = 1.293 \times 10^{-3}$ g/cm^3) as a function of altitude.

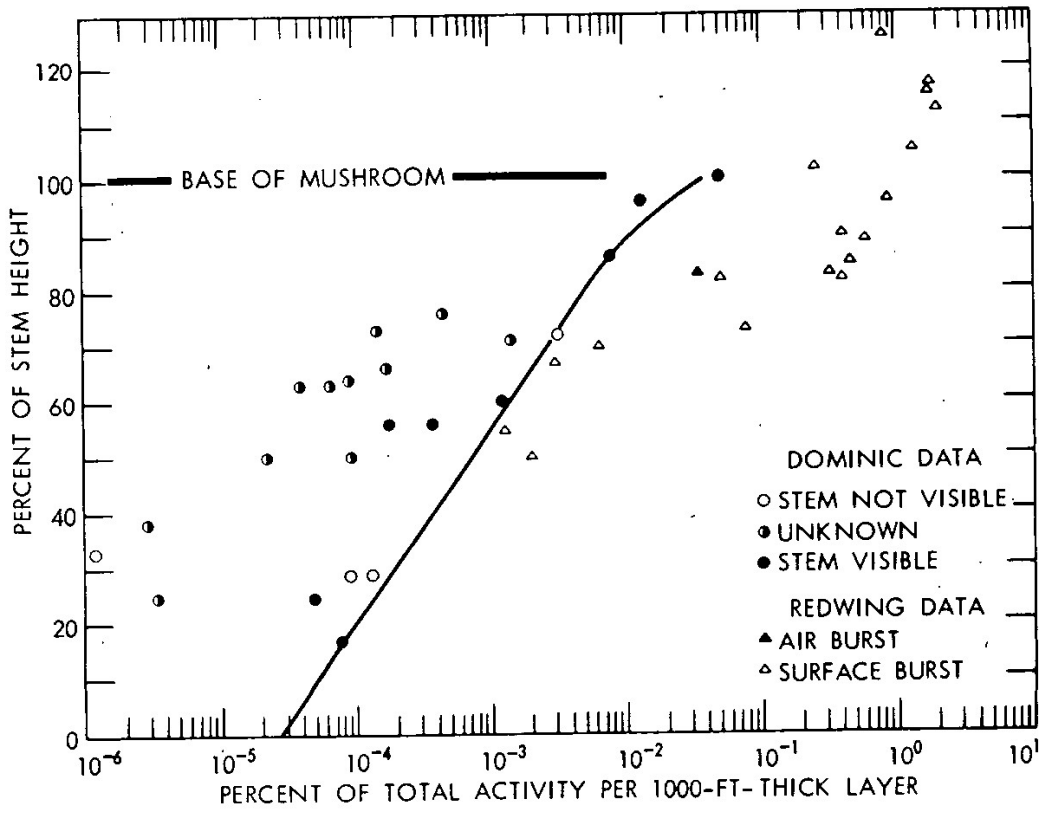

Fig. 3—Variation with height of the percent of the total activity residing in a 1000-ft-thick horizontal layer of the cloud.

also are discussed later. The curve is intended to represent a conservative estimate (for safety considerations) of the stem activity as a function of height for air bursts.

The rather large scatter in the data may be attributed to several factors. It appears that stem visibility may be the most important of these. Most of the higher activity readings occurred during penetrations when the stem cloud was visible to the pilot. The relatively low readings were obtained when the cloud was not visible or when it was not known whether the cloud was visible. It is quite possible that the aircraft did not actually penetrate the stem on these occasions. The dose rates measured inside the aircraft may have been due to "shine" from the stem cloud or to activity from diffuse material outside of the stem core. In those cases where the stem was not visible and where several passes were made at the same altitude, only the highest reading has been used.

Unfortunately, for the lower 80% of the stem, virtually all the data for the larger detonations are questionable because of the stem-visibility problem. Therefore it is impossible to say whether or not the low stem activity found for these shots indicates a real decrease in the fraction of activity in the lower part of the stem with increasing nuclear yield.

The following factors also contribute to the uncertainty in the results:

1. Stem-volume estimates. For the determination of the total activity present in a 1000-ft-thick layer, the stem diameter at the penetration altitude was estimated. The values used were based on visual estimates made by observers on the ground and in the sampling aircraft or, where necessary, on estimates for other detonations in the same yield range. The estimated diameter could be in error by as much as a factor of 2 in some cases.

2. Stem-height estimates. The stem was considered to extend from sea-level to the base of the cloud regardless of the burst height. The cloud bases used were based on visual observations from the ground and from the sampling aircraft and verified, where possible, by radiation readings taken in the sampling aircraft. The uncertainty in the height of the cloud-base (stem height) is about 10%.

3. Representativeness of dose-rate readings. The measured dose rates are assumed to represent those in a uniform, infinite cloud. The assumption appears to be reasonably valid for those penetrations where the stem was visible. The aircraft required 20 sec or more to traverse the cloud at a speed of about 7 miles/min while the mean free path of gamma radiation in air is on the order of a few hundred feet. The navigator reported that the dose rate usually rose sharply on entering the cloud, remained fairly steady (within a factor of 2) during

penetration, and then dropped sharply. (It would be advantageous to use automatic time–intensity recorders in future operations.)

The effect of aircraft shielding on the dose rate in the cockpit is also uncertain. Tests made at the ground, using a point source outside the aircraft, indicated that there was no appreciable shielding effect on gamma radiation by the aircraft. Equation 2 assumes that the receptor is completely surrounded by a uniform radiation field. Actually, of course, the receptor was surrounded by a "blank space" equivalent to the volume of the aircraft. No attempt has been made to correct for this. However, the effect should be small, probably less than a factor of 2, since the mean free path of the gamma radiation is large compared to the dimensions of the aircraft. Experimental determination of the correction factor should be planned in connection with any future operation of this type.

AIRCRAFT SAMPLING IN THE VICINITY OF THE CLOUD BASE

Aircraft equipped with Los Alamos Scientific Laboratory air-filter tanks were used for sampling after five Dominic I detonations. Approximately 1-hr sampling missions were flown at altitudes from 35,000 to 48,000 ft at 2 to 5 hr after detonation. The two sampling tanks were opened simultaneously when contact with the cloud was made and remained open for the entire sampling period. As the sampling patterns were flown, readings in the cockpit were made at 1-min intervals with a hand-held AN/PDR-27J Radiacmeter capable of measuring activity in a range from 0.01 to 500 mr/hr. Sampling missions were successful after four of the five detonations. The radiochemical analyses of the samples are reported elsewhere.[6]

The dose-rate readings obtained during three extended sampling missions were sufficient for estimations of the distribution and the amount of activity in the clouds at the sampling altitudes. Similar analyses were done for all three missions. The results are included in Fig. 3.

One of the clouds was sampled at an altitude of 45,000 ft at approximately 3 to 4 hr after detonation. The base of the cloud was reported to be at about 45,000 ft. Both the shot-time wind data and the position of the cloud indicate east-southeast cloud travel at about 15 knots. For correction for the movement of the cloud during the sampling period, the reported aircraft positions were adjusted to the sampling midtime of $3\frac{1}{3}$ hr after detonation. The corrected radiation field and the actual unadjusted sampling track are shown in Fig. 4. If a decay exponent of -1.2 is assumed, integration of the pattern yields 520 r/hr-cu mi at 1 hr in a 1000-ft-thick layer. From Eq. 2 this is equivalent to 270 Mc, or 4.9×10^{-4} of the total fission products produced by the detona-

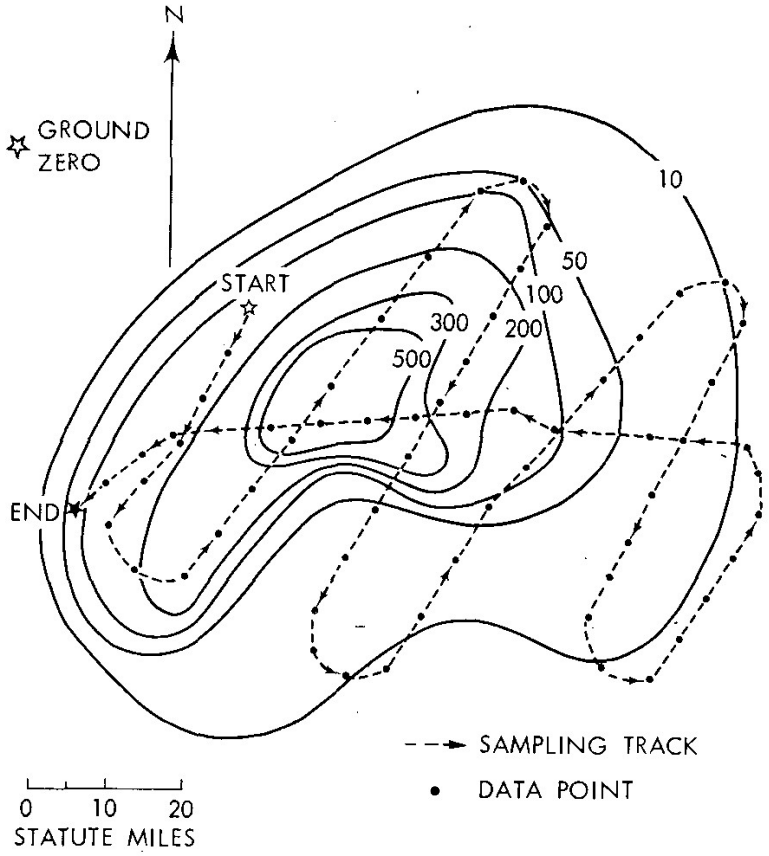

Fig. 4—Sampling track and radiation pattern in a nuclear cloud at 45,000 ft. Values given are in milliroentgens per hour at H + 3⅓ hr.

tion. The cloud covered an area of 5200 square miles at the 45,000-ft altitude.

The sampling track appears to have covered the cloud very well. However, the pilot reported shine from higher portions of the cloud during the last few minutes of sampling when the aircraft was outside the visible cloud. The readings due to shine were about 100 mr/hr. It is possible that a significant fraction of the in-cloud readings may also have been due to shine from the upper portions of the cloud; therefore the estimate of the amount of activity at 45,000 ft may be high.

COMPARISON WITH RADIOCHEMICAL RESULTS

The radiochemical analyses of the samples obtained on the three extended sampling missions provide a check on the method of calculating the amount of debris present from the dose-rate readings in the cloud. The total number of fissions collected in each sample has been determined,[7] based on the number of atoms of ^{99}Mo present corrected for the fission yield of ^{99}Mo for thermal fission of ^{235}U. If the total volume of air passing through the sampling tank and the average dose rate along the sampling path are known, the fissions per sample can be estimated by the same method that was used to estimate the fraction of

the bomb in a 1000-ft-thick layer. The volume sampled is determined from the altitude, the air temperature, the aircraft speed, the sampling time, and the sampling-tank and filter-paper characteristics.[8] The average dose rate is determined from the readings taken in the cockpit at 1-min intervals during the sampling period. From Eq. 2 the gamma megacuries in the sample can be calculated. If it is assumed that 1 kt of fission (1.4×10^{23} fissions) is equivalent to 550 gamma megacuries at 1 hr, the following conversion factor can be used: 1 Mc (H + 1) = 2.64×10^{20} fissions. Table 1 gives the pertinent data and the fissions

Table 1 — COMPARISON OF CALCULATED AND ANALYZED FISSIONS PER SAMPLE

Mission	Altitude, ft	Sample volume, cu ft	Average dose rate, mr/hr at H + 1	Calculated fissions per sample	Fissions per sample (radiochemical analyses)
A	43,000	1.06×10^6	190	1.9×10^{14}	3.3×10^{14}
B	48,000	1.11×10^6	270	2.3×10^{14}	4.9×10^{14}
C	45,000	1.10×10^6	560	5.6×10^{14}	5.8×10^{14}

per sample as calculated from dose-rate readings and as determined from radiochemical analyses of the samples.

The agreement between the calculated values and the results of the sample analyses is remarkably good, considering the uncertainties due to the possibility of shine from other portions of the cloud, aircraft shielding, and aircraft contamination. The calculated values for the samples from missions A and B are low by about a factor of 2, possibly because of the effect of the blank space previously mentioned. The calculated value for the sample from mission C is in almost perfect agreement with the result of the sample analysis. Mission C is the one depicted in Fig. 4 and for which there was reason to suspect a shine contribution to the dose rates which may have compensated for the blank-space effect.

Additional experimental data are needed to evaluate all the factors involved, but the results indicate that the method employed on these missions is a practical and promising way to obtain the distribution of activity in a nuclear cloud.

REDWING IN-CLOUD DOSE-RATE DATA

The doses and dose rates at various altitudes in several nuclear clouds (all but one from surface bursts) were investigated by aircraft penetrations[9] during Operation Redwing in 1956. Some of these penetrations were complete traverses through the cloud. Since the altitude,

the mean speed of the aircraft, the time in the cloud, and the average dose rate are reported, these data can be utilized in the same manner as the Dominic I stem penetrations to compute the device fraction contained in the cloud at the penetration altitudes. The computed device fractions are plotted in Fig. 3 for comparison with the Dominic I data.

Several interesting features may be noted. It appears that the activity in the upper half of the stem is greater for surface bursts than for air bursts and that the difference increases with altitude. The largest gradient of activity with altitude appears at about 70 to 80% of the stem height; this implies that for surface bursts the "radiological base" lies below the visual cloud base. However, this inference may not be warranted since the high activities encountered below the base may be due to the descent of fallout particles.

The values computed for the lower portion of the mushroom indicate about 1 to 2% of the total fission products per 1000 ft. Since the mushroom portion of the clouds investigated averaged about 30,000 ft in vertical extent, the average activity in the mushroom must have been about 3% per 1000 ft. Thus we have some basis for believing that this admittedly crude method can give at least the right order of magnitude for the activity at a given altitude, even when the average dose rate recorded during a single pass through the cloud is used.

We note that the one Redwing data point for an air burst gives about five times the activity indicated by the curve estimated from the Dominic I data. This greater activity might be attributed to the fact that the detonation took place at a lower scaled height than any of the Dominic I air bursts. The burst height was somewhat below the minimum altitude for a true air burst according to our definition (burst height > $180Y^{0.4}$); therefore the activity distribution might be expected to be intermediate between those for air bursts and surface bursts. Although the close-in fallout measured after this detonation was very light, it was considerably more than that found after any Dominic I shot, where shipboard dose rates never exceeded 0.1 mr/hr. However, since only one surface vessel was available for fallout measurements during the Dominic I tests, the very limited number of measurements obtained does not permit the drawing of firm conclusions.

RESULTS AND CONCLUSIONS

Activity in the Stem Cloud for Air Bursts

Although the Dominic I stem-penetration data leave a good deal to be desired for defining the distribution of activity in the stem, the curve in Fig. 3 represents a best estimate based on our interpretation of these data. A major uncertainty lies in the assumption that the distribution in the stem does not vary with yield. As indicated previously,

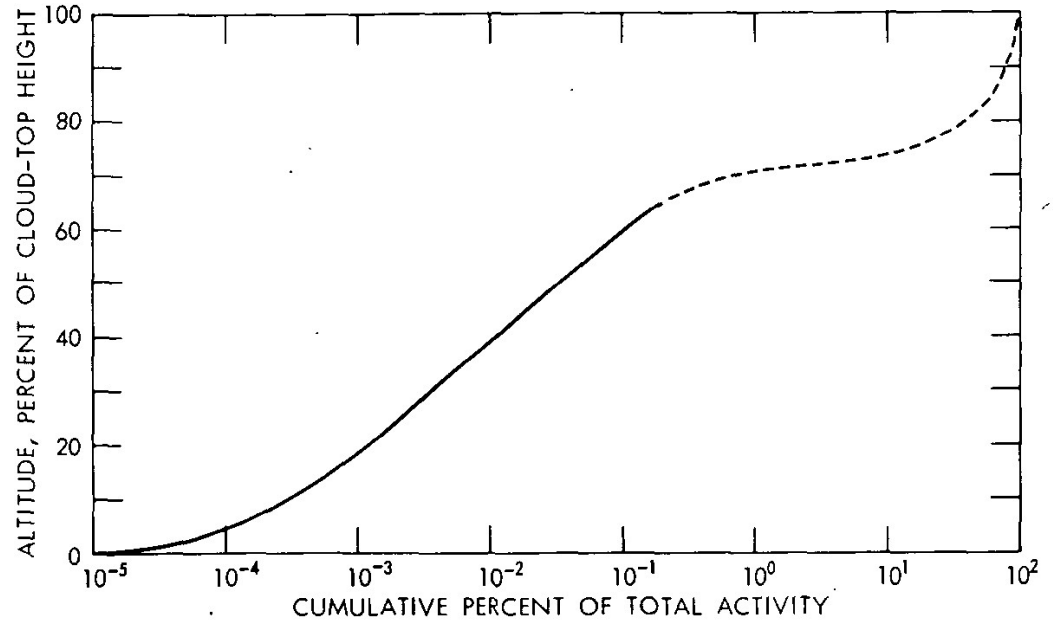

Fig. 5—Cumulative activity as a function of height in the nuclear cloud for air bursts.

this curve may represent an overestimation of the activity in the lower part of the stem for the larger yields (above about 200 kt).

Cumulative Activity with Height in the Nuclear Cloud for Air Bursts

With the use of the stem-activity curve in Fig. 3, an estimate of the cumulative activity with height in the nuclear cloud was derived. The solid portion of the curve in Fig. 5 was obtained from the stem-activity curve by using an average stem height of 40,000 ft and by assuming the stem-top height (or visual cloud base) to be 63% of the cloud-top height (the average for the Dominic I series). Since the entire stem appears to contain less than 1% of the total activity, it is obvious that the activity must increase rapidly with height at or above the base of the cloud. The dashed portion of the curve represents a subjective estimate (based, in part, on the Redwing data for surface detonations) of the distribution of activity in the mushroom portion of the cloud. The activity in the mushroom is assumed to be distributed as follows:

Layer, % of cloud-top height	Fraction of total activity, %
65 to 70	0.6
70 to 75	14
75 to 80	25
80 to 85	25
85 to 90	15
90 to 95	15
95 to 100	5

For air bursts it appears reasonably certain that less than 1% of the total activity is present in the stem and that less than 0.1% stabilizes between the surface of the earth and one-half of the cloud-top altitude. The fraction of activity per unit altitude increases with height throughout the stem, and the region of maximum vertical gradient, which might be termed "the radiological base of the cloud," probably occurs somewhat above the visual cloud base. The peak activity per unit altitude is assumed to occur between 75 and 85% of the distance from the surface to the cloud top. It is also assumed that for air bursts the distribution of activity relative to the cloud-top height does not vary with nuclear yield, burst height, or atmospheric conditions.

Actually, the interaction of these factors must exert some influence on the activity distribution. The estimated top and base heights of the Dominic I clouds indicate that the ratio of base height to top height has a tendency to decrease with increasing yield. However, it is uncertain to what extent these indications are valid since the variation among detonations of about the same yield is almost as great as that for the range of yields from 40 kt to several megatons. The mean ratio is 63%, with individual clouds varying from 53 to 73%. Some of the variation may be attributed to errors in the estimates of the base and top heights, but part of it is undoubtedly real. There is a similar uncertainty concerning the height of the radiological base.

Partition of Activity Between Stratosphere and Troposphere

The height of the tropopause varies with latitude, season, and daily atmospheric changes. The daily and seasonal variations are less in tropical latitudes than elsewhere. The tropopause heights averaged about 54,000 ft above sea level for the Dominic I tests, varying between 50,000 and 58,000 ft on individual shot days. This variation is representative of the tropical tropopause.

With the use of the activity distribution in Fig. 5, a mean tropopause height of 54,000 ft, and the mean cloud-height curve in Fig. 1, a typical curve of the percent of total debris in the troposphere as a function of yield has been calculated. The curve, shown in Fig. 6, is intended to be valid at the time of cloud stabilization for air bursts in a tropical atmosphere. Another curve has been drawn to indicate the likely maximum tropospheric fraction, based on a high tropopause (58,000 ft) and low cloud heights (from the lower curve in Fig. 1). These extremes do not represent absolute maximums since higher tropopauses and lower clouds may occur occasionally. In addition, the uncertainties in the activity–height curve (Fig. 5) make it impossible to define a meaningful and useful absolute maximum tropospheric fraction. No attempt has been made to estimate the minimum tropospheric fraction, but, in the megaton-yield range, it could be several orders of magnitude below the typical fraction.

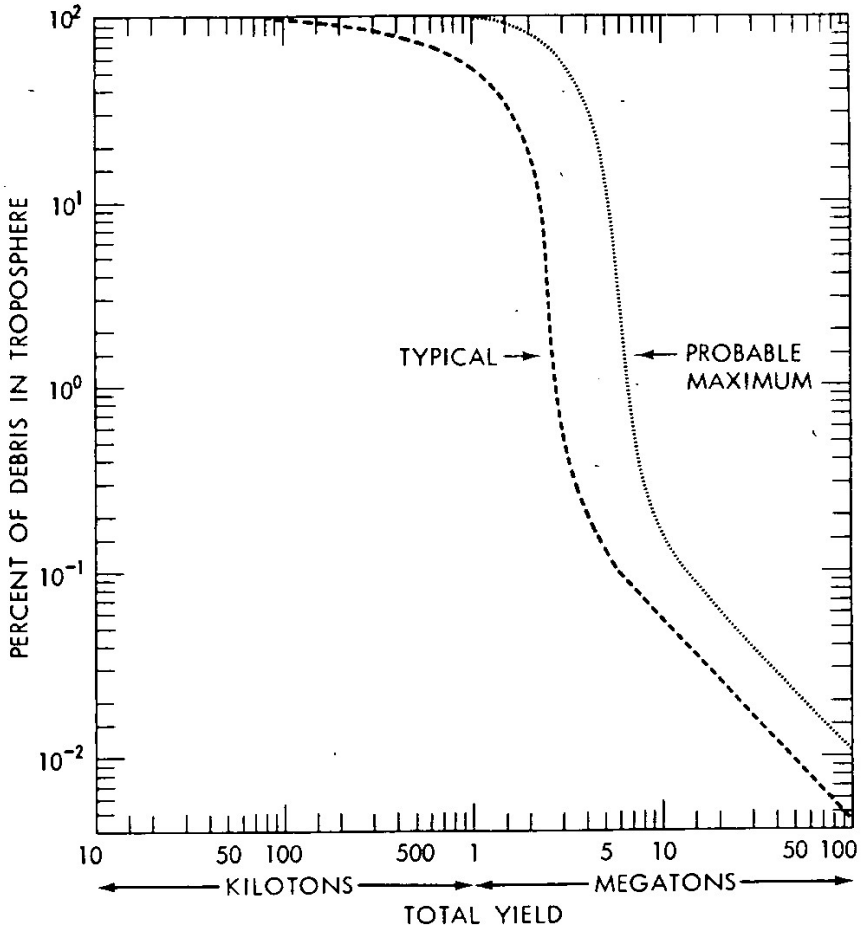

Fig. 6—Percent of total activity initially injected in the troposphere as a function of total yield for air bursts in a tropical atmosphere.

The most critical uncertainty in the estimates is for the range of yields from about 700 kt to about 5 Mt, where the radiological cloud base may lie in the vicinity of the tropopause. For yields less than 700 kt, the tropospheric fraction (at cloud stabilization) can be estimated to within a factor of 2 or less. For yields above about 5 Mt, the fraction in the troposphere becomes very small, although precisely how small it may be has not yet been determined.

An estimate of the kiloton equivalent of fission products stabilized in the troposphere as a function of total yield for air bursts is shown in Fig. 7. The typical and maximum curves are derived from the curves in Fig. 6, based on the assumption that the yield is entirely due to fission. Several interesting features may be noted. The maximum tropospheric contamination is produced by bursts in the low megaton range (assuming 100% fission yield). With typical cloud heights and an average tropopause height of 54,000 ft, the maximum tropospheric contamination is about 500 kt for yields between about 800 kt and 2 Mt. As the yield increases, the tropospheric debris decreases rapidly and then levels off at about 5 kt of fission equivalent for yields from 10 to 100 Mt. The maximum curve, based on a high tropopause and low cloud heights,

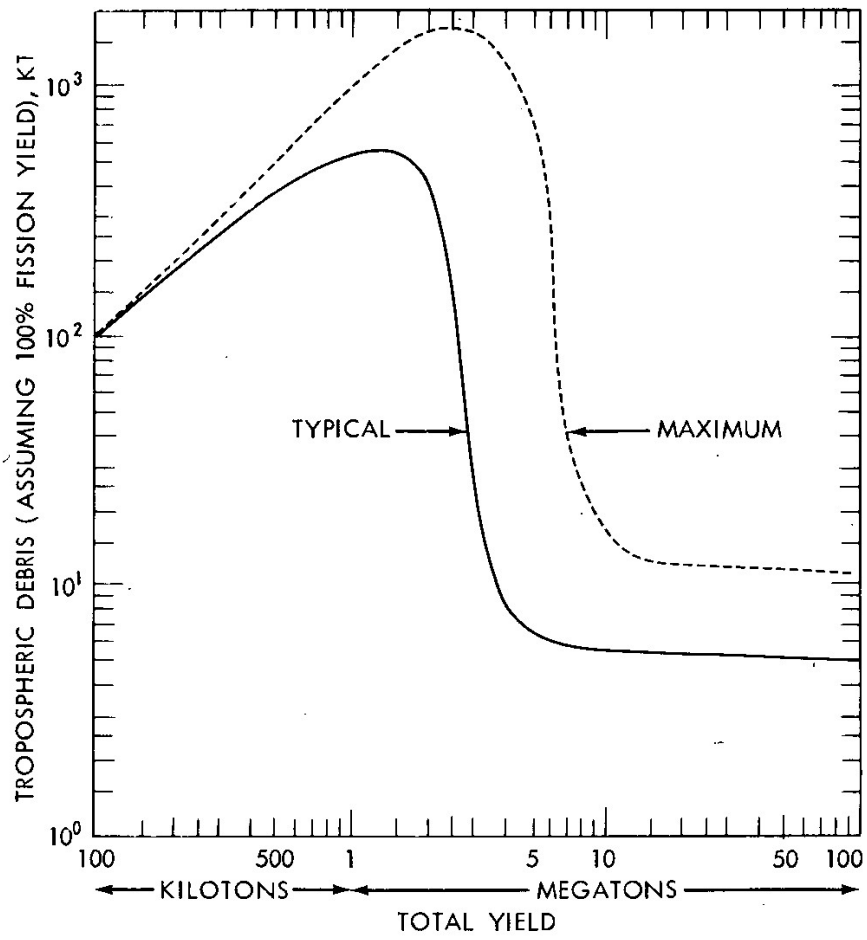

Fig. 7—Amount of debris (kilotons equivalent) initially injected in the troposphere as a function of total yield for air bursts in a tropical atmosphere.

is quite similar with a maximum tropospheric contamination of about 1.5 Mt for yields between 2 and 3 Mt, all fission. This curve also decreases rapidly and then levels off at about 12 kt of tropospheric debris for yields between 15 and 100 Mt. It should be recalled here that these curves are based on the activity–height curve given in Fig. 5 and are subject to the same uncertainties. For thermonuclear devices the amount in the troposphere should be multiplied by the fission fraction of the device.

Dominic I Debris in the Troposphere

With the use of the estimated tropospheric fraction and the fission yield for the individual Christmas Island detonations, it is estimated that about one-third of the total radioactivity initially stabilized in the troposphere. Since a half-residence time of one month is generally accepted for tropospheric debris,[10] about one-sixth of the total activity might be expected to be deposited at the surface, mostly in tropical latitudes, within a month after the conclusion of this test series. A rough integration[11] of the activity found in the AEC Health and Safety Laboratory monthly fallout-deposition collections indicated that only about half this amount was deposited in the latitude band from 30°N to 30°S

through August 1962. The difference between the expected and the measured amounts may be due to the uncertainties in the estimates of the tropospheric fraction and the deposition. However, there are several reasons for believing that the amount deposited in the latitude band was actually less than that estimated from the tropospheric fraction at time of cloud stabilization.

First, some of the debris which initially stabilized below the tropopause may have ascended into the stratosphere in convective cells or as a result of thermally induced direct circulation. Second, some debris was transported to mid-latitudes at altitudes below the tropical tropopause. Since there is a polar tropopause in mid-latitudes, generally between 30,000 and 40,000 ft, the debris which was transported away from the equatorial region at altitudes from about 40,000 to 55,000 ft would have become incorporated into the mid-latitude stratosphere. An interesting example of such transport was provided by the interception of one of the Dominic I clouds by sampling aircraft over the western United States.[12] In addition, sampling of the lower stratosphere over the United States indicates that it contained fresh debris from the Dominic I tests during most of the month of May 1962. Finally, the evidence for a half-residence time of one month for tropospheric debris may actually apply only to debris below the polar tropopause. The residence time for debris in the troposphere, above 40,000 ft, in tropical latitudes has not been established. Only a very small fraction of the debris from the Dominic I tests stabilized below 40,000 ft. The fraction was much smaller than that for previous Pacific test series, which consisted primarily of surface bursts.

In any case, it has become increasingly evident that the potential hazard due to short-lived fission products is not attributable solely to the portion initially injected in the troposphere since there is an exchange of air between the stratosphere and troposphere. Therefore the three-dimensional trajectory of the debris-laden air would have to be considered in determining the fate of a particular debris cloud.

It has also been shown[12] that severe thunderstorms that penetrate the lower stratosphere provide an effective mechanism for bringing stratospheric debris directly to the ground. It appears that thunderstorm scavenging of stratospheric debris from the Dominic I tests accounted for most of the ^{131}I found in milk in the midwestern United States in May 1962.

RECOMMENDATIONS FOR FUTURE WORK

Project Stemwinder has shown in-cloud dose-rate monitoring by aircraft to be a relatively simple and economical way to obtain information on the distribution of radioactive debris in nuclear clouds.

Through the use of this technique, it may be possible to greatly reduce the amount of radiochemical analyses which would be required to obtain a reliable inventory of radioactivity in a nuclear cloud. This type of monitoring might be particularly well suited to clouds from large nuclear cratering detonations such as those contemplated for the Plowshare program. Such clouds should be visible for at least several hours and would probably be confined to the troposphere.

Tentative answers have been found for the questions that led to Project Stemwinder, but large uncertainties still exist. The experience gained in the project indicates that for air bursts the lower stem should be monitored soon after cloud stabilization while it is still visible and that several penetrations should be made at each altitude to ensure that representative readings are obtained. Additional data are particularly needed for yields in the megaton range.

An obvious limitation of Project Stemwinder was the aircraft ceiling of 50,000 ft. A determination of the amount of debris initially stabilized in the troposphere requires sampling to an altitude of 60,000 ft. Aircraft with the capability of operating at this altitude have been used for cloud sampling, but they were not available for Project Stemwinder.

The following recommendations are offered for any future operations:

1. A continuous-recording gamma-intensity instrument package with a range from 1 mr/hr to 1000 r/hr should be used for aircraft cloud penetrations.

2. Experimental determination of the dose-rate reduction due to the aircraft should be attempted.

3. An attempt should be made to monitor the entire cloud from a low- or an intermediate-yield detonation. Thus the distribution of activity throughout the cloud can be ascertained, and the total computed activity can be compared with the fission yield of the device as a check on the method.

ACKNOWLEDGMENTS

Project Stemwinder was originally conceived and coordinated by Joshua Holland, Chief, Fallout Studies Branch, Division of Biology and Medicine, U. S. Atomic Energy Commission, whose vigorous efforts brought the project into being in the space of a few weeks prior to the start of Operation Dominic I. The ideas and efforts of the late A. Vay Shelton, Lawrence Radiation Laboratory (Chief, Hazards Evaluation Branch for Dominic I, Joint Task Force 8) and of Robert J. List, Kosta Telegadas, and Jerome L. Heffter, Atmospheric Radioactivity Research Branch, U. S. Weather Bureau, were instrumental in planning and carrying out the project. The excellent cooperation and high skill of Paul Guthals, Los Alamos Scientific Laboratory, and Harry Hicks

and Edward Fleming, Lawrence Radiation Laboratory, in directing and controlling the sampling aircraft contributed much to the success of the project. Our thanks are also due to Col. Templeton Walker, Commander, 9th Weather Reconnaissance Wing, and to all the members of the 1211th Test Squadron who displayed great enthusiasm and a high degree of professional competence in carrying out the sampling missions.

REFERENCES

1. G. J. Ferber, Operation Dominic I — Project Stemwinder, Operation Dominic Report, WT-2060, U. S. Weather Bureau, May 1964. (Classified)
2. L. Fussel, Jr., Cloud Photography, Operation Redwing Report, ITR-1343, Edgerton, Germeshausen and Grier, Inc., March 1957. (Classified)
3. J. Healy, Radioactive Cloud Dose Calculations, in *Meteorology and Atomic Energy*, D. Slade (Ed.), Chap. 6, U. S. Weather Bureau, Washington, D. C., in preparation.
4. G. Higgins, Calculation of Radiation Fields from Fallout, USAEC Report UCID-4539, Lawrence Radiation Laboratory, University of California. Jan. 25, 1963.
5. E. G. Reid, Average Atmospheric Characteristics at the Eniwetok Proving Ground (April–June 1956), Stanford University, private communication, July 1958.
6. P. A. Benson, The Analysis of Particulate Debris from Pacific Air Shots, Quarterly Progress Reports, 1962–1964, various pages, Tracerlab, Division of Laboratory for Electronics, Inc.
7. P. A. Benson, Total Fissions Collected in Dominic Samples, Tracerlab, Division of Laboratory for Electronics, Inc., private communication, November 1963.
8. K. Telegadas and R. J. List, B-57 Air Sampling Program (1960), USAEC Report HASL-105, Health and Safety Laboratory, Jan. 9, 1961.
9. E. A. Pinson et al., Operation Redwing — Project 2.66a, Early Cloud Penetrations, Report WT-1320, Air Force Special Weapons Center, Kirtland AFB, February 1960. (Classified)
10. United Nations, Report of the Scientific Committee on the Effects of Atomic Radiation, Supplement No. 16, General Assembly, 17th Session, p.248, New York, 1962.
11. R. J. List, U. S. Weather Bureau, private communication, January 1964.
12. R. J. List, K. Telegadas, and G. J. Ferber, Meteorological Evaluation of the Sources of Iodine-131 Contamination in Milk, *Science*, *146:* 59(1964).

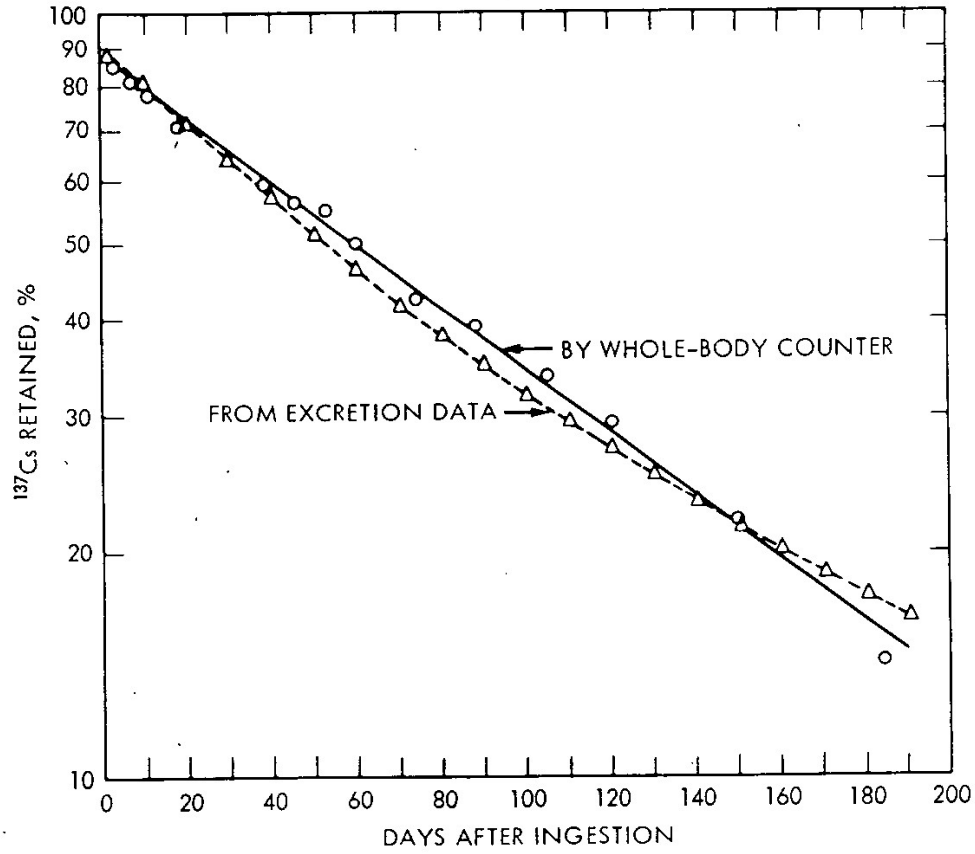

Fig. 5—Percent retention of ^{137}Cs from Rongelap food.

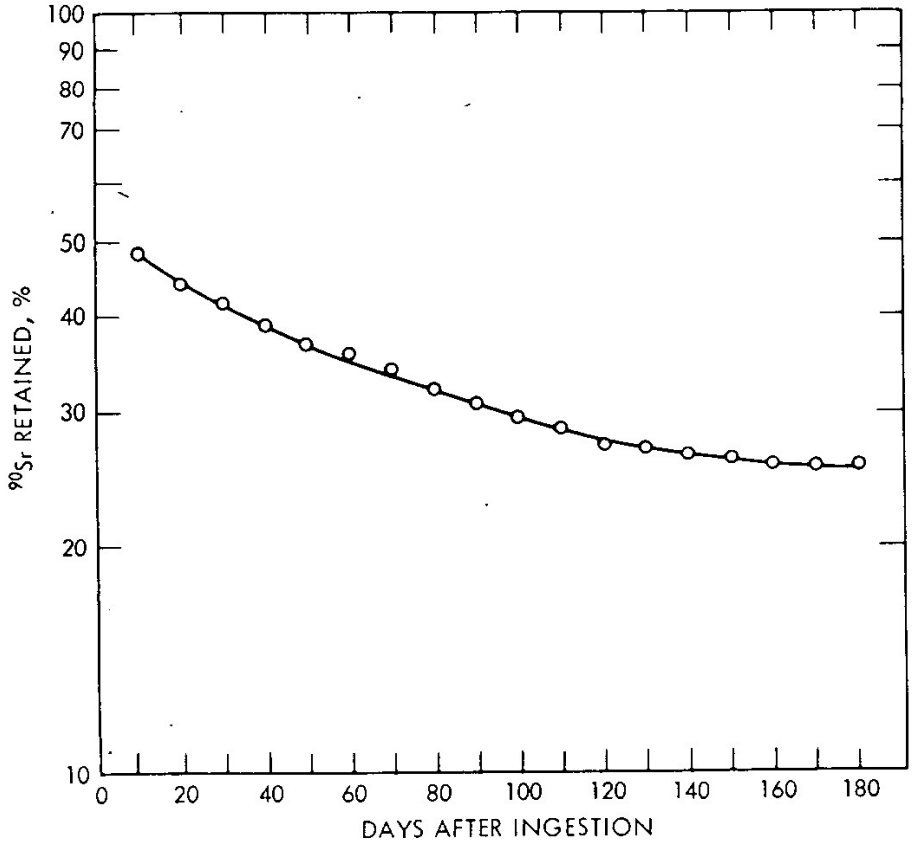

Fig. 6—Percent retention of ^{90}Sr from Rongelap food as measured from excretion.

EARLY FOOD-CHAIN KINETICS OF RADIONUCLIDES FOLLOWING CLOSE-IN FALLOUT FROM A SINGLE NUCLEAR DETONATION

WILLIAM E. MARTIN
University of California at Los Angeles, Los Angeles, California

ABSTRACT

Plant samples and rabbits were collected from representative locations in the Sedan fallout field before and at various times after the detonation. Radiochemical and statistical analyses indicated highly significant correlations between estimates of gamma dose rates and maximum concentrations of ^{89}Sr or ^{131}I in plant samples and in the stomach contents, bone ash, or thyroids of rabbits collected between 15 and 110 miles from ground zero.

The effective half-lives of ^{89}Sr and ^{131}I on fallout-contaminated plants were approximately 18 and 5.0 to 5.5 days, respectively. Maximum concentrations of ^{89}Sr in rabbit bone ash occurred about 30 days after the detonation and remained high for at least 60 days; but maximum concentrations of ^{131}I in rabbit thyroids occurred by or before five days and then declined to pre-Sedan levels in less than 60 days after the detonation.

Deterministic exponential models were formulated and found to function satisfactorily, with parameter values derived from the data, in providing a partial explanation of the quantitative kinetic relations between initial concentrations of ^{89}Sr and ^{131}I on plants and subsequent concentrations in the bone ash or thyroids of rabbits collected in the Sedan fallout field. Major sources of error in the estimation of input-parameter values and in the use of such models to make predictions are described and discussed.

Similar models were proposed for the study of radionuclide kinetics in human food chains (i.e., pasture plants, cow milk, and human

tissues or organs) following environmental contamination by a single fallout event. The results of hypothetical calculations were compared with the Radiation Protection Guides recommended by the Federal Radiation Council.

INTRODUCTION

To explain the kinetics of radionuclide transfers in a given food chain, it is first necessary to describe the routes and rates of transfer affecting specific food-chain compartments. The major route and some of the minor routes of radionuclide transfer and exchange in a terrestrial ecosystem are shown in Fig. 1.

Some of the fallout particles initially deposited on soil surfaces may be redeposited by wind or rain on plants,[1] but most of them are mechanically trapped and not susceptible to redeposition.[2] Material deposited on soil may enter food chains by stem-base absorption,[3] by downward leaching in the soil profile and subsequent root uptake,[4,5] or by accidental ingestion, especially by burrowing animals.[6] Most of the fallout deposited directly on soil can be regarded as unavailable for rapid entry into major food chains.

Some of the radioactivity contained in the fallout particles, mostly $< 44\ \mu$ in diameter,[1,7] retained on foliage may be assimilated by foliar absorption,[8,9] but a much larger fraction is subject to fairly rapid removal by wind or rain.[10,11] While it remains on plant surfaces, this material may be ingested by herbivores.

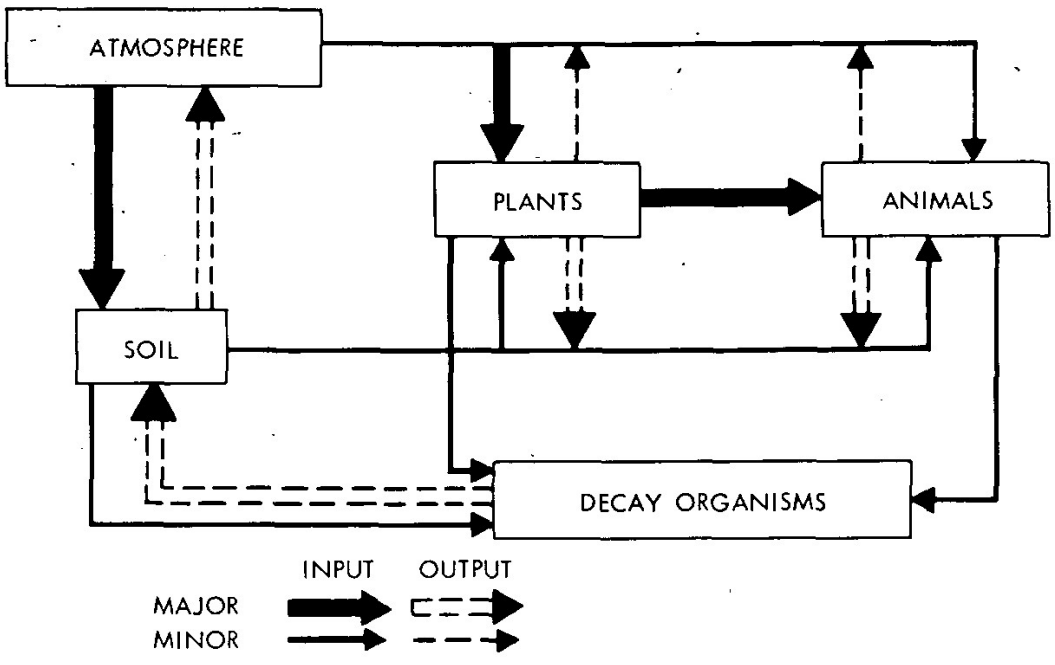

Fig. 1—Major and minor routes of radionuclide transfer and exchange in a terrestrial ecosystem contaminated by radioactive fallout.

Herbivorous mammals may be externally contaminated by direct exposure to fallout or by contact with contaminated plants or soils. Radionuclides may accumulate in animal tissues via inhalation, which, in many cases, is relatively unimportant or via ingestion of contaminated materials. Although inhalation, ingestion of contaminated soil or water, and ingestion of fallout particles while the animal is preening cannot be dismissed entirely, it is probably reasonable to assume that externally contaminated plants are the major sources of radionuclides for assimilation by herbivorous mammals (e.g., jackrabbits or dairy cattle) feeding in a fallout-contaminated environment during the first 30 to 90 days after close-in fallout.

The summer of 1962 provided an excellent opportunity to study the food-chain kinetics of ^{89}Sr and ^{131}I in relation to desert shrubs and rabbits in the Sedan fallout field. These studies included the formulation and testing of mathematical models that can be shown to provide at least a partial explanation of the kinetic relations between initial concentrations of ^{89}Sr and ^{131}I on fallout-contaminated plants and subsequent concentrations of ^{89}Sr in the bone ash or of ^{131}I in the thyroids of rabbits collected in the Sedan fallout field. Although the results of these studies[11–17] are not conclusive, partly because the causes of variation are imperfectly understood, they do provide evidence that mathematical models similar to those used by radiochemists to explain decay-chain kinetics,[18] by physiologists to explain tracer kinetics,[19] and by the International Commission on Radiological Protection (ICRP) to establish maximum permissible concentrations[20] can also be used to study food-chain kinetics under field conditions.

The objectives of this paper are (1) to summarize some of the data related to ^{89}Sr and ^{131}I on desert shrubs and in rabbit tissues following fallout from Project Sedan, (2) to present the deterministic models that provide a partial explanation of these results, and (3) to illustrate the potential value of similar models in studying the food-chain kinetics of radionuclides on pasture plants, in cow milk, and in human tissues following a single fallout event.

METHODS

Project Sedan, a peaceful nuclear-explosives test, involved the detonation of a 100 ± 15 kt thermonuclear device at a depth of 635 ft in alluvium and tuff at the north end of the Nevada Test Site on July 6, 1962. As predicted, the early fallout was relatively light and occurred primarily within a 150-mile sector, N60°W to N60°E, from ground zero in Yucca Flat.

Before and at various times after the detonation, plant samples and rabbits were collected from representative locations in the Sedan fallout field (see Fig. 2). Each sampling station was marked by a metal

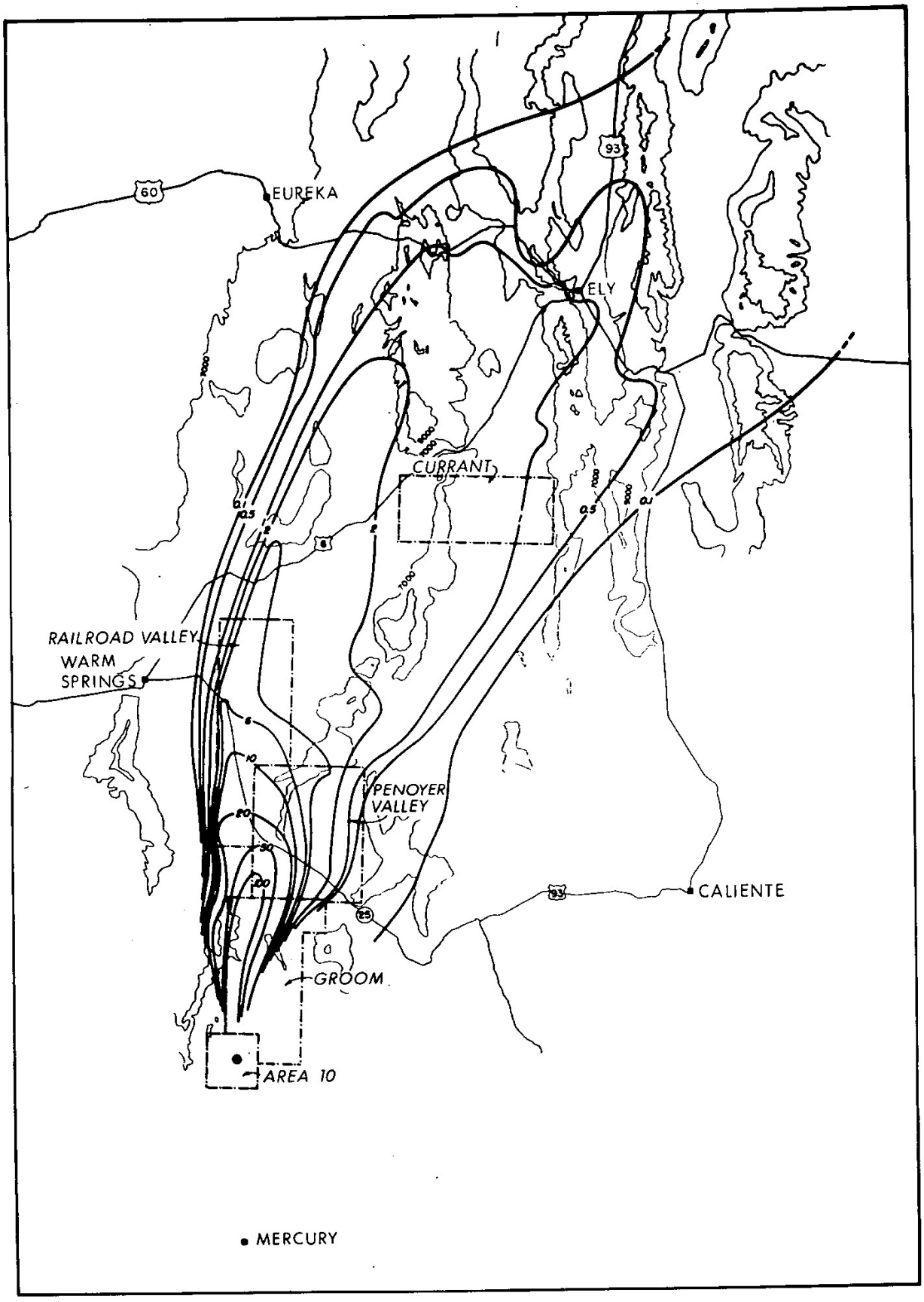

Fig. 2—Approximate locations of study areas and sampling stations in the Sedan fallout field. Dose-rate contours (mr/hr at H + 24) are based on aerial surveys.[22]

post to facilitate its relocation and positive identification. Plant samples were collected by clipping twigs and foliage from the crowns of desert shrubs growing within a radius of 150 ft from each station marker. *Artemisia tridentata* (sagebrush) was the species collected at all stations in Groom Valley and the Currant Area, and *Atriplex confertifolia* (shadscale) was collected at all but three of the stations in Penoyer and Railroad valleys. Most of the rabbits representing a given location were shot within a few hundred yards of a station marker, but rabbits taken within a 1-mile radius were accepted as representatives of the general location. Most of the rabbits collected were blacktailed jackrabbits (*Lepus californicus*), but a few cottontail rabbits (*Sylvilagus auduboni*) were taken in mountainous areas where jackrabbits were not always available.

Radiochemical analyses were made to determine the ^{89}Sr and ^{131}I contents of plant samples, the ^{89}Sr content of rabbit bone ash, and the ^{131}I content of rabbit thyroids. The stomach contents of rabbits were analyzed for ^{131}I, but the samples remaining after aliquots were removed for this purpose were too small to be used in making analyses for ^{89}Sr. Following each determination, a decay correction was made to indicate the ^{89}Sr or ^{131}I concentration at the time the sample was collected. The procedures followed in making these analyses are described elsewhere[11,16,21] in considerable detail.

For simplicity, the only samples considered in this paper are those collected at the 20 representative locations indicated in Fig. 2. Additional data are given in other publications.[13,16] Estimates of the initial gamma dose rates (R_0 = mr/hr at 3 ft aboveground at H + 24) were obtained from a tracing of Guillou's[22] original large-scale map prepared from aerial surveys made before and after the detonation.

Correlation and regression analyses were made to examine the relation between initial gamma dose rates, R_0, and initial concentrations of ^{89}Sr or ^{131}I on plants, P_0; between P_0 and maximum concentrations of ^{89}Sr in rabbit bone ash, B_{30}; and between P_0 and maximum concentrations of ^{131}I in rabbit thyroids, A_5. Similar analyses were also made to determine the relations between S_0 and R_0, A_5, and S_0, where S_0 represents the initial concentration of ^{131}I in rabbit-stomach contents.

Estimates of ^{89}Sr and ^{131}I retention by plants in relation to theoretical deposition rates, different parts of the fallout field, and different plant species were based on Eq. 1:

$$f_p = \frac{a_p}{a_s} \tag{1}$$

where f_p = retention index of N_i deposited on plants, sq ft/g [N.B. This index multiplied by G = g (dry weight) of plants per square foot would give the fraction of N_i deposited on plants]

a_p = pc N_i/g (dry)/R_0 deposited on plants

a_s = pc N_i/sq ft/R_0 deposited on uniform plane
N_i = a given radionuclide (e.g., ^{89}Sr or ^{131}I)

Estimates of a_p were based on the results of radiochemical analyses, P_t, and estimates of a_s (theoretical values) were based on Eq. 2:

$$a_s = \frac{0.693 F_k Y}{T_r D_d C R_k} \tag{2}$$

where $F_k = 1.43 \times 10^{23}$ fissions (^{235}U)/kt (Ref. 23)
Y = percent fission yield (atoms/fission) of N_i (4.79% ^{89}Sr, 3.1% ^{131}I) (Ref. 24)
T_r = radioactive half-life of N_i in days (50.5-day ^{89}Sr, 8.04-day ^{131}I)
$D_d = 3.2 \times 10^3$ dis/pc/day
$C = 2.79 \times 10^7$ sq ft/sq mile
$R_k = 4.5 \times 10^4$ mr/hr/kt/sq mile at 3 ft aboveground at H ± 24 (Ref. 25)

The relations between initial gamma dose rates, R_0, and initial concentrations of ^{89}Sr or ^{131}I on fallout-contaminated plants, P_0, were tentatively defined by linear regression formulas. For example, where $\overline{P}_0$ and $\overline{R}_0$ are the means of P_0 and R_0 and b_{xy} is the coefficient of regression of P_0 on R_0,

$$P_0 = \overline{P}_0 \pm b_{xy} (R_0 - \overline{R}_0) \tag{3}$$

The deterministic exponential models used to describe and explain the time-specific relation between ^{89}Sr or ^{131}I concentrations on plants, P_t, and of ^{89}Sr in bone ash, B_t, or of ^{131}I in thyroids, A_t, are given (if at $t = 0$, $P = P_0$, $B = 0$, and $A = 0$) by Eqs. 4 to 6:

$$P_t = P_0 e^{-\lambda_p t} \tag{4}$$

$$B_t = P_0 \frac{W_p f_b}{W_b} \left(\frac{e^{-\lambda_p t}}{\lambda_b - \lambda_p} + \frac{e^{-\lambda_b t}}{\lambda_p - \lambda_b} \right) \tag{5}$$

$$A_t = P_0 W_p f_a \left(\frac{e^{-\lambda_p t}}{\lambda_a - \lambda_p} + \frac{e^{-\lambda_a t}}{\lambda_p - \lambda_a} \right) \tag{6}$$

where t = days after fallout deposition
P_t = pc ^{89}Sr/g (dry) or pc ^{131}I/g (dry) on plants at $t > 0$
B_t = pc ^{89}Sr/g of rabbit bone ash at $t > 0$
A_t = pc ^{131}I (total) in rabbit thyroid at $t > 0$
W_p = g (dry) of contaminated plant material consumed per rabbit per day
W_b = g (dry) of bone ash per rabbit

f_b = fraction of ingested ^{89}Sr deposited in the rabbit's skeleton
f_a = fraction of ingested ^{131}I deposited in the rabbit's thyroid
$\lambda_p = 0.693/T_p$ where T_p = effective half-life of ^{89}Sr or ^{131}I on plants
$\lambda_b = 0.693/T_b$ where T_b = effective half-life of ^{89}Sr in rabbit's skeleton
$\lambda_a = 0.693/T_a$ where T_a = effective half-life of ^{131}I in rabbit's thyroid

RESULTS

Estimates of average gamma dose rates, of ^{89}Sr concentrations in plant samples and in the bone ash of rabbits, and of ^{131}I concentrations in plant samples, in the stomach contents of rabbits, and in rabbit thyroids are given in Tables 1 and 2. The approximate locations at which these samples were collected are shown in Fig. 2.

The wide range of values and the relatively large standard errors of the means given in Tables 1 and 2 indicate a high degree of apparently inherent variability.* The wide range of ^{89}Sr and ^{131}I concentrations in plant samples and in rabbit tissues or stomach contents is partly a reflection of the wide range of initial contamination levels as indicated by estimated gamma dose rates; but much of the inherent variability is undoubtedly related to the probabilistic nature of the environmental and biological processes that influence the external contamination of plants and the accumulation of radionuclides in animal tissues. The probabilistic approach to the study of food-chain kinetics and the use of stochastic models to simulate these processes are considered in this symposium by Turner.†

The results of correlation and regression analyses given in Table 3 show that the quantitative interrelations of initial dose-rate estimates and estimates of maximum ^{89}Sr or ^{131}I concentrations in plants and animal tissues are highly significant in spite of their inherent variability. As might be expected, the correlation between initial gamma dose rates, R_0, and initial concentrations of ^{89}Sr or ^{131}I on plants, P_0, are highly significant. The correlations and regressions of plant contamination on maximum concentrations of ^{89}Sr in bone ash, B_{30}, and of ^{131}I in thyroids, A_5, are also highly significant. The somewhat higher correlation between ^{131}I concentrations in stomach contents, S_0, and in thyroids, A_5, suggests some difference between the plants collected for radiochemical analyses and those actually eaten by the rabbits in the Sedan fallout field.

---

*Since the standard deviations (= sx $\sqrt{n}$) are large in relation to the means, the frequency distributions of these variates are sharply skewed. Preliminary investigations indicate that they may be lognormal rather than normal.

†See paper by Frederick B. Turner, this volume.[15]

Table 1 — AVERAGE GAMMA DOSE RATES, R_0, AND AVERAGE CONCENTRATIONS OF ^{90}Sr IN PLANT SAMPLES AND IN THE BONE ASH OF RABBITS COLLECTED FROM DIFFERENT PARTS OF THE SEDAN FALLOUT FIELD AT VARIOUS TIMES AFTER THE DETONATION*

Study areas	Initial gamma dose rates†			Days after detonation	Plant samples, pc ^{89}Sr/g (dry)			Rabbit bone ash, pc ^{89}Sr/g (dry)		
	$\bar{x}$	$s\bar{x}$	n		$\bar{x}$	$s\bar{x}$	n	$\bar{x}$	$s\bar{x}$	n
Groom Valley	45.0	±30%	5	5	4059	±30%	5	1459	±42%	5
				15	2716	±38%	5	3648	±62%	5
				30	1544	±50%	5	3667	±41%	5
				60	788	±38%	5	3581	±74%	5
Penoyer Valley	16.8	±45%	5	5	948	±37%	5	1363	±51%	5
				15	470	±30%	5	2024	±37%	5
				30	332	±39%	5	2283	±61%	5
				60	283	±44%	5	552	±34%	5
Railroad Valley	6.8	±32%	5	5	397	±14%	5	334	±30%	5
				15	269	±13%	5	620	±68%	5
				30	164	±19%	5	783	±33%	5
				60	127	±30%	5	462	±33%	5
Currant Area	1.5	±33%	5	5	318	±20%	5	295	±54%	5
				15	183	±23%	5	323	±31%	5
				30	136	±18%	5	427	±26%	5
				60	55	±15%	5	280	±31%	5
All areas	17.5	±30%	20	5	1436	±32%	20	863	±29%	20
				15	909	±37%	20	1680	±38%	20
				30	544	±40%	20	2097	±30%	20
				60	313	±32%	20	1389	±34%	20
		Pre-Sedan concentrations			30	±17%	14	56	±30%	16

*$\bar{x}$ = mean, $s\bar{x}$ = standard error expressed as a percentage of the mean, and n = number of samples. (Based on data given by Martin and Turner.[13])

†R_0 = mr/hr at 3 ft aboveground at H + 24.

When P_0 or S_0, B_t, and A_t are given, the parameter values required to solve Eqs. 4 to 6 are W_p, W_b, T_p, T_b, T_a, f_b, and f_a. Some of these parameter values can be obtained from experimental results reported in the literature, and others can be obtained from the data given in Tables 1 and 2. For our purposes those obtained from the field data may be more accurate.

Various studies[26,27] have indicated that adult jackrabbits consume approximately 100 g of dry plant material per day; therefore W_p = 100 g. Unpublished data collected during this and previous studies[1,2,28] indicate that the average adult jackrabbit in Nevada weighs about 2000 g and has a skeleton weighing 200 g (fresh). Since the ratio of fresh bone weight to bone-ash weight is approximately 4 to 1, W_b = 50 g. The ratio, W_p/W_b = 100/50, indicates a feeding rate of approximately 2.0 g of dry plant material per gram of bone ash per rabbit per day. The feeding

Table 2— AVERAGE CONCENTRATIONS OF ^{131}I IN PLANT SAMPLES AND IN THE STOMACH CONTENTS AND THE THYROIDS OF RABBITS COLLECTED FROM DIFFERENT PARTS OF THE SEDAN FALLOUT FIELD AT VARIOUS TIMES AFTER THE DETONATION*

Study areas	Days after detonation	Plant samples, pc ^{131}I/g (dry)			Rabbit stomach contents, pc ^{131}I/g (dry)			Rabbit thyroids, nc ^{131}I per thyroid		
		$\bar{x}$	$s\bar{x}$	n	$\bar{x}$	$s\bar{x}$	n	$\bar{x}$	$s\bar{x}$	n
Groom Valley	5	11966	±33%	5	5194	±29%	5	467	±34%	5
	10	6671	±39%	5	1283	±32%	4	386	±43%	4
	15	3192	±34%	5	1018	±47%	5	139	±52%	5
	20	1224	±49%	5	424	±28%	5	83	±35%	5
	25	526	±36%	5	161	±50%	5	61	±31%	5
	30	273	±30%	5	149	±32%	5	16	±31%	5
Penoyer Valley	5	1244	±33%	5	1853	±31%	5	257	±34%	5
	10	659	±30%	5	1212	±20%	4	141	±14%	4
	15	412	±36%	5	638	±17%	4	88	±34%	5
	20	227	±46%	5	311	±40%	5	40	±48%	5
	25	192	±64%	5	115	±44%	5	29	±52%	5
	30	81	±41%	5	81	±52%	4	1.5	±70%	5
Railroad Valley	5	713	±11%	5	693	±41%	2	111	±65%	4
	10	376	±10%	5	604	±34%	4	85	±36%	5
	15	211	±11%	5	348	±39%	3	61	±34%	5
	20	119	±17%	5	148	±31%	5	22	±45%	5
	25	96	±14%	5	75	±19%	5	29	±52%	5
	30	48	±25%	5	33	±24%	4	11	±27%	5
Currant Area	5	501	±15%	5	322	±37%	3	26	±27%	5
	10	200	±20%	5	57	±12%	3	7	±23%	5
	15	121	±57%	5	46	±28%	4	6	±50%	5
	20	56	±27%	5	42	±36%	5	6	±30%	5
	25	35	±26%	5	28	±50%	4	1.6	±10%	5
	30	26	±15%	5	7	±43%	5	1.1	±34%	5
All areas	5	3606	±40%	20	2506	±29%	15	221	±28%	19
	10	1977	±44%	20	838	±21%	15	143	±34%	18
	15	984	±40%	20	554	±31%	16	74	±36%	20
	20	406	±43%	20	231	±23%	20	38	±26%	20
	25	212	±32%	20	96	±27%	19	30	±27%	20
	30	113	±27%	20	69	±29%	18	12	±50%	20
Pre-Sedan concentrations		312	±57%	14	207	±51%	17	5.4	±61%	15

*$\bar{x}$ = mean, $s\bar{x}$ = standard error expressed as a percentage of the mean, and n = number of samples. (Based on data given by Turner and Martin.[16])

rate applicable to the accumulation of ^{131}I in the thyroid was taken as 100 g of dry plant material per whole thyroid per rabbit per day.

As shown in Table 1 and Fig. 3, the apparent rate of ^{89}Sr loss from fallout-contaminated plants tended to decrease with increasing time after the detonation, but the average effective half-life, T_p, from D + 5 to D + 30 (5 to 30 days after the detonation) was approximately 18 days. The average concentration of ^{89}Sr in bone ash, B_t, increased rapidly from D + 5 to D + 15 and then more slowly to a maximum (apparent

Table 3—RESULTS OF CORRELATION AND REGRESSION ANALYSES BASED ON ESTIMATES OF INITIAL GAMMA DOSE RATES AT 20 REPRESENTATIVE LOCATIONS IN THE SEDAN FALLOUT FIELD AND ON THE CONCENTRATIONS OF ^{89}Sr AND ^{131}I IN PLANT SAMPLES OR IN THE STOMACH CONTENTS, BONE ASH, OR THYROIDS OF RABBITS COLLECTED AT THE SAME LOCATIONS

Variables* [x(y)]	Correlation coefficients	Regression coefficients	Regression formulas [$x = \bar{x} + b_{xy}(y - \bar{y})$]
^{89}Sr			
$P_0(R_0)$	0.755†	83.75 ± 16.65†	$P_0 = 83.75\ R_0 + 335$
$B_{30}(P_0)$	0.698†	0.742 ● 0.250†	$B_{30} = 0.742\ P_0 + 761$
^{131}I			
$P_0(R_0)$	0.738†	0.405 ± 0.187†	$P_0 = 0.405\ R_0 + 0.147$
$S_0(R_0)$	0.835†	0.184 ± 0.029†	$S_0 = 0.184\ R_0 + 0.817$
$A_5(P_0)$	0.626†	12.76 ± 3.72†	$A_5 = 12.76\ P_0 + 122$
$A_5(S_0)$	0.769†	38.82 ± 7.59†	$A_5 = 38.82\ S_0 + 57$

*R_0 = mr/hr at 3 ft aboveground at H + 24; $P_0(^{89}Sr) = 1.26\ P_5$ (pc/g on plants at t = 0); $P_0(^{131}I) = 2.00\ P_5$ (nc/g on plants at t = 0); $S_0(^{131}I) = 2.00\ S_5$ (nc/g in stomachs at t = 0); $B_{30}(^{89}Sr)$ = observed values (pc/g in bone ash at t = 30 days); and $A_5(^{131}I)$ = observed values [nc(total) in thyroids at t = 5 days].

†Statistically significant at the 1% level of probability.

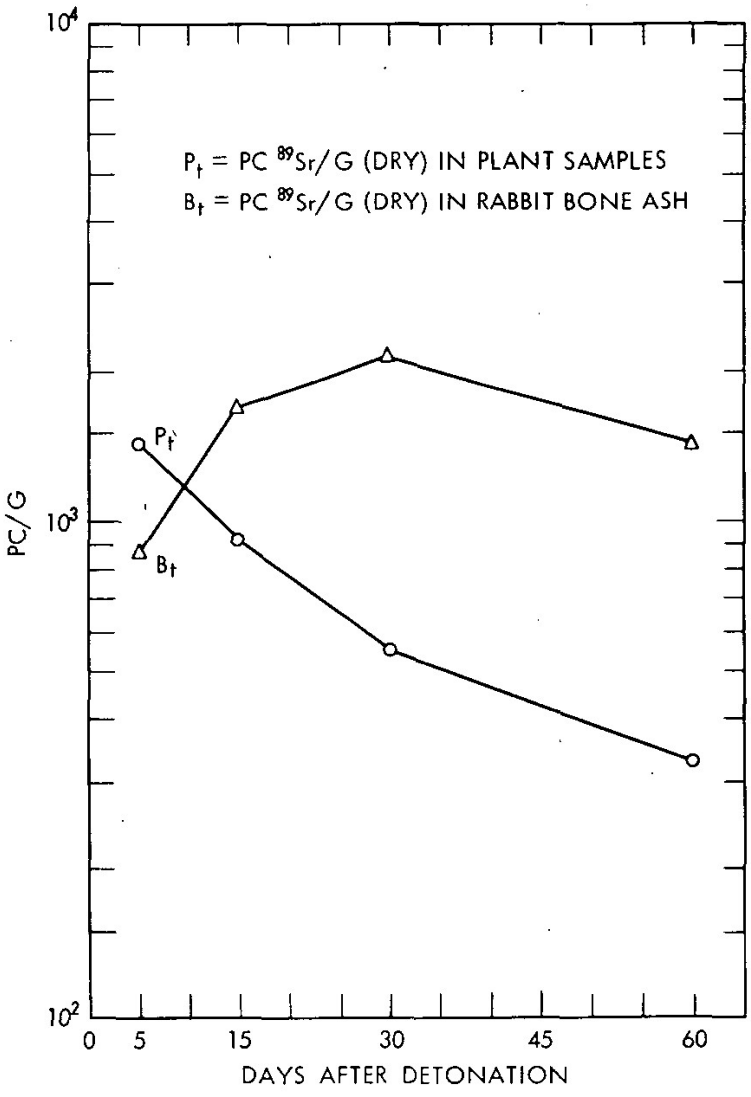

Fig. 3—Average concentrations of ^{89}Sr in plant samples, P_t, and in the bone ash of rabbits, B_t, collected from representative locations (see Fig. 2) in the Sedan fallout field at various times after the detonation.

equilibrium) about D + 30. The rate of decline from D + 30 to D + 60 approximated the radioactive half-life of ^{89}Sr. Estimates of the effective half-life of ^{89}Sr in rabbit bone (T_b = 20 days) were based on the average rates of loss from plants and the average rates of accumulation in bone ash. After estimates of the other required parameter values were obtained, these and the observed values for B_t were used to solve Eq. 5 for f_b. The average value thus obtained was $f_b = 0.0575$.

As shown in Table 2, the average concentrations of ^{131}I in plant samples (sagebrush) from Groom Valley and the Currant Area were higher than the average concentrations in the stomach contents of rabbits from the same locations. In the Penoyer and Railroad valleys, ^{131}I concentrations in the stomach contents of rabbits were somewhat higher than those in plant samples (mostly shadscale) from the same locations. Apparently the rabbits in these areas were feeding on plants other than sagebrush and shadscale.

This supposition is supported by the estimates of f_p given in Table 4. The average f_p values based on the plant samples from all locations are approximately the same for ^{89}Sr and ^{131}I. However, the average f_p value for ^{131}I based on concentrations in plant samples is higher than the average based on concentrations in the stomach contents of rabbits. For both ^{89}Sr and ^{131}I, the f_p values for sagebrush are higher than those for shadscale. The differences between f_p values for ^{89}Sr and ^{131}I in the different study areas are probably due to disparities between actual and theoretical, a_s, deposition rates, i.e., to fractionation or to errors in the estimation of average gamma dose rates. In general, these results indicate that the plants (probably grasses and broad-leaved herbs) representing the average rabbit's diet were less efficient than sagebrush but somewhat more efficient than shadscale in regard to the interception of fallout particles.

As shown in Table 2 and Fig. 4, the average concentrations of ^{131}I in plant samples from all stations were higher than the average ^{131}I concentrations in the stomach contents of rabbits from the same areas;

Table 4 — ESTIMATES OF f_p BASED ON EQS. 1 AND 2 AND OF INITIAL CONCENTRATIONS OF ^{89}Sr AND ^{131}I IN PLANT SAMPLES, P_0, AND OF ^{131}I IN THE STOMACH CONTENTS OF RABBITS, S_0*

Study areas†	Plant species	^{89}Sr	P_0	^{131}I	P_0	^{131}I	S_0
Groom Valley	Sagebrush	4.86	$\times 10^{-3}$	5.61	$\times 10^{-3}$	2.42	$\times 10^{-3}$
Penoyer Valley	Shadscale‡	3.03	$\times 10^{-3}$	1.56	$\times 10^{-3}$	2.32	$\times 10^{-3}$
Railroad Valley	Shadscale	3.14	$\times 10^{-3}$	2.21	$\times 10^{-3}$	2.24	$\times 10^{-3}$
Currant Area	Sagebrush	11.9	$\times 10^{-3}$	7.02	$\times 10^{-3}$	4.51	$\times 10^{-3}$
Average for all locations		4.40	$\times 10^{-3}$	4.34	$\times 10^{-3}$	3.02	$\times 10^{-3}$

*$P_0(^{89}Sr) = 1.26\ P_5$, $P_0(^{131}I) = 2.00\ P_5$, and $S_0(^{131}I) = 2.00\ S_5$.
†Locations of study areas are shown in Fig. 2.
‡Some of the plant samples from this area were *Grayia spinosa*.

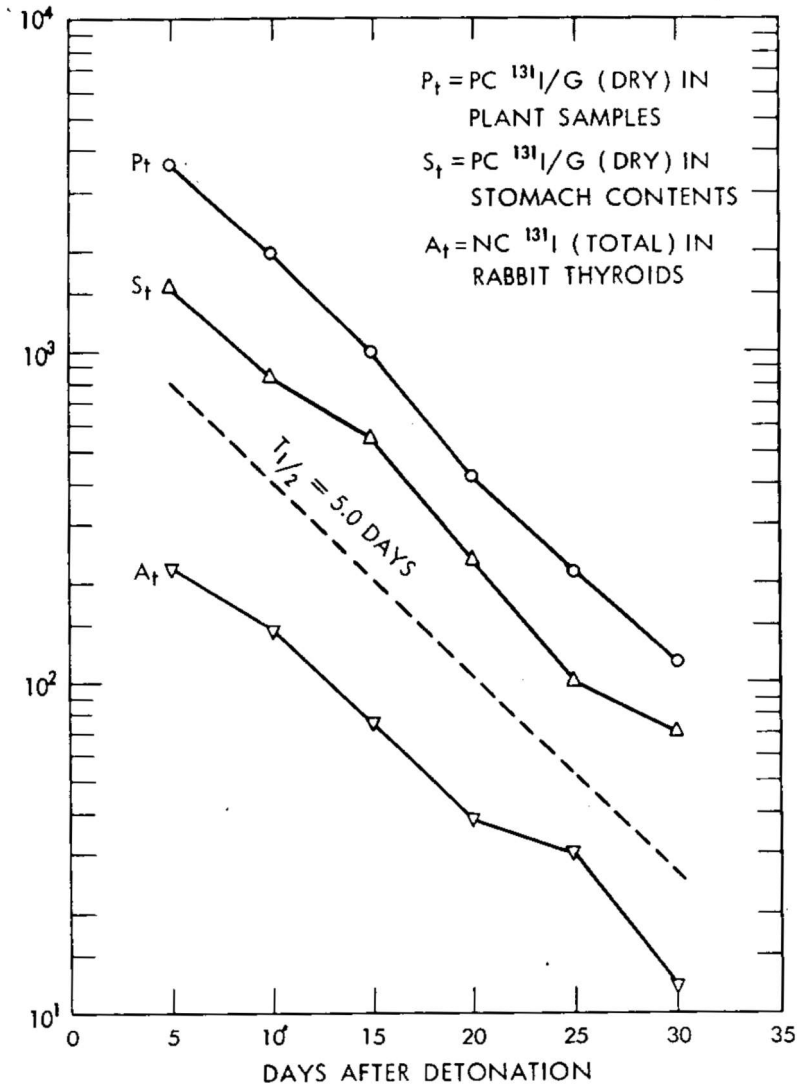

Fig. 4—Average concentrations of ^{131}I in plant samples, P_t, in the stomach contents, S_t, and in thyroids, A_t, of rabbits collected from representative locations (see Fig. 2) in the Sedan fallout field at various times after the detonation.

but the apparent rates of loss, indicating an effective half-life, T_p, of 5.0 to 5.5 days, were about the same. The average concentrations of ^{131}I in rabbit thyroids attained a maximum by or before D + 5 and declined at a half-time rate of 5 to 6 days.

French[27] and French and Van Middlesworth[29] did some experimental work with jackrabbits near the National Reactor Testing Station in Idaho. Their reports give estimates of T_a ranging from 1.5 to 2.5 days and of f_a ranging from 0.29 ± 0.09 to 0.158 ± 0.086. A more recent report by McBride[30] gives estimates of T_a = 2.0 days and f_a = 0.29. By trial and error we have found that estimates of T_p = 5.0 days and T_a = 2.0 days are reasonable approximations in relation to the data given in Table 2 and Fig. 4. With the use of these parameter values and the observed average values of A_t, Eq. 6 was solved for f_a. The results based on plant data, $\bar{P}_0$, indicate f_a = 0.18, and the results based on stomach-

contents data, $\bar{S}_0$, indicate $f_a = 0.26$. (N.B. If stomach-contents data were available for ^{89}Sr, one might expect to find a similar difference in estimates of f_b required to fit the observed data points.)

Figures 5 and 6 show the relatively close agreement between observed average concentrations of ^{89}Sr in rabbit bone ash and of ^{131}I in rabbit thyroids and the hypothetical values obtained through solution of Eqs. 5 and 6. Because of variations within and between the different study areas (Groom, Penoyer, Railroad, and Currant), the parameter values that apply to the Sedan fallout field as a whole may or may not apply with equal accuracy to different areas within the fallout field. For example, if they were based on initial ^{131}I concentrations in plant samples, estimates of ^{131}I concentrations in thyroids, A_t, would be higher than those observed in the Groom and Currant study areas but lower than those observed in the Penoyer and Railroad valleys. However, the disparities between hypothetical and observed ^{89}Sr concentrations in the bone ash of rabbits from different parts of the Sedan fallout field, based on R_0 rather than physiography, are generally less than the standard errors of the observed means.[13]

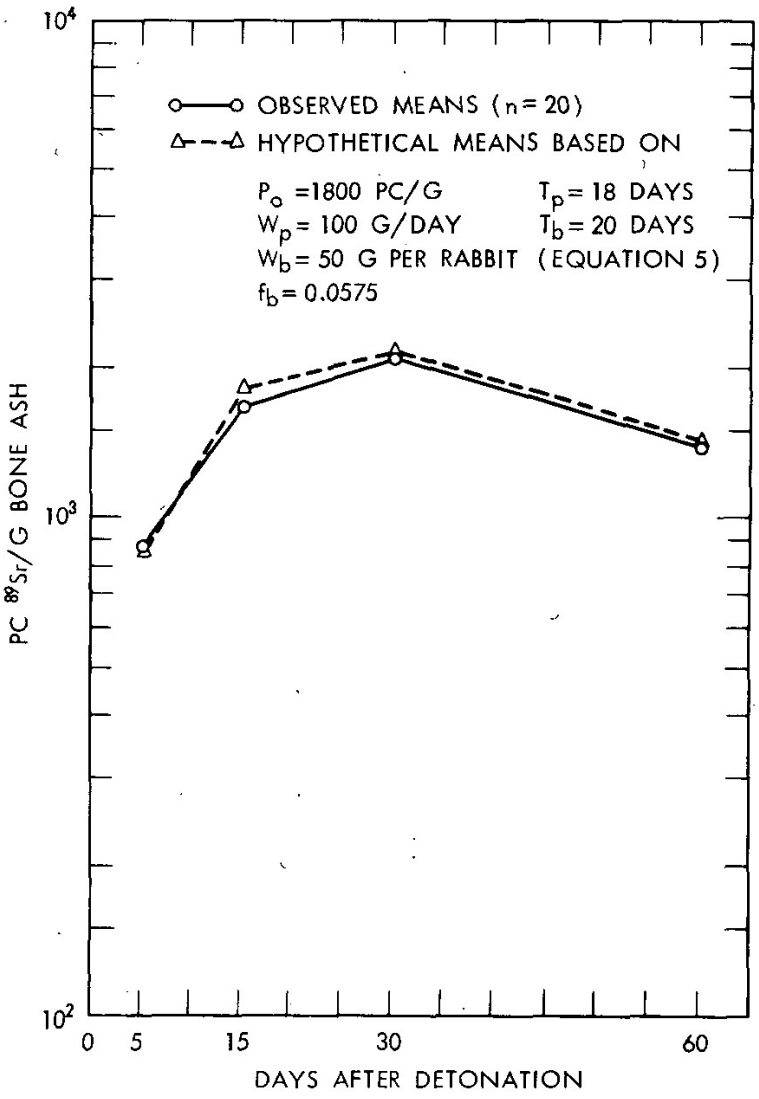

Fig. 5—Observed and hypothetical average concentrations of ^{89}Sr in the bone ash of rabbits collected from representative locations (see Fig. 2) in the Sedan fallout field at various times after the detonation.

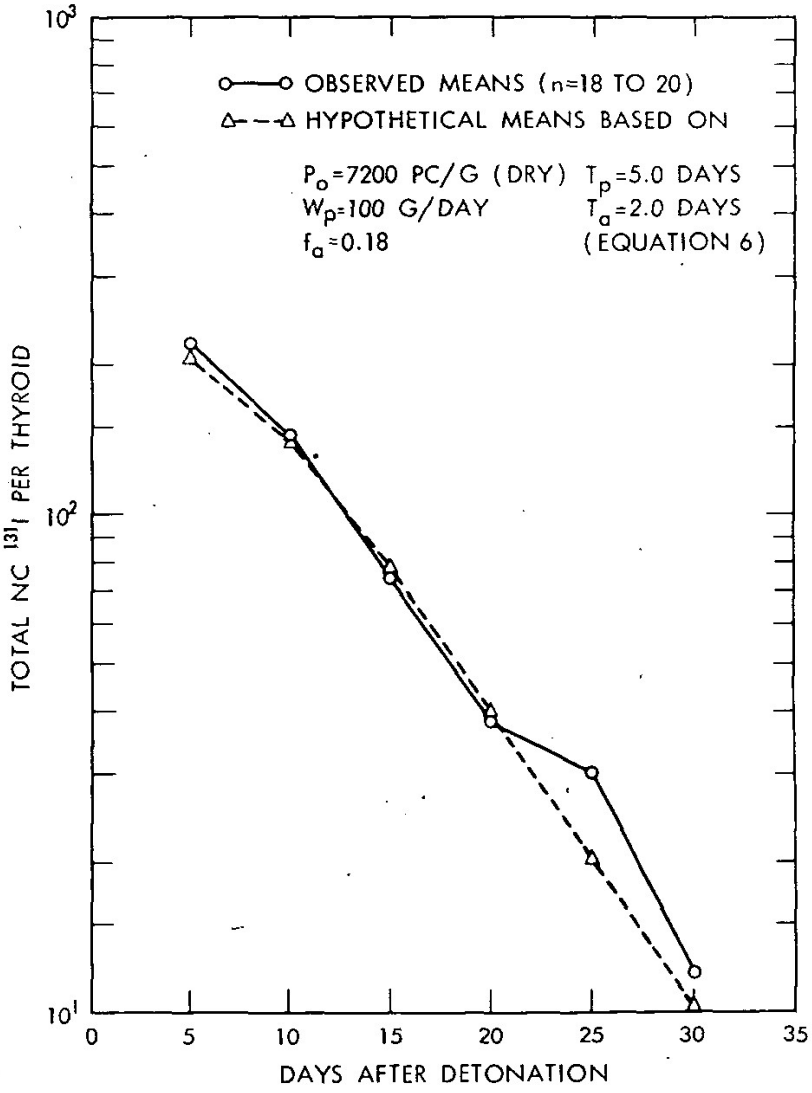

Fig. 6—Observed and hypothetical average concentrations of ^{131}I in the thyroids of rabbits collected from representative locations (see Fig. 2) in the Sedan fallout field at various times after the detonation.

DISCUSSION

These results seem to indicate that Eqs. 4 to 6 function satisfactorily, with estimated parameter values based on observed means, in explaining the early food-chain kinetics of ^{89}Sr and ^{131}I on plants and in the skeletons or thyroids of rabbits collected from 20 representative locations in the Sedan fallout field at between 5 and 60 days after the detonation. The input parameters for Eqs. 4 to 6 (W_p, W_b, f_b, f_a, T_p, T_b, and T_a) are known to vary; but the means of these values can be used, with fair success, as though they were constants. This deterministic approach to the problem permits us to describe and explain certain aspects of food-chain kinetics in relatively simple mathematical terms. It may also permit us to make errors in estimating parameter values; these errors are difficult to detect because the several parameters are

interdependent. The variations within and between different study areas and the twofold difference between estimates of f_a based on ^{131}I concentrations in plant samples and in the stomach contents of rabbits are good examples of the kinds of disparities to be anticipated.

Although it is quite tempting to use such models to predict the biological consequences of close-in fallout, there are many good reasons for proceeding with caution. Some of the uncertainties, possible sources of error, and other obstacles to the achievement of this goal are described and discussed below.

From our analyses, the relation between initial gamma dose rates, R_0, and initial concentrations of radionuclides on fallout-contaminated plants, P_0, appears to take the form of a linear regression formula. There are several reasons for viewing this apparently simple relation with suspicion. For example, Guillou[22] has noted that the probable accuracy of R_0 estimates based on aerial-survey data is no greater than $\pm 50\%$. Consequently the regression coefficients given in Table 3 could be in error by $\pm 50\%$, and errors associated with extrapolations beyond the standard regression formula limits could be even greater.

Because of nuclide fractionation and downwind variations in the particle-size composition of fallout, one might not expect to find significant correlations between gross gamma dose rates and concentrations of specific radionuclides on plants or soils in fallout fields resulting from surface or low-altitude nuclear detonations. Previous studies[1,7,28] along the hot lines of fallout from balloon- and tower-supported detonations have shown correlations between plant and animal contamination and the distribution of fallout particles $< 44\ \mu$ in diameter.* In several cases, the highest percentages of fallout $< 44\ \mu$ in diameter and the highest levels of plant and animal contamination were found at intermediate distances from ground zero and hence at intermediate levels of gross gamma dose rate. Under these conditions, it would not be possible to predict plant contamination levels by means of linear regression formulas involving R_0 as the independent variable.

As shown in Table 4, it is also necessary to consider those factors which influence a plant's ability to intercept and retain the fallout particles deposited on it. Other things being equal, it may be assumed that plants with dense foliage composed of oily, resinous, or pubescent leaves should have higher f_p values than plants with sparse foliage composed of smooth or waxy leaves; but more data are needed to determine f_p values for a variety of wild and cultivated plant species in relation to specific morphological features, the particle-size composition of fallout, and various deposition rates.

*Autoradiographs and microscopic examinations have shown that virtually all the radioactive particles on plant foliage in the Sedan fallout field were $< 50\ \mu$ in diameter and that about half of those measured were $< 20\ \mu$ in diameter.

Also needed are data to indicate the effects on f_p of plant density (e.g., g/sq ft) and other phytosociological characteristics of vegetation such as species composition, community structure, and phenology. In desert-shrub communities, for example, shrubs are widely spaced, and it is probably safe to assume that the f_p value for plants in a given area is independent of plant density. In pasture or forest, where plants are more crowded and where some may grow in the shade of others, f_p may decrease as density increases. Some evidence of this relation in regard to ^{131}I has been cited recently by Straub and Fooks.[31]

Many of these factors (fractionation, particle-size composition and distribution, and retention factors, $a_L = f_p$) are considered in the fallout model proposed by Miller.[32] If suitable plant data were available for a given situation, Miller's model would surely provide a theoretically sounder basis than unqualified linear regression formulas for the prediction of the initial concentrations of radionuclides on plants at different locations in a close-in fallout field. If one wanted to use the food-chain model described earlier (Eqs. 3 to 6) to make predictions of P_0, P_t, B_t, and A_t, a fallout model such as Miller's should be substituted for Eq. 3.

After the deposition of fallout, the concentration of a given radionuclide on fallout-contaminated plants can be expected to decline at a rate significantly faster than would be predicted on the basis of its radioactive half-life. Our estimates of effective half-lives on plants in the Sedan fallout field, 18 days for ^{89}Sr and 5.0 to 5.5 days for ^{131}I, indicate environmental half-lives (i.e., half-time rates of loss due to all causes other than radioactive decay) of approximately 28 days for ^{89}Sr and 15 days for ^{131}I. Since there was little or no rain in the area of the Sedan fallout field during the period of this study, the environmental half-life of ^{89}Sr on plants can be attributed primarily to wind action that removed particles from foliage or foliage from plants. The shorter environmental half-life of ^{131}I on plants may reflect the combined effects of wind action and sublimation.[11,12]

Other studies have indicated that our estimates of environmental and effective half-lives may not be applicable to other situations. For example, Bartlett et al.[10] sprayed solutions of different fission products on grass that was then exposed to both wind and rain for periods up to 60 days. Their results indicated an average environmental half-life of about 14 days for each of the radionuclides used. The difference between their results and ours is probably due to the effects of rain in removing soluble materials, but rain should have similar effects on particulate materials.

Considering the large number of variables involved (e.g., plant species, local weather conditions, the particle-size composition of material deposited on plants, the developmental stage of foliage, etc.), one should expect to find a wide range of apparent effective half-lives

of different radionuclides on fallout-contaminated plants. In the absence of pertinent measurements, it is reasonable to assume an environmental half-life of 14 days or less for ^{131}I and for other radionuclides on fallout-contaminated plants in humid regions. Except for ^{131}I, an environmental half-life of 28 days should be more accurate for arid regions. In general, the effective half-life of a given radionuclide on plants, T_p, could be estimated, where T_e is the environmental half-life and T_r is the radioactive half-life, by

$$T_p = \frac{T_r \times T_e}{T_r + T_e} \tag{7}$$

Our method[13] of estimating the effective half-life of ^{89}Sr in rabbit bone (T_b = 20 days) was made necessary by the absence of pertinent experimental data, and our only confidence in the accuracy of our estimate is based on the results obtained (Fig. 5) when we used it to solve Eq. 5. Our estimate of the effective half-life of ^{131}I in rabbit thyroids (T_a = 2.0 to 2.5 days) was well within the range of experimental results reported by French[27] (T_a = 1.5 to 2.5 days). Whenever possible, the effective half-lives of radionuclides in animal tissues or organs should be determined by experimental as well as by empirical methods. One can then judge which of several possible values should be applied to a given set of circumstances.

Animal retention factors, e.g., f_b and f_a, are especially difficult to evaluate; and, as shown in Eqs. 5 and 6, errors in the estimation of these parameter values would result in proportional errors in the prediction of tissue burdens. Our estimates of retention factors for ^{89}Sr (f_b = 5.75%) and for ^{131}I (f_a = 18% if based on P_0 or f_a = 26% if based on S_0) represent mathematically arbitrary numbers calculated to obtain reasonably good fits between hypothetical and observed average tissue burdens. Because of the methods used in the estimation of these values, their physiological significance is doubtful; but these values may be just as useful as those obtained from feeding experiments. For example, French's experimental results indicated f_a values ranging from < 10 to >30% for jackrabbits, whereas the averages obtained for Dutch rabbits under laboratory conditions were only half as high. We collected samples of sagebrush and shadscale from the Sedan fallout field and fed them to Dutch rabbits in the laboratory. The results reported by Turner[14] indicated f_a values ranging from 2.0 ± 0.6% (based on samples from the Currant Area) to 12.0 ± 8.0% (based on samples from Groom Valley). Because of the difference in animal species (Dutch rabbits vs. jackrabbits) and because our field data indicate that jackrabbits in the Sedan fallout field were feeding on plants other than sagebrush and shadscale, these results are of dubious value in relation to the food-chain model.

DETERMINISTIC MODELS FOR HUMAN-FOOD-CHAIN KINETICS

The data summarized and discussed in the preceding pages have served to illustrate the usefulness of deterministic exponential models in providing at least a partial explanation of the early food-chain kinetics of radionuclides following a single fallout event. Although the results of these studies are not conclusive, they are promising and provide a basis for the supposition that similar models should be useful in the study of radionuclide transfers in food chains leading to man.

For example, suppose that an ordinary pasture is contaminated by fallout from a single nuclear detonation or from a reactor accident and that the milk produced by dairy cattle grazing in the contaminated pasture is consumed by people living on the farm or in a nearby village. If an estimate of the initial concentration of a given radionuclide, N_i, on pasture plants, P_0, can be obtained from direct measurement or predicted by a suitable fallout model, the subsequent concentration of N_i on pasture plants, P_t, in cow milk, M_t, and in the human tissue or organ of reference, H_t, can be estimated, with the assumptions that $P = P_0$, $M = 0$, and $H = 0$ at $t = 0$, by Eqs. 8 to 10:

$$P_t = P_0 e^{-\lambda_p t} \tag{8}$$

$$M_t = P_0 K_m f_m \left(\frac{e^{-\lambda_p t}}{\lambda_m - \lambda_p} + \frac{e^{-\lambda_m t}}{\lambda_p - \lambda_m} \right) \tag{9}$$

$$H_t = P_0 K_m f_m K_h f_h \left[\frac{e^{-\lambda_p t}}{(\lambda_m - \lambda_p)(\lambda_h - \lambda_p)} + \frac{e^{-\lambda_m t}}{(\lambda_p - \lambda_m)(\lambda_h - \lambda_m)} + \frac{e^{-\lambda_h t}}{(\lambda_p - \lambda_h)(\lambda_m - \lambda_h)} \right] \tag{10}$$

where t = days after fallout
N_i = a given radionuclide (e.g., ^{89}Sr or ^{131}I)
P_0 = pc N_i/g (dry) on pasture plants at $t = 0$
P_t = pc N_i/g (dry) on pasture plants at $t > 0$
M_t = pc N_i/ml (fresh) in milk produced at $t > 0$
H_t = pc N_i/g (fresh) in the human tissue or organ of reference at $t > 0$
K_m = dry weight (g) of plants consumed/volume (ml) of milk produced per day
K_h = volume (ml) of milk consumed per day/weight (g) of human organ or tissue
f_m = fraction of ingested N_i secreted in cow milk
f_h = fraction of ingested N_i deposited in human tissue or organ of reference
$\lambda = 0.693/T$
T_p = effective half-life of N_i on pasture plants
T_m = effective half-life of N_i in cow milk production
T_h = effective half-life of N_i in human tissue or organ of reference

To illustrate the potential value of the model formulated above, we have adopted the parameter values listed in Table 5. Most of these values are based on experimental data reported in the literature; but, when two or more estimates of a given parameter value were found, we usually selected the one resulting in higher concentrations in milk or

Table 5—PARAMETER VALUES USED WITH EQS. 8 TO 10 TO CALCULATE HYPOTHETICAL CONCENTRATIONS OF ^{89}Sr AND ^{131}I ON PASTURE PLANTS, IN COW MILK, AND IN HUMAN TISSUES FOLLOWING A SINGLE FALLOUT EVENT*

Parameter†	^{89}Sr	^{131}I	References
P_0	100 pc/g	400 pc/g	Arbitrary values
K_m	1.4 g/ml/day	1.4 g/ml/day	33
f_m	0.02	0.06	34, 35
K_h (adult)	1/7 ml/day/g	50 ml/day/g	20
K_h (infant)	10/7 ml/day/g	500 ml/day/g	20
f_h	0.21	0.30	20
K_r‡	1.43×10^{-4}	1.17×10^{-5}	20
T_p	18.0 days	5.5 days	13, 16
T_m	2.5 days	2.0 days	34
T_h	50.4 days	7.5 days	20

*Results are shown in Figs. 7 and 8.
†Parameters are defined in the text.
‡Used with Eq. 11 to calculate tissue doses.

human tissues. The results of calculations based on Eqs. 8 to 10 and the parameter values listed in Table 5 are shown in Figs. 7 and 8. Obviously, for different values of P_0, the corresponding values of M_t and H_t would be proportionally larger or smaller than shown in Figs. 7 and 8. Using the same effective half-lives but different estimates of K_m, f_m, K_h, or f_h would also result in proportionally higher or lower estimates of M_t and H_t.

The total dose, D_t, delivered by N_i to the human tissue or organ of reference is given, for $t = 0$ to $t = \infty$, by

$$D_t = P_0 K_m f_m K_h f_h K_r \left[\frac{1 - e^{-\lambda_p t}}{\lambda_p(\lambda_m - \lambda_p)(\lambda_h - \lambda_p)} + \frac{1 - e^{-\lambda_m t}}{\lambda_m(\lambda_p - \lambda_m)(\lambda_h - \lambda_m)} + \frac{1 - e^{-\lambda_h t}}{\lambda_h(\lambda_p - \lambda_h)(\lambda_m - \lambda_h)} \right] \quad (11)$$

where D_t = total dose (rem) delivered by N_i, from $t = 0$ to $t > 0$, to the human organ or tissue of reference

$K_r = [(3.20 \times 10^3 \text{ dis/pc/day})\ (E)/(6.24 \times 10^7 \text{ Mev/100 ergs/g})]$

E = effective absorbed energy (Mev) per disintegration of N_i [Mev absorbed/disintegrations of N_i × relative biological effectiveness (RBE)]

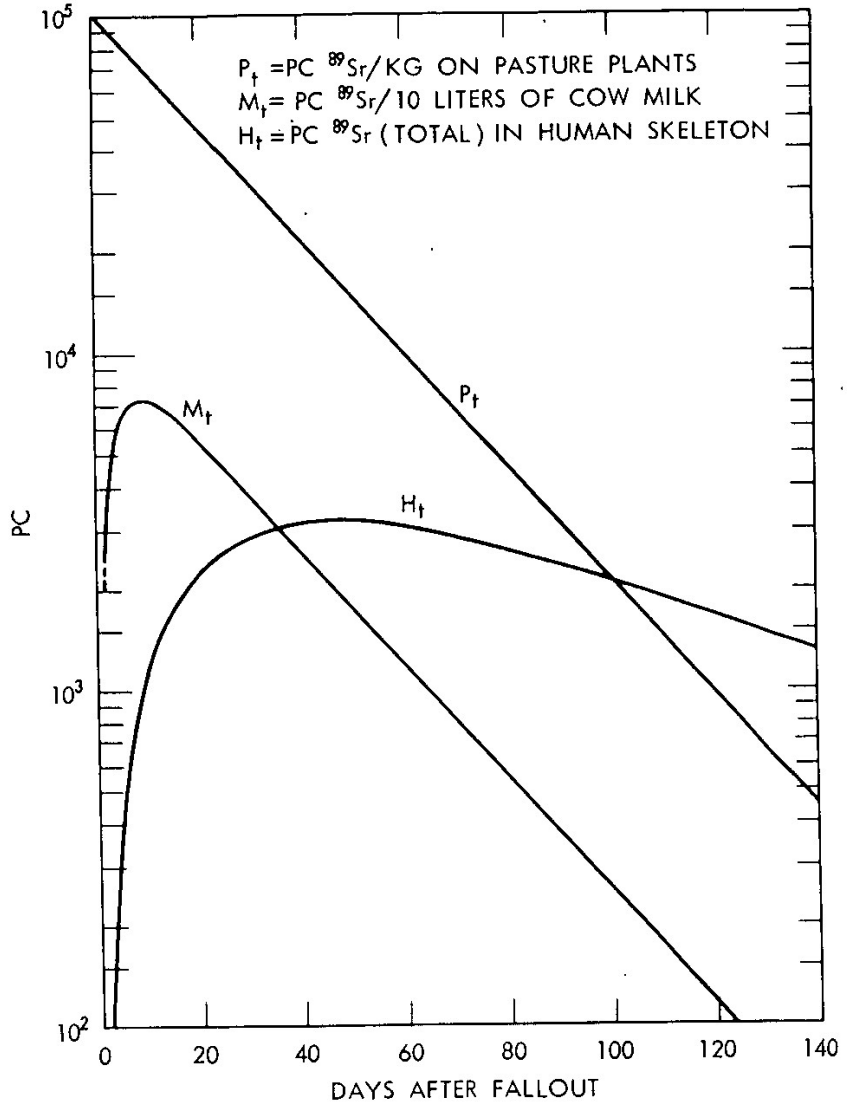

Fig. 7—Hypothetical concentrations of ^{89}Sr on pasture plants, in cow milk, and in human skeletons following environmental contamination by a single fallout event.

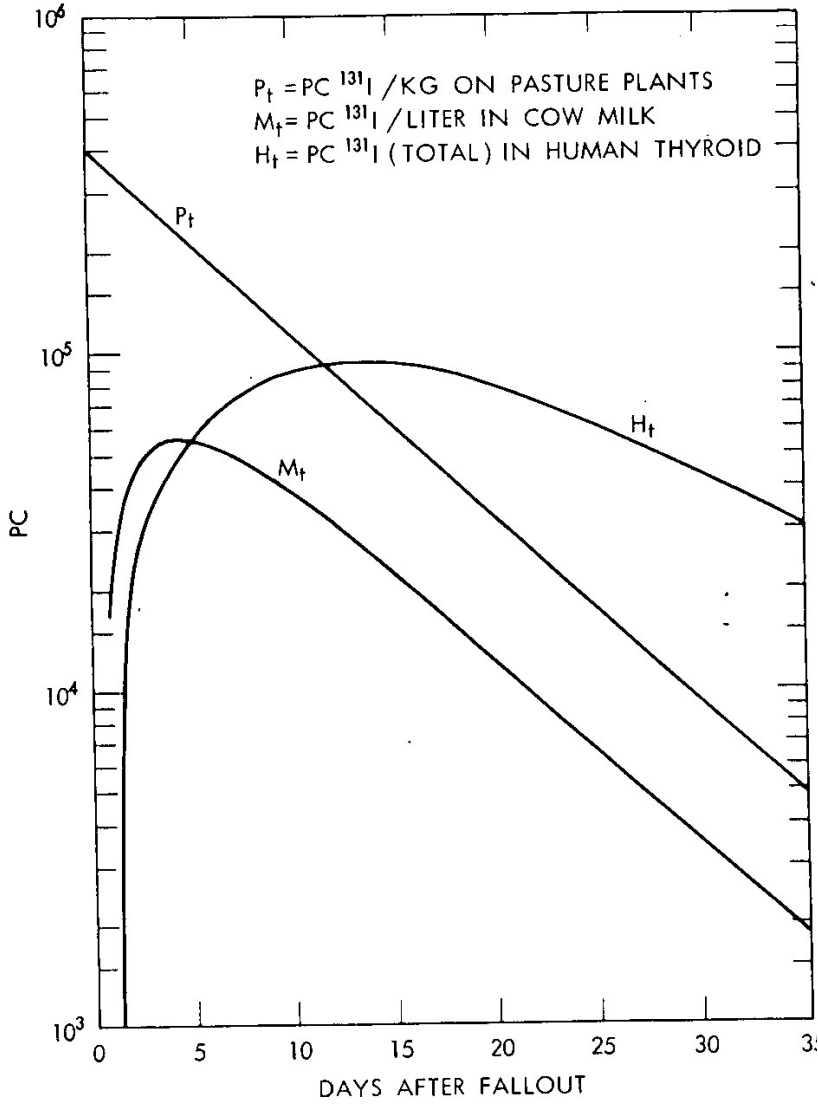

Fig. 8—Hypothetical concentrations of ^{131}I on pasture plants, in cow milk, and in human thyroids following environmental contamination by a single fallout event.

If the concentration of N_i on pasture plants is not known, estimates of doses to human tissue can be based on concentrations in milk (M_t = pc N_i/ml). If the time of fallout is known and M_t is given for a specified time of milking, Eq. 9 can be simplified, as shown in Eq. 12, to obtain an integration constant, I_0, that can then be substituted for the expression $P_0K_mf_m$ in Eqs. 10 and 11 to obtain estimates of concentrations in, H_t, and doses to, D_t, the human tissue or organ of reference:

$$M_t = I_0 \frac{e^{\lambda_p t} - e^{\lambda_m t}}{\lambda_m - \lambda_p} \tag{12}$$

James[36] recently used a similar method to estimate human thyroid doses resulting from a single fallout event, but many of his parameter values (i.e., $f_h = 0.25$, $K_r = 1.0 \times 10^{-5}$, $T_p = 5.0$ days, and $T_m = 1.9$ days) were not as pessimistic as those given in Table 5. James concluded from his investigation that a maximum concentration of 2800 pc of ^{131}I per liter of milk resulting from a single fallout event would, if a milk consumption of 1 liter/day were assumed, result in a total dose of 0.5 rad to a 2.0-g thyroid. Our results (Table 6) indicate that a maximum concentration of only 1850 pc of ^{131}I per liter of milk would be required for a potential dose of 0.5 rem to a 2.0-g human thyroid. (N.B. In this case 1 rem = 1 rad × RBE, and RBE = 1.0; therefore 1 rem = 1 rad.)

Pendelton et al.[37] based their estimates of thyroid doses on estimates of total ^{131}I intake, I_t, by people consuming 1 liter of milk per day in various parts of Utah during the summer of 1962. According to our hypothesis, the value of I_t would be given by

$$I_t = I_0 V_h \left[\frac{1 - e^{-\lambda_p t}}{\lambda_p(\lambda_m - \lambda_p)} + \frac{1 - e^{-\lambda_m t}}{\lambda_m(\lambda_p - \lambda_m)} \right] \tag{13}$$

where I_0 is an integration constant obtained from Eq. 12 and V_h is the volume of milk in milliliters consumed per person per day.

With the use of I_t from Eq. 13, the total thyroid dose would be given, where W_h is the thyroid weight (fresh) in grams, by

$$D_t = \frac{I_t K_r f_h}{\lambda_h W_h} \tag{14}$$

The Radiation Protection Guides (RPG's) recommended by the Federal Radiation Council (FRC)[38] are said to represent "... a reasonable balance between biological risk and benefit to be derived from useful applications of radiation and atomic energy." The RPG's for human bone and thyroid are based on average rates of radiostrontium and radioiodine intakes which, in the opinion of the FRC, should result in doses no greater than 1.5 rem/year to "... individuals in the gen-

Table 6—SUMMARY OF HYPOTHETICAL VALUES THAT, IF INDICATED BY MEASUREMENTS MADE AFTER ENVIRONMENTAL CONTAMINATION BY A SINGLE FALLOUT EVENT, WOULD IMPLY TOTAL DOSES OF 0.5 REM TO THE SKELETONS OR THYROIDS OF INFANTS CONSUMING 1 LITER OF MILK PER DAY

Hypothetical values*	^{89}Sr	^{131}I
Initial concentrations on pasture plants, P_0	61.0 pc/g	13.7 pc/g
Maximum concentrations in milk, M_t	4500 pc/liter	1850 pc/liter
Time after fallout, t_{max}	8 days	4 days
Total intake (to $t = \infty$)	1.60×10^5 pc	2.63×10^4 pc
Maximum concentration in human tissue, H_t	27 pc/g†	1580 pc/g†
Time after fallout, t_{max}	50 days	15 days
Total dose (at $t = \infty$)	0.5 rem†	0.5 rem†

*Calculations were based on Eqs. 8 to 14 and the parameter values listed in Table 5.

†Based on a 700-g skeleton or a 2.0-g thyroid.

eral population..." or an average of 0.5 rem/year "... to be applied to suitable samples of an exposed population group." Average annual intakes of >2000 pc ^{89}Sr/day or >100 pc ^{131}I/day "... would be presumed to result in exposures exceeding the RPG...."

With the assumptions of a skeleton weight of 700 g and a thyroid weight of 2.0 g, Eq. 14 and the parameter values listed in Table 5 indicate that total annual intakes of 160,000 pc of ^{89}Sr or of 26,300 pc of ^{131}I could result in doses of 0.5 rem/year to the bones and the thyroids of infants. These values are lower than those indicated by the FRC (i.e., 720,000 pc ^{89}Sr/year and 36,500 pc ^{131}I/year) because the parameter values in Table 5 are more pessimistic than those adopted by the FRC.

For further comparison with the FRC's recommendations, we have estimated the hypothetical values of various measurements which, if obtained following a single fallout event, could result in doses of 0.5 rem to the bones and thyroids of infants. These hypothetical values are given in Table 6.

Tables 1 and 2 show that initial concentrations of ^{131}I on plants in various parts of the Sedan fallout field were about four times higher than the initial concentrations of ^{89}Sr. The estimates given in Table 6 indicate that initial concentrations of ^{89}Sr about 4.5 times higher than those of ^{131}I are required to deliver comparable doses to human tissues. We might therefore suppose that ^{131}I is considerably more hazardous than ^{89}Sr in an area contaminated by close-in fallout.

The data given in Table 2 indicate that the initial concentration of ^{131}I on plants in the vicinity of Currant, Nev., was approximately 1000 ± 150 pc/g. Similar plant samples collected in a hot spot (centered near Fruitland, Utah), which was discovered after the Small Boy detonation

on July 14, 1962, indicated an initial ^{131}I concentration (on July 15) of approximately 800 ± 200 pc (n = 6). If we assume an f_p value of about 3.0×10^{-3} for pasture plants compared to approximately 7.5×10^{-3} for desert shrubs, the initial concentrations of ^{131}I on pasture plants in the vicinity of Currant, Nev., and Fruitland, Utah, could have been 400 and 320 pc/g, respectively.

If our hypothetical pastures, dairy herds, and human populations had been located in these areas, the total ^{131}I intakes by people drinking 1 liter of milk per day could have ranged from 670,000 to 825,000 pc, and the doses to the thyroids of children could have been 11.4 to 14.6 rem. With the use of the more optimistic parameters adopted by the FRC, the estimated doses based on these intakes would be 9.2 and 11.3 rem. (N.B. These estimates are comparable to the highest estimates reported by Pendelton et al.[37] for stations located in other parts of Utah).

Actually, there are very few milk cattle in the area of the Sedan fallout field, and, since we collected no milk samples, our treatment of the problem is strictly hypothetical. However, one sample collected near Ely, Nev., and analyzed by the U. S. Public Health Service[39] contained 2800 pc ^{131}I/liter on July 24, 18 days after the detonation. If this value represents the concentration at the time of milking, it could indicate a possible thyroid dose of 2.6 rems.

Solutions to Eq. 13 indicate that ^{131}I intakes during periods of 7, 14, or 21 days following environmental contamination by a single fallout event should account for 42, 85, or 97%, respectively, of the total potential intakes from $t = 0$ to $t = \infty$. Therefore the simplest countermeasures to avoid 85% or more of the potential biological hazard related to ^{131}I would be (1) to feed cattle on stored feed for a period of two or more weeks after a detonation or (2) to use the milk produced during that period for making cheese or other dairy products that would not be consumed for a period of three or more weeks after milk production.

REFERENCES

1. R. L. Lindberg, E. M. Romney, J. H. Olafson, and K. H. Larson, Factors Influencing the Biological Fate and Persistence of Fallout, Operation Teapot, Report WT-1177, University of California at Los Angeles, January 1959.
2. K. H. Larson, H. A. Hawthorne, and J. H. Olafson, Nevada Test Site Fallout: Some Characteristics, Its Apparent Environmental Equilibrium and Biological Availability, in Radioactive Fallout from Nuclear Weapons Tests, A. W. Klement, Jr. (Ed.), USAEC Report TID-7632, pp. 4-24, February 1962.
3. R. S. Russell, Deposition of Sr^{90} and Its Content in Vegetation and in Human Diet in the United Kingdom, *Nature, 182:* 834-839 (1958).
4. National Academy of Sciences, the Behavior of Radioactive Fallout in Soils and Plants, *Natl. Acad. Sci.—Natl. Res. Council Publ. No. 1092,* 37 pp., 1963.

5. H. Nishita, E. M. Romney, and K. H. Larson, Uptake of Radioactive Fission Products by Crop Plants, *Agri. Food Chem., 9:* 101-106 (1961).
6. N. R. French and K. H. Larson, Environmental Pathways of Radioactive Iodine from Nuclear Tests in Arid Regions, USAEC Report UCLA-499, University of California at Los Angeles, December 1961.
7. E. M. Romney, R. G. Lindberg, H. A. Hawthorne, B. G. Bostrom, and K. H. Larson, Contamination of Plant Foliage with Radioactive Fallout, *Ecology, 44:* 343-349 (1963).
8. L. J. Middleton, Absorption and Translocation of Strontium and Cesium by Plants from Foliar Sprays, *Nature, 181:* 1300-1303 (1958).
9. A. A. Selders and F. P. Hungate, the Foliar Sorption of Iodine by Plants, USAEC Report HW-44890, Hanford Atomic Products Operation, Sept. 1, 1956.
10. B. O. Bartlett, L. J. Middleton, G. M. Milbourn, and H. M. Squire, the Removal of Fission Products from Grass by Rain, United Kingdom Agricultural Research Council Report ARCRL-5, pp. 52-54, 1961.
11. W. E. Martin, Losses of Sr^{90}, Sr^{89}, and I^{131} from Fallout Contaminated Plants, *Radiation Botany,* in press.
12. W. E. Martin, Loss of I^{131} from Fallout-contaminated Vegetation, *Health Phys., 9:* 1141-1148 (1963).
13. W. E. Martin and F. B. Turner, Food-chain Relationships of Radiostrontium in the Sedan Fallout Field, USAEC Report PNE-237F, University of California at Los Angeles, March 1965.
14. F. B. Turner, Quantitative Relationships Between Fallout Radioiodine on Native Vegetation and in the Thyroids of Herbivores, *Health Phys., 9:* 1241-1247 (1963).
15. F. B. Turner, the Uptake of Fallout Radioisotopes by Mammals and a Stochastic Simulation of the Process, this volume.
16. F. B. Turner and W. E. Martin, Food-chain Relationships of Radioiodine Following Two Nuclear Tests in Nevada, USAEC Report PNE-236P, University of California at Los Angeles, May 10, 1963.
17. F. B. Turner and W. E. Martin, Food-chain Relationships of I^{131} in Nevada Following the Sedan Test of July 1962, USAEC Report PNE-236F, University of California at Los Angeles, July 24, 1964.
18. G. Friedlander and J. W. Kennedy, *Nuclear and Radiochemistry,* Chap. 5, pp. 127-144, John Wiley & Sons, Inc., New York, 1955.
19. W. E. Siri, *Isotopic Tracers and Nuclear Radiation,* Chap. 15, pp. 388-402, McGraw-Hill Book Company, Inc., New York, 1949.
20. International Committee on Radiation Protection, Report of Committee II on Permissible Dose for Internal Radiation, *Health Phys., 3:* 1 (1960).
21. Health and Safety Laboratory, Manual of Standard Procedures, USAEC Report NYO-4700(Rev.), August 1962.
22. R. B. Guillou, Part II, Aerial Radiometric Survey, Project Sedan, USAEC Report PNE-225P, pp. 36-64, University of California at Los Angeles, August 1962.
23. S. Glasstone (Ed.), *The Effects of Nuclear Weapons,* U. S. Government Printing Office, Washington, D. C., 1962.
24. S. Katcoff, Fission-product Yields from Neutron-induced Fission, *Nucleonics, 18*(11): 201-208 (1960).
25. G. Higgins, Calculation of Radiation Fields from Fallout, USAEC Report UCID-4539, University of California Lawrence Radiation Laboratory, Jan. 25, 1963.
26. A. D. Arnold, Forage Consumption and Preferences of Experimentally Fed Arizona and Antelope Jack Rabbits, *Univ. Ariz. Agri. Expt. Sta. Tech. Bull., 95:* 51-86 (1961).
27. N. R. French, Iodine Metabolism in Wild Jack Rabbits, in Oklahoma Conference — Radioisotopes in Agriculture, Held April 2 and 3 at Oklahoma State University, Stillwater, Oklahoma, USAEC Report TID-7578, pp. 113-121,

Associated Midwest Universities and Argonne National Laboratory, Apr. 13, 1960.
28. K. H. Larson and J. W. Neel, Summary Statement of Findings Related to the Distribution, Characteristics, and Biological Availability of Fallout Debris Originating from Testing Programs at the Nevada Test Site, USAEC Report UCLA-438, University of California at Los Angeles, Sept. 14, 1960.
29. N. R. French and L. Van Middlesworth, Biological Monitoring of Recent Airborne Fission Products, in *Proceedings of the Second International Conference on the Peaceful Uses of Atomic Energy, Geneva, 1958*, Vol. 18, pp. 516-518, United Nations, New York, 1958.
30. R. McBride, Radioiodine Uptake at the NRTS and Environs, *Health Phys., 9:* 1127-1230 (1963).
31. C. P. Straub and J. H. Fooks, Cooperative Field Studies on Environmental Factors Influencing I^{131} Levels in Milk, *Health Phys., 9:* 1195-1204 (1963).
32. C. F. Miller, *Fallout and Radiological Countermeasures* (2 volumes), Stanford Research Institute, Menlo Park, Calif., 1963.
33. A. C. Chamberlain, J. F. Loutit, R. P. Martin, and R. S. Russell, The Behaviour of I^{131}, Sr^{89}, and Sr^{90} in Certain Agricultural Food Chains, in *Proceedings of the International Conference on the Peaceful Uses of Atomic Energy, Geneva, 1955,* Vol. 13, pp. 360-363, United Nations, New York, 1956.
34. C. L. Comar and R. H. Wasserman, Radioisotopes in the Study of Mineral Metabolism, in *Progress in Nuclear Energy, Biological Sciences*, Series IV, Vol. 1, pp. 153-196, Pergamon Press, Inc., New York, 1956.
35. F. W. Lengemann and E. W. Swanson, Secretion of Iodine in Milk of Dairy Cows Using Oral Doses of I^{131}, *J. Dairy Sci., 40:* 216-224 (1957).
36. R. A. James, Calculation of Radioactive Iodine Concentrations in Milk and Human Thyroid as a Result of Nuclear Explosions, USAEC Report UCRL-7716, University of California Lawrence Radiation Laboratory, Feb. 14, 1964.
37. R. C. Pendelton, C. W. Mays, R. D. Lloyd, and A. L. Brooks, Differential Accumulation of I^{131} from Local Fallout in People and Milk, *Health Phys., 9:* 1261-1270 (1963).
38. Federal Radiation Council, Background Material for the Development of Radiation Protection Standards, Report No. 2, U. S. Government Printing Office, Washington, D. C., 1961.
39. U. S. Atomic Energy Commission, Off-site Environmental Contamination from Nuclear Explosives at the Nevada Test Site, September 15, 1961–September 15, 1962, USAEC Report TID-18892.